Titre: Title:	Mechanical properties of white layers formed by different machining processes on nickel-based superalloy
Auteur: Author:	Édouard Proust
Date:	2007
Type:	Mémoire ou thèse / Dissertation or Thesis
Référence: Citation:	Proust, É. (2007). Mechanical properties of white layers formed by different machining processes on nickel-based superalloy [Mémoire de maîtrise, École Polytechnique de Montréal]. PolyPublie. https://publications.polymtl.ca/8503/

URL de PolyPublie: PolyPublie URL:	https://publications.polymtl.ca/8503/
Directeurs de recherche: Advisors:	Jolanta-Ewa Sapieha, & Ludvik Martinu
Programme: Program:	Non spécifié

UNIVERSITÉ DE MONTRÉAL

MECHANICAL PROPERTIES OF WHITE LAYERS FORMED BY DIFFERENT MACHINING PROCESSES ON NICKEL-BASED SUPERALLOY

ÉDOUARD PROUST
DÉPARTEMENT DE GÉNIE PHYSIQUE
ÉCOLE POLYTECHNIQUE DE MONTRÉAL

MÉMOIRE PRÉSENTÉ EN VUE DE L'OBTENTION
DU DIPLÔME DE MAÎTRISE ÈS SCIENCES APPLIQUÉES
(GÉNIE PHYSIQUE)
DÉCEMBRE 2007

Your file Votre référence
ISBN: 978-0-494-69163-2
Our file Notre référence
ISBN: 978-0-494-69163-2

UNIVERSITÉ DE MONTRÉAL

ÉCOLE POLYTECHNIQUE DE MONTRÉAL

Ce mémoire intitulé:

MECHANICAL PROPERTIES OF WHITE LAYERS FORMED BY DIFFERENT MACHINING PROCESSES ON NICKEL-BASED SUPERALLOY

présenté par: PROUST Édouard

en vue de l'obtention du diplôme de : Maîtrise ès sciences appliquées

a été dûment accepté par le jury d'examen constitué de:

M. YELON Arthur, Ph.D., président

Mme. SAPIEHA Jolanta Ewa, Ph.D., membre et directrice de recherche

M. MARTINU Ludvik, Ph.D., membre et codirecteur de recherche

M. BALAZINSKI Marek, Ph.D., membre

ACKNOWLEDGEMENTS

I wish to thank my thesis supervisors Dr. Jolanta Sapieha & Professor Ludvik Martinu for giving me the opportunity to work on this innovative project, for supervising my work and for their patience.

I would also like to express my thanks to Professor Arthur Yelon and Professor Marek Balazinski for accepting to evaluate this work and be members of my jury.

I want to express my sincere gratitude to Dr. Nihad Ben-Salah from the research and development group – materials engineering of Pratt & Whitney Canada for the time she spent answering my numerous questions, for her helpful advice and for her helps with advancing my project.

A special thank to Etienne Bousser and Samih Beskri for sharing their knowledge with me, helping when it was hard to go on and for supporting me throughout this time. Good luck with your respective projects.

I also wish to thank my friends and colleagues of the Functional Coating and Surface Engineering Laboratory at École Polytechnique for their help and friendly environment: Oleg, Maxime, Francis, Yves, Moushab, Eda, David, Jiri, Pierre-Yves, Philippe, Guru, Bill, Matej, Jean-Michel, Stéphane and Richard.

Finally, thanks to my parents, family and friends for their support during my studies here, in Montreal.

RÉSUMÉ

Les superalliages de nickel présentent d'excellentes propriétés mécaniques et une importante résistance à la corrosion à haute température de sorte qu'ils sont largement utilisés dans l'industrie aéronautique pour la fabrication de disques et d'aubes de turbines.

Bien que très performants, ces alliages restent difficiles à usiner. Leur structure provoque une usure rapide des outils de coupe. De plus, sous certaines conditions d'usinage, les parties superficielles du matériau subissent un changement de phase résultant en la formation d'une couche mince à la surface des pièces usinées appellée couche blanche. Les disques de turbine sont des pièces critiques et aucun défaut ne peut être accepté. De plus, il faut s'assurer que la couche blanche ne peut influer sur la vie en fatigue de la pièce, rendant son exploitation dangeureuse.

Même si l'existence de la couche blanche est bien connue, ses propriétés mécaniques n'ont jamais été étudiées d'une façon systématique. Dans ce mémoire nous présentons une étude des propriétés mécaniques (dureté et module d'Young) et microstructurales de couches blanches formées à la surface de disques de turbines en superalliage de nickel IN100 par différents procédés d'usinage. L'étude vise à étudier l'influence du procédé d'usinage et de sollicitations en fatigue sur les propriétés mécaniques et sur la microstructure de la couche blanche résultant de l'usinage.

La principale originalité de ce travail vient de la technique de caractérisation employée. En utilisant la nanoindentation nous avons pu determiner de façon très précise de quelle façon varient la dureté et le module d'Young des couches blanches étudiées. De plus, l'utilisation d'un système d'indentation spécifique nous a permis de réaliser des images de grande qualité de la surface des échantillons et ainsi d'étudier la microstructure des couches blanches formées.

Cette recherche a démontré que les propriétés mécaniques et microstructurales des couches blanches sont directement liées aux conditions d'usinage du matériau. Ainsi, notre travail permettra, à terme, de mieux comprendre les processus de formation des

couches blanches sur les superalliages de nickel IN100 et de trouver des solutions pour éviter leur apparition, une étape d'importance considérable pour l'industrie aéronautique.

ABSTRACT

Nickel-based superalloys are widely used in the aerospace industry in the production of turbine discs and blades because of their good mechanical properties and great corrosion resistance at high temperature.

Although very useful, these alloys are hard to machine. Their structure is responsible for rapid wear of cutting tools. Moreover, under certain machining conditions, near-surface regions of the material undergo a phase transformation resulting in the formation of a thin layer called "white etching layer" at the surface of the machined workpiece. Because turbine discs are safety critical components, no defects can be tolerated on the workpiece. Therefore, efforts should be made to ensure that this white etching layer can't influence the operating life of the workpiece and make its operation unsafe.

Even if the existence of the white etching layer is well known, its mechanical properties have never been assessed in detail. In this thesis, we present a study of the mechanical (hardness and Young's modulus) and microstructural properties of white etching layers formed at the surface of nickel-based superalloy IN100 turbine discs fabricated by different machining processes. This work aims at evaluating the impact of the machining process and of fatigue on the properties of the white etching layers under study.

The originality of this study primarily lies in the employed characterization technique. Using nanoindentation has allowed us to very precisely assess the variations of both the hardness and the Young's modulus along the white etching layers. Also, the use of a sophisticated indentation system has enabled the acquisition of very precise surface images of the samples and therefore to study the microstructure of the white etching layers.

This research has demonstrated that the mechanical and microstructural properties of the white etching layers are closely linked to the machining conditions of the material. Therefore, our study will help researchers gain a better understanding of white etching

layer formation mechanisms on IN100 nickel-based superalloy and find ways to prevent their formation: a point of crucial importance for the aerospace industry.

CONDENSÉ

Les superalliages de nickel sont d'un intérêt considérable pour l'industrie aéronautique étant donné qu'ils maintiennent d'excellentes propriétés mécaniques et de résistance à la corrosion à haute température. Cette caractéristique en fait d'excellents choix lors de la conception de moteurs à réaction et notamment de leurs parties dites "chaudes". Ainsi, on retrouve ces alliages dans la réalisation des disques et des aubes de turbines.

La structure diphasique des superalliages de nickel est responsable de leur excellente tenue en température. Ces alliages sont constitués d'une matrice appellée phase γ et d'une phase durcissante connue sous le nom de phase γ'. En bloquant le mouvement des dislocations à haute température, les plans de glissements de la phase γ' limitent les pertes de performance du matériau en opération.

Bien que très performants, les superalliages de nickel présentent de grandes difficultés d'usinage. La phase durcissante γ' cause une usure rapide des outils de coupe. De plus, la faible conductivité thermique de ces alliages limite la diffusion vers l'intérieur du matériau de la chaleur produite pendant l'usinage. Ces caractéristiques imposent d'avoir recours à des procédés d'usinages spécifiques pour mettre en forme ces matériaux.

Les contraintes mécaniques et thermiques appliquées au matériau durant son usinage sont responsables d'un changement de phase à la surface des pièces usinées. Cette transformation se manifeste par la formation d'une couche superficielle qui est résistante aux attaques chimiques et apparait blanche en microscopie optique. Cette dernière propriété lui a vallu le nom de "couche blanche".

Les pièces de moteurs d'avion sont des pièces dites "de sécurité", ce qui implique qu'elle ne doivent pas présenter le moindre défaut pour être considérées comme fonctionnelles. Cette couche blanche n'étant pas désirée, il convient de l'étudier afin de comprendre les mécanismes conduisant à sa formation ainsi que de déterminer ses propriétés. Ainsi, au cours de cette étude nous avons caractérisé des couches blanches

produites par deux différents procédés d'usinage : l'électroérosion et le brochage. Ces deux procédés contraignent le matériau usiné de façon très différente ce qui laisse à penser que les couches blanches formées peuvent avoir des propriétés spécifiques. Pour reproduire les conditions de fonctionnement des pièces de moteurs d'avions, nous avons également caractérisé des échantillons ayant été soumis à des sollicitations cycliques. Cette étude soulève deux questions :

- les propriétés mécaniques et microstructurales des couches blanches sont-elles liées entre-elles et influencées par le procédé d'usinage utilisé ?
- La fatigue a-t-elle une influence sur les propriétés mécaniques et microstructurales des couches blanches ?

Ce mémoire commence par des considérations théoriques incluant une description des superalliages de nickel, de leur propriétés et des techniques d'usinage employées pour les mettre en forme. Les mécanismes de formation des couches blanches ainsi que leurs propriétés sont ensuite développés. Par la suite la méthodologie expérimentale est décrite en détail. Elle est suivie par la présentation des résultats expérimentaux. Dans un premier temps sont étudiés les échantillons de référence avant et après test en fatigue. Ensuite sont présentés successivement les résultats pour les échantillons usinés par électroérosion puis par brochage. Comme pour les échantillons de référence, on présente dans un premier temps les résultats des échantillons n'ayant pas subi de test en fatigue. Enfin, les résultats sont analysés et les conclusions du travail sont exposées ainsi que des perspectives pouvant mener à des recherches futures.

La première tâche du travail a été de développer la méthodologie expérimentale. L'extrême finesse des couches blanches étudiées a imposé l'utilisation d'un système de nanoindentation équipé d'un dispositif d'imagerie en contact à force constante. L'imagerie a été employée pour positionner avec précision l'indenteur au dessus des régions d'intérêt. Après avoir identifié les couches blanches sur les échantillons, il a fallu

tester différents paramètres d'imagerie permettant d'obtenir des images de qualité avant d'effectuer les mesures des propriétés mécaniques.

Dans un deuxième temps, nous avons caratérisé par nanoindentation un échantillon du superalliage de nickel IN100 ayant subi des tests en fatigue après avoir été usiné par abrasion. Le procédé d'usinage par abrasion a été spécialement adapté pour diminuer au maximum les contraintes induites dans les pièces usinées. L'échantillon ainsi caractérisé a fourni des valeurs de référence pour les propriétés mécaniques du superalliage de nickel étudié.

Nous avons ensuite réalisé des mesures de nanoindentation sur les échantillons usinés par électroérosion et brochage et n'ayant pas été soumis à des tests de fatigue. Les mesures ont été réalisées perpendiculairement à l'interface entre le matériau de base et les couches blanches afin d'obtenir des profils en fonction de la distance à la surface des échantillons. Dans le cas des couches les plus minces, les mesures ont été effectuées parallèlement à cette même surface. Chaque zone d'étude a été imagée avant et après indentation par imagerie afin de pouvoir localiser les traces laissées par l'indenteur et ainsi tracer les profils d'évolution de la dureté et du module d'Young en fonction de la distance à l'interface entre la couche blanche et le superalliage de nickel. Ces mesures ont permis de mettre en évidence le fait que les couches blanches formées sont plus dures que le matériau de base et que leur microstructure diffère de celle des superalliages de nickel.

Enfin, nous avons répété les mêmes étapes de mesure avec les échantillons ayant subi des tests de fatigue afin d'étudier la réponse du matériau et des couches blanches à une sollicitation cyclique. Dans ce cas, nous avons observé un durcissement de la couche blanche et du matériau de base. Ce phénomène de durcissement est causé par écrouissage lors des tests de fatigue. Les contraintes cycliques causent une accumulation de dislocations autour de la phase γ'. L'augmentation de la dureté des couches blanches par fatigue a de plus démontré qu'elles sont ductiles et non fragiles comme le laissait penser la littérature.

Les résultats de ce travail ont contribué à l'avancement général des connaissances sur les couches blanches formées sur les superalliages de nickel par usinage en permettant

l'évaluation des rélations entre la microstructure, les propriétés mécaniques et le procédé d'usinage. Les résultats originaux de cette étude sont les suivants :

- développement d'une méthodologie pour la caractérisation mécanique et microstructurale de couches blanches par nanoindentation assistée par imagerie,
- caractérisation des propriétés mécaniques et microstructurales de couches blanches formées par différents procédés d'usinage,
- preuve de l'influence du procédé d'usinage sur les propriétés mécaniques et microstructurales des couches blanches étudiées.
- démonstration de l'influence de contraintes cycliques sur les propriétés mécaniques et microstructurales des couches blanches.

Cette étude constitue une première dans le domaine des couches blanches formées sur des superalliages de nickel. Elle donnera lieu à des développements futurs. Ce travail peut notamment servir de base à l'étude :

- des mécanismes de rupture dans les couches blanches et de leur impact sur la vie en opération des pièces de moteurs d'avions,
- des mécanismes d'usure par contact présents dans les moteurs à réaction,
- des mécanismes de formation des couches blanches sur les superalliages de nickel.

TABLE OF CONTENTS

LIST OF TABLES

LIST OF FIGURES

LIST OF SYMBOLS

A	Constant, expressed in μN/nm^2.
$A(h_c)$	Projected contact area at peak load in nm^2.
AFM	Atomic force microscopy.
D	Diameter in m of the workpiece in turning.
DL, Dl	Deformed layer(s).
E	Young's modulus of the material in GPa.
E_i	Young's modulus of the indenter in GPa.
E_{IT}	Indentation Young's modulus in GPa.
E_r	Reduced Young's modulus of the indentation contact in GPa.
EDM	Electrical-discharge machining.
F	Indentation force in μN.
F_{max}	Maximum test force in μN.
f	Feed motion in mm/min.
h	Total displacement of the tip in nm.
h_c	Depth of the contact of the indenter with the test piece at F_{max} in nm.
h_f	Constant, expressed in nm.
H_{IT}	Indentation hardness in GPa.
h_{max}	Maximum indentation depth at F_{max} in nm.
IN100	Nickel-based superalloy Inconel IN100.
IN718	Nickel-based superalloy Inconel IN718.
LSG	Low-stress grinding.
m	Constant (dimensionless).
N	Rotation speed in rev/min.
Ni	Nickel-based superalloy.
ν_S	Poisson's ratio of the test piece.
ν_i	Poisson's ratio of the indenter.

S	Initial unloading contact stiffness in μN/nm.
SDL, Sdl	Severely deformed layer(s).
AFM	Scanning probe microscopy.
τ	White layer thickness in μm.
V_c	Cutting speed in m/min.
WEL, Wl	White etching layer(s).

LIST OF APPENDICES

CHAPTER 1 – INTRODUCTION

From the very first human flights to the most recent technical developments, aeronautics has played a major role in the development of mankind since the early 1900's. By allowing faster journeys between continents and cities, modern commercial airlines have had a great impact on complex multinational projects and therefore on the life of millions of people around the world [1-5]. Aeronautics being the science of making an airplane, several fields such as aerodynamics, propulsion, materials science, structures and control systems must be understood. Today, most civilian and military aircraft are powered by gas turbine engines (Figure 1.1) which delivering thrust in order to drive the plane forward [3-5]. In order to meet the demands of the aerospace industry, designers are pushing the limits still further, particularly by upgrading material properties and design capabilities, and therefore offering engines with much better performances. These improvements are often linked with the fabrication of lighter components with improved mechanical and chemical properties and capable of operating at higher temperatures [5-7].

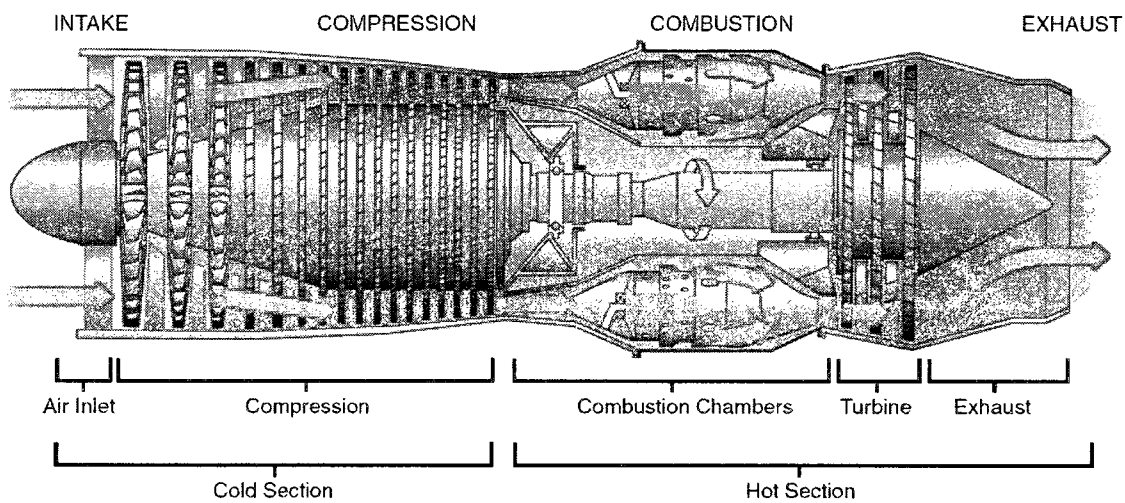

Figure 1.1 – Main components of a jet engine [8].

Airplane and helicopter engines are highly complex and sophisticated assemblies of components that are safety critical, meaning that the smallest defect on the workpiece will result in its discard for safety reasons. Turbine discs (Figure 1.2) are one of the numerous defect free components present in an engine. Because of the high mechanical solicitations to which they are exposed and the corrosive environment in which they operate, special requirements concerning the materials to be employed have to be met in their conception. Nickel-based superalloys are the most advanced materials employed today in the design of airplane and helicopter turbine discs. They possess high strength and high resistance to corrosion, two properties that are necessary to withstand the operating conditions of modern turboprop engines (high temperatures, great centrifugal forces and highly corrosive environment), making them very attractive for the production of turbine discs. Furthermore, theses alloys maintain their properties even at high temperatures [9, 10].

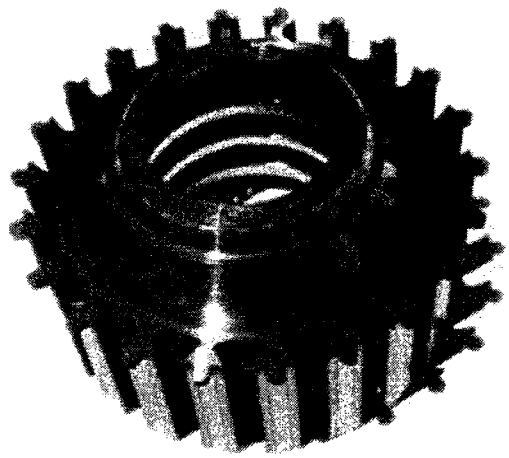

Figure 1.2 – Turbine disc [11].

These turbine discs are produced by powder metallurgy and their very specific characteristics are related to their microstructure, composed of two different phases: an γ phase and a hardening γ' phase [9-10, 12]. The γ' phase is responsible for some of the interesting mechanical properties of nickel-based superalloys, but it also accounts for the

difficulty of machining these materials [13, 14]. Nickel alloys are considered to be "hard-to-machine" materials.

Today, several machining techniques exist to shape these alloys but, some difficulties can appear. Powder metallurgy allows for a gross shaping of the workpiece, followed by machining to attain the required dimensions and surface finish. In this work, the effects of two machining techniques employed in the aerospace industry, namely broaching and electrical discharge machining (EDM), on the bulk material's surface are assessed. A third technique (low-stress grinding) is also studied as a guiding thread between broaching and EDM as it provides reference values of the hardness and Young's modulus. While considering the effect of machining on the workpiece, one should understand that on a small scale, machining can only have an influence on the properties (mechanical, chemical and structural) of the near-surface region justifying the approach we apply in this work.

Some very specific and small geometries machined on turbine discs (turbine blades fixings known as tree roots fixings) require special machining techniques. Broaching is a good solution because, a well shaped tool (called a broach), allows one to produce complex shapes such as tree root fixings in one cut [15, 16]. If adapted to actual production standards, broaching is not without serious limitations. Employing a cutting tool to produce defect-free workpieces involves very stringent monitoring of manufacturing conditions. If any wear on the cutting edges of the broach is detected, a long process of sharpening results in an increase of the production time and therefore of the cost. Also, broaching is a relatively "violent" machining technique in which the tool is moved by force into the workpiece resulting in serious plastic deformation causing alterations of the near surface region in certain conditions [16].

Therefore, in the past decades, major efforts have been made to develop a new technique that will enable one to machine small and complex geometries on hard-to-machine materials without the drawbacks of broaching. As it does not operate by metal cutting but by melting of the machined material, EDM is a very promising alternative [17]. No contact between the tool and the workpiece's surface is needed, thus reducing

the tool's pressure on the machined material when compared to broaching. However, the melting of the material inevitably means a change in its microstructure, possibly leading to negative effects to the parts properties.

Even if they are efficient for shaping hard-to-machine materials, such as nickel-based superalloys, both broaching and EDM present a very serious problem. In certain "violent" machining conditions they can lead to the formation of a surface layer on the workpiece. This layer is known as the "white layer" (WL) or "white etching layer" (WEL) because it is resistant to etching and appears white under optical microscopy [18-20]. The phenomenon has been reported in many studies and on many different materials [18-25]. WEL formation is a phase transformation which happens when sufficient energy is brought to the material's surface during machining operations. This energy can be transferred by a thermal process, a plastic strain or a combination of both [18]. Therefore, this WEL is not confined to the machining workshops and some reports have also mentioned the formation of WEL on railroad tracks [26] and wires [21].

The WEL typically exhibits different mechanical properties from those of the bulk material [18-20, 22-25]. When producing "defect-free" workpieces, it is necessary to determine the exact mechanical properties and microstructure of this white layer to ensure that it does not have an influence on the fatigue life of the workpiece. That is why, in this thesis, we focus on the mechanical properties of the WEL produced during the machining of tree roots fixings by broaching and EDM on Inconel 100 turbine discs and on the near surface region of the samples studied, in order to evaluate the effect of the machining technique on the surface of the workpiece.

1.1 OBJECTIVES

The objective of this thesis is to advance the state of knowledge on WEL produced on Inconel IN100 nickel-based superalloy by different machining processes (broaching and EDM), and more specifically on the materials mechanical properties. The following aspects represent specific objectives of this work:

- To develop a methodology for the mechanical characterization of the WEL.
- To establish a relation between the elasto-plastic properties, the microstructure of the WEL, and the characteristics of the machining process.
- To evaluate the impact of cyclic stresses (fatigue tests) on the microstructure and other properties of the WEL.

1.2 ORGANIZATION OF THE THESIS

The thesis is divided into five chapters. After this introduction, Chapter 2 provides a review of the studies already published on stainless steel and on nickel-based superalloys, their properties, and machining techniques. In Chapter 3, we describe the samples studied and the experimental techniques used during this project. A brief description of the systems and models used to characterize the mechanical and microstructural properties of the studied WEL are also provided. In Chapter 4, we describe the results obtained by nanoindentation on the studied WEL, and we then correlate them to their microstructure. Finally, in Chapter 5, we conclude and present further considerations, which may improve our knowledge of the WEL, in the future.

CHAPTER 2 – LITERATURE REVIEW

Nickel-based superalloys are very interesting materials for jet engine applications in the aerospace industry where excellent mechanical properties and good corrosion resistance at high temperature are needed. However, these alloys are hard to machine leading to extra production costs. Some techniques, like high speed machining or high pressure lubrication, were developed to improve productivity. However, higher productivity means faster machining and therefore "hard machining" operations. Unfortunately, hard machining also leads to abusive machining conditions (above the machined material capabilities) that often promote the forming of a white etching layer (WEL) at the surface of the machined geometry. This WEL is a defect that has specific properties (mechanical, chemical, microstructural) and can modify the behavior of the workpiece in operation.

In the first two sections of this chapter we will focus on nickel-based superalloys (specifically Inconel IN100) and their machining and then, we will describe WEL formation mechanisms on steels and their typical properties.

2.1 NICKEL-BASED SUPERALLOYS

A superalloy is a metallic alloy which can be used at high temperatures (0,7 times the melting temperature), creep and oxidation resistance being the prime design criteria [27]. Developed initially to maintain their mechanical properties at high temperatures in a corrosive environment, nickel-based superalloys are widely used in the aerospace industry for the manufacturing of turboprop engines parts such as turbine discs or blades. Machining of aerospace components often implies a high rate of material removal [12, 27] making production time a major issue. Companies are always looking for improvement in this field. Some solutions (high speed machining, high pressure lubrication, coated tools, ...) were developed to shape these parts with traditional metal

cutting techniques (turning, broaching, ...). However, WEL formed at the surfaces of workpieces during hard machining processes lead to uncertainty with regards to the reliability of the component during normal operation cycles.

Nickel-based superalloys are formed by powder metallurgy. Powder metallurgy is a general term for all the sciences and production techniques by sintering, the process that allows the shaping of workpieces from powders of different sizes. During sintering, the powders are compressed into a mould having the shape of the desired part and then heated to just below the fusion point of at least one of the powders. While a high temperature, the grains weld together giving the part its cohesion and as there is no fusion of at least one type of particle, sintering allows for a very close control of the microstructure. Sintering is a good technique to preform nickel-based superalloy turbine discs before finishing by the machining of the tree root fixings (Figure 2.1).

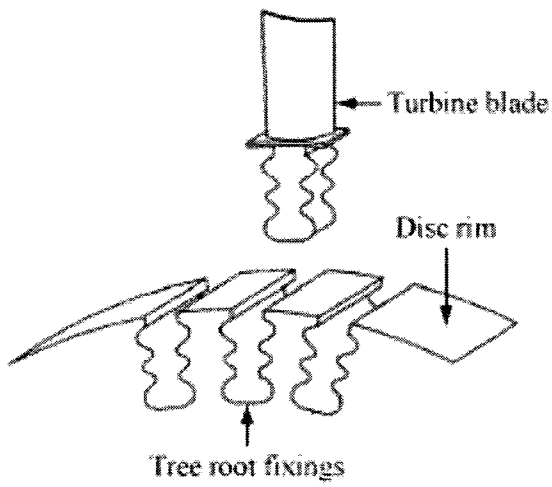

Figure 2.1 – Example of fixings on a turbine disc [15].

Nickel-based superalloys are composed of two different phases. Nickel is the base material and is referred to as the "γ phase" or "γ matrix". During sintering, nickel-based superalloys are precipitation hardened by metallic precipitates of the type $Ni_3(Al-Ti)$ named the "γ' phase" (Figure 2.2) and by carbides located at the grain boundaries. The sintering process is performed below the fusion point of precipitates. It has been shown

that the mechanical properties at high temperatures of nickel-based superalloys depend on the distribution, size and fraction of the γ' phase. The best properties are obtained when the percentage of the γ' phase reaches 55% [12, 27-29].

Most metals loose strength at high temperatures because the movement of dislocations is facilitated by thermal activation. In nickel-based superalloys, the slip of dislocations is blocked at high temperature by the $Ni_3(Al-Ti)$ precipitates. Above 600°C the thermal activation is sufficient to allow dislocations to move [27].

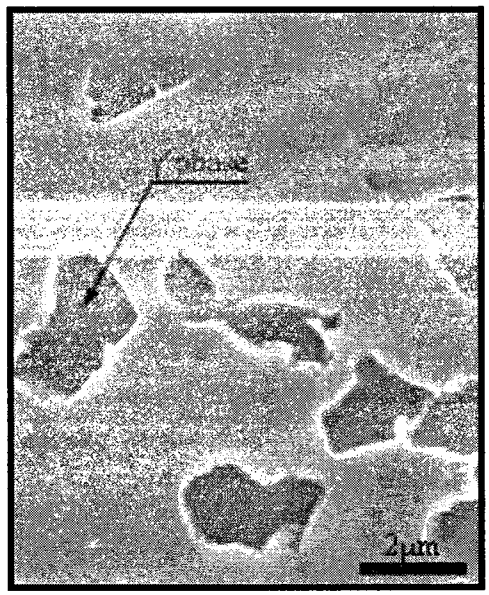

Figure 2.2 – Microstructure of IN100 nickel-based superalloy showing the γ' phase [30].

The oxidation resistance (to dry corrosion especially) of nickel-based superalloys is ensured by the large amounts of nickel in the material. The chemical composition of an IN100 superalloy used by Pratt & Whitney is given bellow.

Table 2.1 – Chemical composition [in wt%] of IN100 superalloy [30].

Ni	Al	Mo	Ti	V	Cr	Co	Zr	B	C
Base	5	3,2	4,3	0,8	12,4	18,5	0,07	0,02	0,07

2.2 MACHINING OF NICKEL-BASED SUPERALLOYS

Before continuing any further, it is necessary to describe in more detail some of the machining processes reported in the literature resulting in the formation of a WEL. We will focus on turning, milling, broaching, low-stress grinding (LSG) and electrical-discharge machining (EDM) as most references discussing the formation of a WEL involve one of these techniques. The first four are chip forming operations and are regrouped in section 2.2.1 of this chapter. EDM is considered to be an unconventional machining technique and is presented in section 2.2.2. WEL produced by chip forming techniques and by EDM are very different. Their formation mechanisms and mechanical properties differ completely. These differences will be highlighted in section 2.3 and in Chapter 4.

2.2.1 METAL CUTTING PROCESSES

"Metal cutting process" is a generic term for every action in which metal workpieces are shaped by a cutting tool. Machining processes have a great influence on both the microstructure and the mechanical properties of the formed white layer [31]. The parameters involved are, the contact length between the tool and the workpiece, the contact time between the tool and the workpiece, the contact induced stress, the residual stresses penetration and the machining conditions.

Turning, milling, broaching and LSG are machining processes in which material is removed from the workpiece using a cutting tool. What differs between these four techniques is the geometry of the employed tool, the relative movements between the

cutting tool and the workpiece and the resulting part geometry that can be obtained from the machining operation.

The list of machining techniques employing a cutting tool presented above is not exhaustive. In fact, many other techniques exist (drilling, reaming, tapping, threading, ...) but won't be discussed in this work.

2.2.1.1 TURNING [32, 33]

In turning, a cutting tool is fed into a rotating workpiece which is turned around its axis at a speed noted N, expressed in rev/min. This movement of the workpiece is called the cutting motion. The tool is led by a movement of translation called the feed motion (noted f and expressed in mm/min) permitting the shaping of the workpiece. The combination of these two motions, as well as the shape of the cutting edge of the tool, allows the machining of surfaces that are concentric with the workpiece's axis of rotation (Figure 2.3). Turning operations are therefore well suited for the machining of cylindrical parts such as shafts, casings, etc...

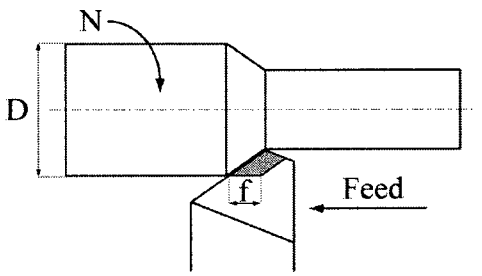

Figure 2.3 – Principle of turning.

Turning operations are accomplished on lathes: one of the oldest conventional machine tools. The workpiece is typically mounted horizontally on a spindle but a vertical configuration can be used especially when machining large workpieces. During machining, the cutting speed V_c is given in m/min and it is selected to take into

consideration tool and workpiece materials, lubrication method, desired tool life and other machining parameters (feed rate, depth of cut, ...). It can be expressed by,

$$V_c = \pi \frac{N \cdot D}{1000} \tag{2.1}$$

where, D is the diameter in m of the workpiece to machine.

Numerous authors have reported the formation of WEL on steel during hard turning processes [19, 23, 24, 31, 34-37]. Hard turning refers to turning operations on hard metals in which the parts are finished using ceramic or polycrystalline tools. Hard turning is employed on materials such as high speed steels, hardened steels and hard irons. This process allows very fine finishing and tolerances but requires very stiff tool holders and machines. Hard turning can be used in place of grinding.

2.2.1.2 MILLING [32, 33]

In milling, metal is removed by a rotating tool. The tool is given a rotating motion around its axis (cutting motion) while the workpiece is fed into the tool (feed motion). Milling tools have more than one cutting edge but several which are distributed regularly around the tool holder. The number of cutting edges is set depending on materials in contact (workpiece and tool), dimensions of the workpiece, vibrations, surface roughness, power of the machine tool, feed per tooth and the obligation to maintain at least two teeth in the workpiece at all time (to avoid impacting cutting edges on the workpiece). The space between two successive edges is called the pitch. A high pitch is synonymous with less teeth on the tool, thus meaning more space in order to accumulate chips produced during the cutting process and to evacuate them out of the machining zone. A high pitch is employed during preform operations and when vibrations are to be avoided. On the other hand, a reduced pitch will result in a higher number of teeth on the tool, thus reducing the available space to move chips out of the machining zone.

Milling operations are divided in two categories: face (or end) milling and peripheral milling (Figure 2.4). Face milling generates a surface normal to the axis of rotation of the tool while peripheral milling generates a surface parallel to the axis of rotation.

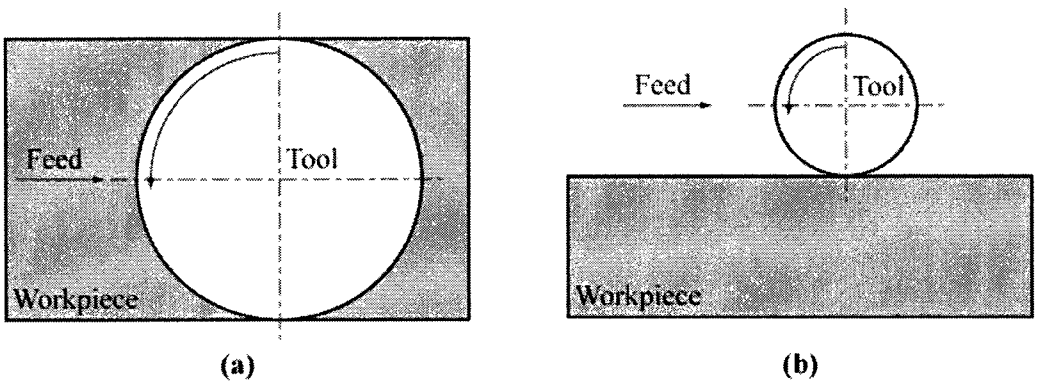

Figure 2.4 – (a) Face milling, (b) peripheral milling.

Milling operations are further separated into conventional and down milling. In conventional milling, the feed motion of the workpiece is in opposite direction than the tool rotation direction while in down milling these two motions are in the same direction (Figure 2.5). In conventional milling, cutting forces have a tendency to lift the workpiece from its worktable. Therefore, special attention during the design of the machining fixture is required. In down milling, however, cutting forces are reduced and firmly maintain the workpiece on the table surface.

As the workpiece is not rotating during milling operations, this technique is adapted to the machining of large prismatic workpieces like the spars of commercial airplanes with lengths of up to several dozens of meters.

Several authors have reported the formation of WEL during milling operations [38-42].

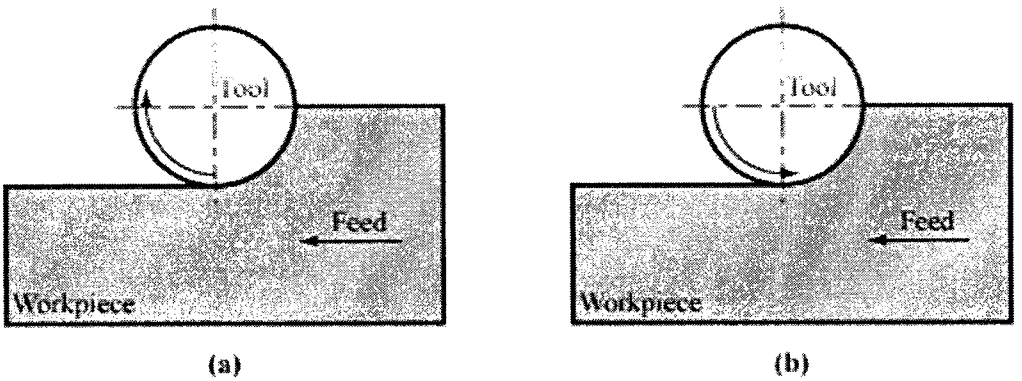

Figure 2.5 – (a) Down milling, (b) conventional milling.

2.2.1.3 BROACHING

Where turning and milling are used to machine cylindrical and prismatic workpieces, machining of complex profiles can be performed more easily by broaching. Also, broaching can lead to higher productivity for large series, by performing roughing and finishing cuts at the same time, thus producing precise geometries with low roughness. The term "broaching" appears for the first time in 1873 when Anson and Stephenson file a patent concerning a broaching machine. The first machine was built in 1898.

In broaching, the cutting tool (broach) is translated linearly across the workpiece [16, 32], and depending on the application, the tool can be either pulled or pushed. Broaching operations are divided in two categories: internal and external broaching (depending on whether machining is occurring on the inside or the outside of the workpiece). For each technique, vertical and horizontal broaching machines can be employed. Today, vertical broaching machines are almost always preferred except in the case of large workpieces but whatever the employed technique, broaching requires a prior hole in the workpiece to enable the installation of the tool.

The broach is composed of progressively taller and regularly spaced teeth mounted on a tool body (Figure 2.6). The space between two successive teeth serves to store the chips during machining.

In industry, broaching is commonly used to manufacture geometries difficult to machine by other processes such as splines or square keyways on gears and driveshafts. This technique is also widely employed in the aerospace industry to manufacture turbine disc tree root fixings (Figure 2.1) as the broach can be given the shape of the desired fixing leading to faster machining operations.

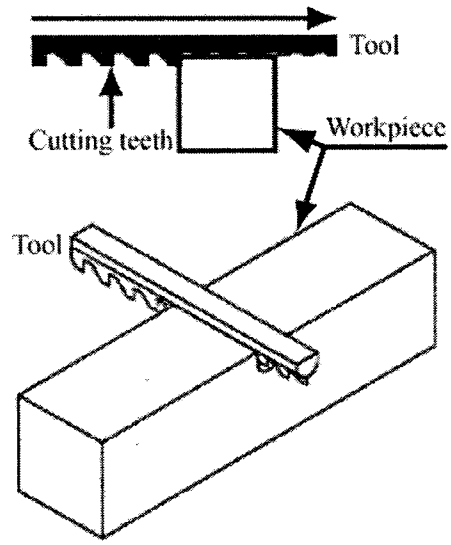

Figure 2.6 – Principle of broaching [16].

Broaching is similar to turning and milling in that metal cutting is obtained by generating a sufficient shear stress to remove metal chips from the workpiece. However, where in the other techniques a combination of two motions is necessary to achieve metal removal, only one is needed in broaching. As the tool moves linearly through the workpiece, both the cutting and feed motions are in the same direction. If well designed, a broaching tool can produce roughing, semi-finishing and finishing cuts in one stroke. Broaching can consequently be considered as a highly productive process. However, in some applications like jet engine parts, the need of defect-free components involves an inspection of all the tool's cutting edges after every stroke and if needed, the sharpening of some of the edges or the replacement of the complete broach by a new tool. All these

controls require the tool to be dismounted from the machine obliging the operator to set the tool back into position, introducing production delays.

2.2.1.4 GRINDING [32]

Grinding is a general term describing processes in which an abrasive surface is pressed against a workpiece, resulting in the removal of material from both the workpiece and the abrasive. Grinding is a common technique that can be employed to produce precise parts with fine surface finishes. Grinding can also be used to produce complex geometries. Low-stress grinding (LSG) is a type of grinding were machining parameters are set to ensure minimum stress generation within the near surface region of the machined workpiece. No WEL is usually formed during LSG but this technique is to slow to be employed on a production line.

The main difference between grinding and traditional chip forming techniques (turning, milling and broaching for example) is the type of cutting tool. It is composed of numerous abrasive and irregularly shaped grains, randomly spaced on a wheel surface. Because of this configuration, metal cutting in grinding takes place on a smaller scale than for all the other techniques already described in this section. The chip is also much thinner (2 to 50 μm) than in other traditional techniques where thicknesses of several millimeters can be achieved.

Numerous reports on the formation of a WEL on different netals by grinding have been published [20, 26, 43-46].

2.2.2 EDM

As previously mentioned, the wear of the tool is an issue of prime importance since it implies extra production costs. Therefore, over the past decades, major efforts have been devoted to developing a process that would allow machining of complex geometries

without the problems linked to the use of cutting tools. In some applications where metal cutting processes are very inconvenient, like the machining of superalloys, electrical-discharge machining (EDM) is a promising solution [17, 47] as it operates by fusion.

EDM is a process for eroding and removing metal from electrically conductive materials by the use of electric sparks. Although EDM was invented in the 1940's it was not accepted as a machining process until 1950. Today, the EDM industry continues to develop along with superalloys used in aircraft turbines and other hard to machine materials. If conductive, these materials are good candidates for EDM while other machining processes are expensive and/or complex [17,48].

EDM is a nontraditional machining method that involves series of electric arcing discharges between an electrode (the cutting tool) and the workpiece in the presence of a high electric field and inside a dielectric fluid. EDM does not require a direct contact between the tool and the workpiece reducing damage to the machined surface from excess tool pressure. The electrode can be given a specific shape for drilling EDM operations or can also be a wire (wire cut EDM). In wire cut EDM a metal wire (made of brass and zinc for example) is fed through the workpiece. This type of EDM allows for the realization of very precise machining [17].

During an EDM cycle, a spark is generated producing series of small craters on workpiece's surface by melting and vaporization of the machined material. Debris from the crater are continuously flushed away by the dielectric. This fluid has a double role, first it insures a good electrical conduction between the electrode and the machined material and second it carries the removed metal particles out of the path of the electrode after each spark [17].

In EDM, every spark generates heat that locally melts and sometimes evaporates the machined material. All the evaporated and some of the melted material is quenched and flushed by the dielectric. The remaining melted material recasts on the surface in the form of a WEL. In addition, on the surface of the workpiece, a heat affected zone is formed due to the rapid heating and cooling during EDM cycles [17, 50]. Numerous reports on the formation of a WEL by EDM have been published [25, 47, 49-51].

2.2.3 MACHINING IMPROVEMENTS

The resistance of nickel-based superalloys to common cutting techniques comes mainly from four of their properties [52-54]:

- A high mechanical resistance, even at high cutting temperatures.
- A high percentage of hard γ' phase in nickel alloy leading to rapid wear of cutting tools.
- A poor thermal conductivity of superalloys preventing any conduction of the heat generated during machining into the workpiece leading to a rise of the cutting edge's temperature and a fast wear of the tool.
- An austenitic structure responsible for a strain hardening of the machined surfaces increasing cutting edge's wear at the next passage of the tool.

All these properties of nickel-based superalloys are responsible for a loss of productivity. Machining these alloys with conventional techniques implies to reduce cutting speeds by up to 90% [55].

In this section we present some ideas that were developed to increase the efficiency of the machining of the hard-to-machine materials. A major issue resides in the improvement of cutting speeds to reduce machining times and therefore machining costs.

A high cutting speed is defined as a cutting speed which leads to a rise of temperature of material's surface [32]. Therefore, the value of the cutting speed for which a machining process is said to be a high speed process depends on the properties of the machined material (Figure 2.7). It also depends on the machining process, the tool, the tool holder and the machine tool [56].

When increasing the cutting speed from conventional machining values, one will reach a range of speeds for which the wear of the tool will increase and the quality of the machined surface will decrease (to clarify the Figure 2.7 these zones were not represented). Once the high speed zone is reached, the machining conditions become

excellent (reduced wear of the tool, low vibrations and good surface quality). The low and high values of the cutting speeds defining these zones are set arbitrary [56, 57].

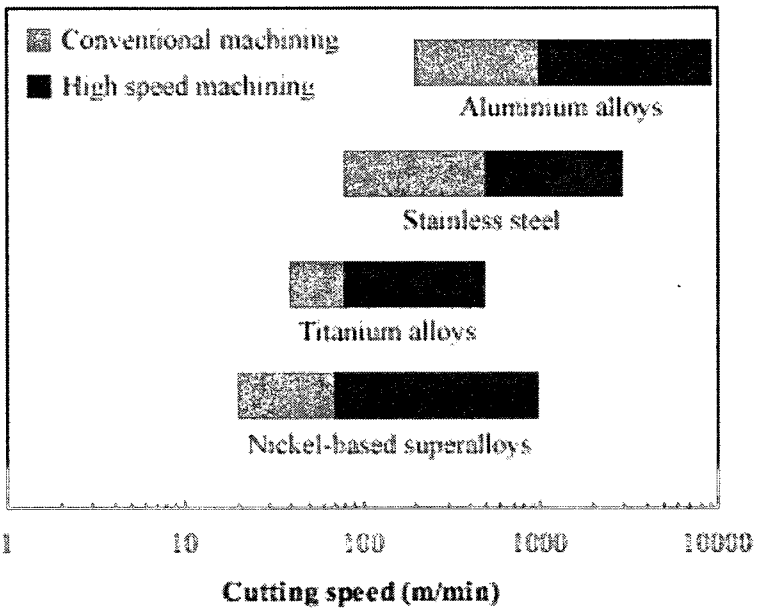

Figure 2.7 – Cutting speeds for different materials in conventional and high speed machining (turning and milling) [57].

In the case of nickel-based superalloy IN718, the cutting temperature is a function of cutting speed (Figure 2.8) [52, 58]. Common solutions to improve tool life during high speed machining include:

- The use of a high pressure lubrication system [53].
- The coating of the cutting edge of the tool with suitable materials designed to resist high temperature, oxidation and friction [32]. Figure 2.9 presents a comparison of cutting speeds that can be reached with coated and uncoated tools.
- The use of unconventional machining techniques like EDM where no contact between the cutting tool and the workpiece is needed.

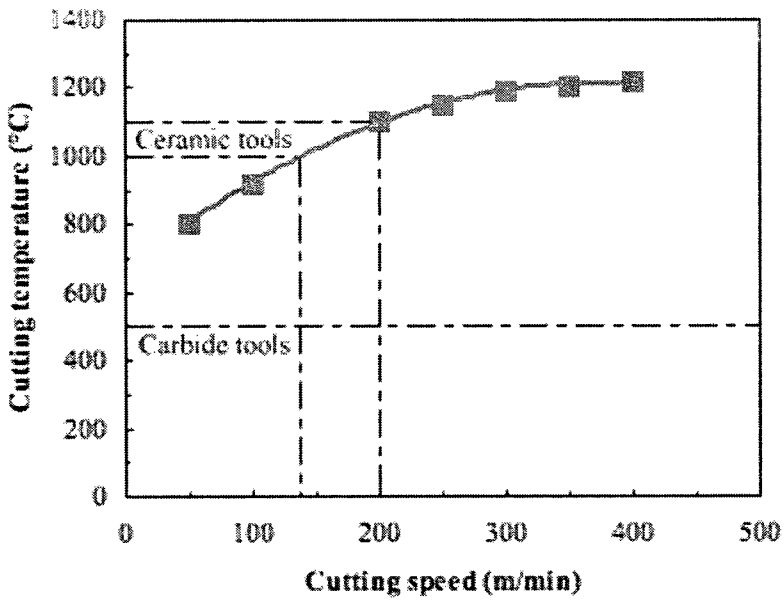

Figure 2.8 – Cutting temperature of IN718 as a function of the cutting speed [57].

For the machining techniques described previously, several machining parameters have a direct impact on the formation of a WEL. These parameters are [59]:

- In turning: the cutting speed, the feed speed, the shape of the cutting edge of the tool and the cooling technique.
- In milling: the cutting speed, the feed speed, the number of teeth of the tool engaged at a time in the workpiece, the shape of the tool and the cooling technique.
- In broaching: the rake angle (angle, in a diametrical plane, formed by the face of the tool and a radial line from the cutting edge [32]), the cutting speed, the chip load and the shape of the cutting edges.
- In EDM: the peak current, the pulse-on duration, the electrode material, the type of dielectric.

All these parameters have important effects on both the mechanical and microstructural properties of the resulting WEL as we will see further in Chapter 4. In the

following section of this chapter we discuss the formation mechanisms and the properties of the white layers.

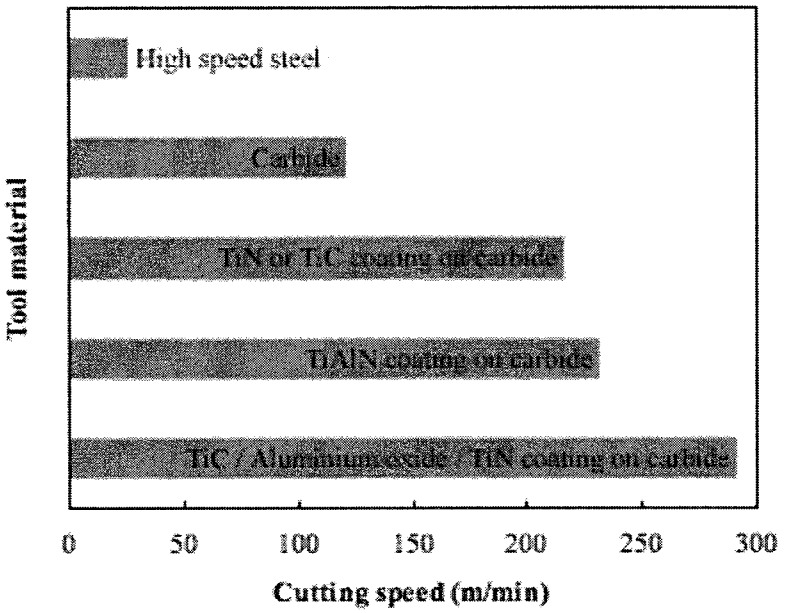

Figure 2.9 – Comparison of cutting speeds for coated and uncoated tools [32].

2.3 WHITE ETCHING LAYERS (WEL)

WEL are hard compounds that can be formed at the surface of machined metallic materials when the machining process is too aggressive meaning that it induces high temperatures or strains at the surface of the workpiece. They are named thus because of their appearance under optical microscopy after etching (Figure 2.10). WEL are resistant to etching and appear featureless under optical microscopy [18,19, 24, 34]. References to WEL in the literature can be found as early as 1912. Stead seems to be the first to have identified the so-called WEL on steel wire ropes [21]. Since then, WEL have been observed in various situations and on a variety of ferrous and non-ferrous materials [18, 60, 61].

Because the lack of published work on WEL formed on nickel-based superalloy, we mainly discuss WEL formation on steel in this section. Further in the thesis we will investigate properties of WEL formed on a nickel-based superalloy (IN100) by broaching and EDM.

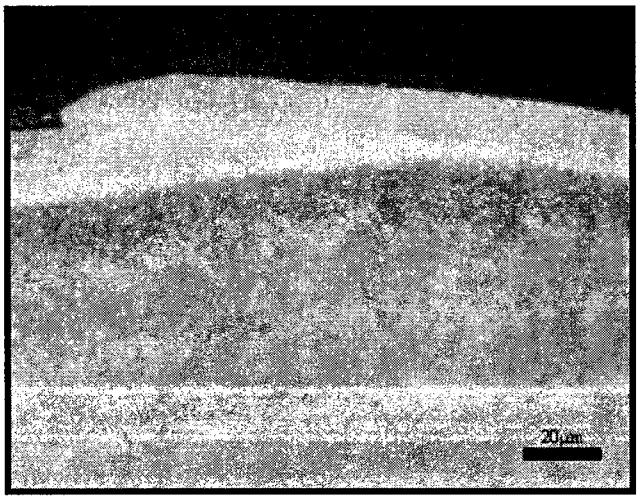

Figure 2.10 – Optical microscopy image of a WEL formed by EDM on steel [25].

2.3.1 WEL FORMATION MECHANISMS

It is commonly admitted that there are three main mechanisms responsible for the formation of WEL on steel [18]. These are:

- The thermal mechanism consisting of a rapid heating followed by quenching resulting in a phase transformation at the surface of the machined workpiece.
- The plastic flow mechanism producing a homogenous or a fine grain structure.
- The surface reaction mechanism whereby the surface is chemically modified by its surrounding environment.

These three mechanisms are promoted by high cutting speeds and tool wear [18-19, 23-24, 34-35, 62]. A high cutting speed creates high strains and is accountable for permanent deformation of the machined material. It also disrupts the evacuation of chips produced by metal cutting techniques from the Tool/Workpiece contact zone. Because a great part of the heat produced during machining is carried by chips, this phenomenon can lead to local overheating of both the tool and the workpiece. Tool wear can also locally increase the temperature near the Tool/Workpiece contact zone.

To these three main mechanisms should be added three other factors that have a demonstrated influence on the formation of WEL. These complementary factors are [18]:

- The cutting pressure of the tool onto the workpiece for conventional metal cutting techniques (turning, milling, broaching, grinding, ...).
- The strain rate induced by the cutting tool in metal cutting techniques.
- The quench rate of the surface of the workpiece after the passage of the tool.

In machining, the formation of WEL is a result of the presence of both high temperature and important deformation. In some cases only one of these mechanisms plays a role in the formation process. In turning, milling and broaching, the formation mechanisms of WEL are the same. The main difference lying in the relative importance of the heating and of the plastic deformation for each machining technique. This difference is expressed by the following relation,

$$\left(\frac{Heating}{Deformation}\right)_{Turning\,/\,Milling} > \left(\frac{Heating}{Deformation}\right)_{Broaching} \tag{2.2}$$

illustrating the predominance of the thermal mechanism in turning and milling, while in broaching, WEL are formed by the combined actions of severe plastic deformation and heating on the near surface region of the workpiece [59].

On nickel-based superalloys, the formation mechanism involves a very high deformation of both the γ matrix and the γ' phase. The energy produced by this deformation induces the homogenization of these two phases. In fact, when the

deformation is not fully achieved, residual deformed γ' could still be observed in the WEL [59].

The strain rate also plays a role in the transformation of the base material. The successive teeth of the broach cause severe deformations and friction leading to a microstructural modification of the plastically and thermally affected zone. It was shown [63] that deformation mechanisms alone cannot cause the formation of WEL without being combined with the effect of heat treatment of the surface. In addition to the WEL, broaching produces a sub-surface zone of highly deformed material called the deformed layer (DL) which is located between the WEL and the bulk material. The amount of deformation and the thickness of the DL depend on the strain rate produced by the broach. DL on nickel-based superalloys can be identified under optical microscopy (Figure 2.11) by identifying the deformed γ' phase inclusions in the near surface region, these are generally deformed in the direction of the machining. The DL is always present in broaching processes and the severity of the deformation depends on the harshness of the machining process [15-16].

It is important to point out the differences between the formation mechanisms of WEL produced by traditional machining and by EDM. WEL produced by EDM (Figure 2.12) are recast layers where a small portion of material is melted after each spark and then rapidly quenched by the dielectric. These rapid variations of temperature cause phase transformations in the machined material [25, 47, 49-50]. Therefore, the thermal mechanism is the only one involved in the formation of WEL during EDM processes and no deformation process occurs. Because EDM operates by fusion, the near surface region of the machined material is thermally affected by the machining process even if it does not melt. The microstructure and the properties of this affected portion of the material are different from those of the bulk and of the WEL. The thermally affected zone is visible on Figure 2.12. The thickness of the WEL and of the heat affected zone depend notably on the heat produced during machining [49].

WEL produced by EDM can be found all along the machined surface as the heat produced by the machining process is continuous throughout the cutting process. The

thickness of the WEL varies with the pulse current (Figure 2.12) and "liquid drop" patterns can be observed at the surface of the machined material. It was found that the thickness of WEL produced on steel by EDM is a function of the pulse-on duration of the process. Also, an increase of the pulse current causes a greater variation in the thickness of the WEL [47].

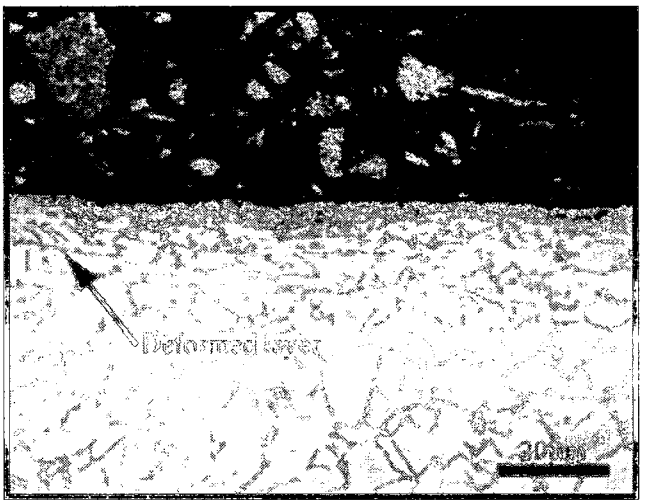

Figure 2.11 – Optical microscopy image of IN718 machined by broaching showing the presence of a DL [15].

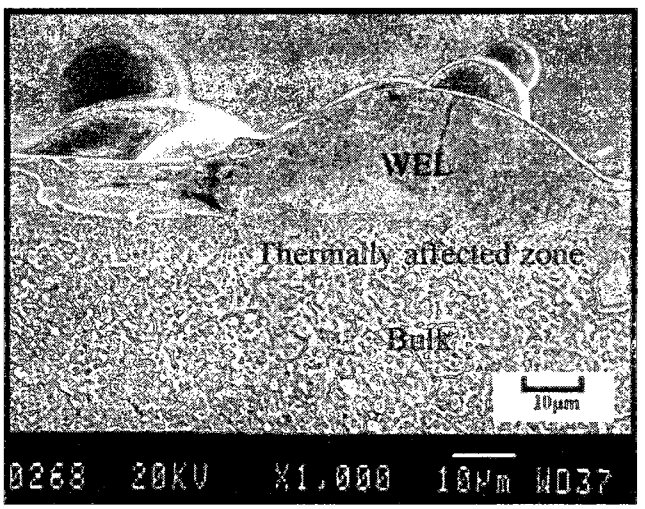

Figure 2.12 – WEL formed on steel by EDM [47].

2.3.2 WEL PROPERTIES

Properties of WEL (mechanical properties, surface structure, microstructure, ...) are closely related to those of the bulk material. The literature shows a great variety of WEL structures formed in very different situations (machining, service operation, ...). Therefore, there are as many WEL as there are formation situations [64, 65]. However, it was found that very fine grain structure is a common characteristic of WEL formed on different materials [18]. As it would be too exhaustive to describe all the situations where the formation of a WEL was reported we will only address WEL formed during machining operations on steel.

WEL formed on different types of steels appear featureless under optical microscopy as it is etching resistant. However, studies found that they have a polycrystalline [34] or even nanocrystalline [19, 35] structure, with grain sizes in the order of 10 nm but being a function of the cutting speed [35]. A study on WEL formed on steel by grinding showed that this type of WEL is the only WEL that can be etched and revealed clear microstructures [24].

WEL that form on steel are composed of untempered Martensite and Austenite phases. Austenite is a solid solution of carbon in iron and Martensite is a metastable, hard and brittle phase resulting from the transformation without diffusion of carbon into the Austenite. The exact proportion of Martensite and Austenite in WEL has been subject to controversy between scientists [18,19, 23, 34]. This type of mixed structure could explain why some studies found that such WEL are characterized by an increased hardness [18-20, 31, 34, 36]. Namely, the hardness values reported for WEL on steel are $10-14$ GPa while the bulk hardness of the material is $5-10$ GPa. This difference of hardness is explained by the presence of hard particles embedded in the softer matrix. If the hardness of a WEL is higher than that of the bulk, the Young's modulus behaves oppositely with lower values for the WEL when compared to those of the bulk material [19-20, 31, 34, 36]. Thicknesses reported are between several microns to several dozens of microns [19, 31, 34-36].

On turned steels, formation of a WEL is accompanied by the formation of a dark layer (named after its color under optical microscopy) [31, 36]. This dark layer is located between the WEL (Figure 2.13) and the bulk material. It is softer than the WEL [31] because of its composition of overtempered Martensite [18, 19]. Thicknesses of the dark layer are close to those of the WEL. The thickness ratio of dark to WEL changes with the machining parameters and the material.

WEL formation on steels by turning is facilitated by high cutting speeds ($V_c \geq 100$ m/min) and tool wear, these two factors being responsible for a rise of temperature in the contact zone between the tool and the workpiece. This rise of temperature leads to the austenisation of the near surface layers of the machined material.

Steels machined by grinding present WEL having different properties from those of steels machined by turning. A turned WEL is more strained. Also, the ratio of dark to WEL thickness is larger for a ground surface than for a turned one. Finally the percentage of retained Austenite in the WEL is lower by $10-12\%$ in the case of grinding.

In EDM, WEL were found to be twice as hard as the bulk material with a higher elasticity [50]. As a consequence of the rapid quenching process, WEL formed by EDM frequently present cracks that come from a difference of volume of the martensitic and austenitic phases existing in the layer.

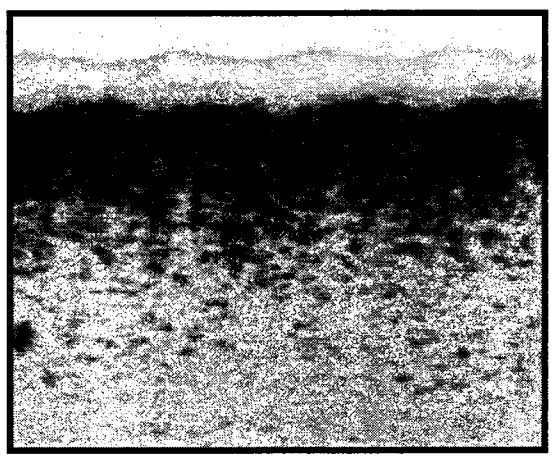

Figure 2.13 – Optical microscopy image of a WEL formed by turning on steel showing the WEL, the dark layer and the bulk material [19].

CHAPTER 3 – EXPERIMENTAL METHODOLOGY

In this section we expose the characteristics of the studied samples and the characterization techniques employed to determine their mechanical and microstructural properties.

3.1 MATERIALS

As part of a collaborative project, the Functional Coatings and Surface Engineering Laboratory at the École Polytechnique de Montréal received nickel based superalloy samples from Pratt and Whitney Canada. These samples were machined using three different techniques with undisclosed sets of machining parameters: electrical-discharge machining (EDM), broaching and low-stress grinding (LSG). EDM and broaching formed a white layer with different properties than those of the bulk material. This white layer is thin and can be scattered or continuous but has different mechanical and microstructural properties from those of the nickel alloy. The studied samples are divided into three groups:

- Group #1, samples machined by EDM.
- Group #2, samples machined by broaching.
- Group #3, reference samples machined by LSG.

In the rest of this work, the undisclosed sets of machining parameters are referred as "A" and "B" for samples of group #1, "C", "D" and "E" for samples of group #2 and "Ref" for samples of group #3.

Following their machining, some samples have undergone low cycle fatigue testing performed on a hydraulic servoactuator in air, at high temperature (650 °C). The load was varied to expose the samples to cyclic tensile stresses. Fatigue tests are of prime

importance in the aerospace industry (especially for "defect free" parts like turbine discs) because they simulate the behavior of the material during its lifecycle. The tests were set to reproduce the most extreme operating conditions of the alloy during normal operation of a turboprop engine (cyclic mechanical solicitation, temperature of operation and corrosive environment).

Prior to fatigue testing, two samples (one machined by EDM and one machined by broaching) were shot peened, a commonly used technique in the aerospace industry. By impacting the workpiece's surface with balls (made of ceramic or steel), shot peening produces a compressive residual stress layer at the surface of metallic parts. Therefore, this technique is very efficient in reducing the speed of crack propagation during normal operation. Shot peening produces a series of successive plastic deformations and thus, modifies the mechanical properties and surface roughness of the peened samples. Effects of fatigue testing and shot peening on the mechanical properties of the studied samples are investigated in Chapter 4 of this work.

Machining processes, sets of machining parameters and fatigue test conditions are given in Tables 3.1, 3.2 and 3.3. In Table 3.1, "EDM-F" and "EDM-R" stand for "EDM-Finishing" and "EDM-Roughing".

Table 3.1 – Samples machined by EDM (group #1).

Sample	Machining parameters	Fatigue test	Shot peening	Fatigue behavior
EDM-F	A	No	-	-
EDM #35	B	No	-	-
EDM-R	B	No	-	-
J7	A	Yes	No	Good
H7	A	Yes	No	Poor
H11	A	Yes	Yes	Very good
H14	B	Yes	No	Poor

Table 3.2 – Samples machined by broaching (group #2).

Sample	Machining parameters	Fatigue test	Shot peening	Fatigue behavior
Broaching #2	C	No	-	-
Broaching #4	D	No	-	-
Broaching #41	D	No	-	-
Broaching #X2	E	No	-	-
H18	C	Yes	No	Good
J5	C	Yes	No	Poor
H22	C	Yes	Yes	Good

Table 3.3 – Samples machined by LSG (group #3).

Sample	Machining parameters	Fatigue test	Shot peening	Fatigue behavior
REF	Ref	No	-	-
H3	Ref	Yes	No	Excellent

3.2 DEPTH SENSING INDENTATION

On each sample we performed depth sensing indentation (commonly referred to as nanoindentation) cross-section profiles from the surface down to the bulk. Most of these indentations were made in the white etching layer (WEL). Furthermore, in order to maximize the accuracy of our measurements and to demonstrate the homogeneity of the WEL we performed additional measurements in a different region of the WEL on selected samples. Finally, we performed indentations in the bulk far from the White layer/Bulk material interface to obtain reliable values of the hardness and reduced Young's modulus of the bulk material. These measurements were performed to demonstrate the influence of the machining processes on the mechanical properties of the bulk material.

For very thin WEL (samples EDM-F, H7, J7, H11, Broaching #2 and H18), the indentations were performed along the edge of the sample as there was no room for a cross-section measurement. For all other samples, cross-section measurements were performed. We maintained a spacing of three times the size of an indentation between two successive indentations sites in order to reduce the impact of subsurface plastic deformation [66] on neighbouring indentation measurements.

In the bulk material, the spacing between two successive indentations varied as a function of the distance to the WEL interface. In the near-surface regions, the spacing was set lower than 5 μm to evaluate with precision the impact of the machining process on the material. Further in the bulk material, the spacing was set over 5 μm.

On all the studied samples, the γ' phase have been removed from the sample surfaces during polishing leaving holes in the γ matrix. Thus, it has been impossible to assess the mechanical properties of this phase. The presence of holes resulting from the existence of the γ' phase in the bulk material (and in the WEL for Broaching #4 sample) forced us to change the spacing between our indentations in order to avoid tip sliding in the voids left by the removed γ' phase.

To determine the ideal indentation force, we performed several indentations at various loads (from 3000 μN to 6000 μN) on a WEL sample. After imaging the surface of the indented WEL we selected the force giving indentation marks sufficiently large to be easily observed by imagery but sufficiently small not to exceed the size of the thinnest WEL. Finally, the indentation force was set to 5000 μN.

From the indentation experiments, nanohardness H_{IT} and reduced Young's modulus E_r were determined using a Hysitron Triboindenter equipped with a Berkovich three-sided pyramidal tip with a total included angle of 142,35° (from one edge to the opposite side) in agreement with ISO standards. The aspect ratio of the tip is 1 : 8 and the radius of curvature is in the order of 150 nm [66, 67]. The test procedure involves a continuous monitoring of the load and of the indenter's position during loading and unloading cycles. The hardness is defined as the resistance to plastic deformation of a given material and the Young's modulus (E_{IT}) as the elastic constant linking the stress and the deformation for a homogenous and isotropic material.

The reduced Young's modulus (E_r) was first introduced to take into account the effects of non-rigid indenters on the Load/Displacement behavior of materials. In opposition to the Young's modulus of a material, the mechanical properties of the indenter are not needed to measure the reduced Young's modulus, facilitating the experimental work [67]. Both E_{IT} and E_r are related by the following equation:

$$\frac{1}{E_r} = \frac{1-\nu_S^2}{E_{IT}} + \frac{1-\nu_i^2}{E_i} \tag{3.1}$$

or,

$$E_{IT} = \frac{E_r.E_i\left(1-\nu_S^2\right)}{E_i - E_r\left(1-\nu_i^2\right)} \tag{3.2}$$

where, E_{IT} and E_i are respectively the indentation Young's modulus and the Young's modulus of the indenter expressed in GPa and ν_S and ν_i are respectively the Poisson ratios of the sample and of the indenter.

For a diamond indenter, $E_i = 1140$ GPa and $\nu_i = 0{,}07$ [68]. For the studied WEL, we assumed the Poisson ratio ν_S to be identical to the one of the bulk material. This assumption was made because measuring the Poisson ratio of WEL is very difficult. Also, we made the hypothesis that the Poisson ratios of the WEL and the bulk material should be sufficiently close not to influence our results [59]. For example, a reduced Young's modulus of 175 GPa gives Young's modulus of 194 and 188 GPa for Poisson ratios values of 0,25 and 0,3 respectively.

The value we used in our calculations was determined by Pratt & Whitney Canada by acoustic microscopy. This technique is based on the fact that the velocity of an acoustic wave traveling through a material is related to some of its elastic parameters such as the Young's modulus and Poisson ratio [69]. The measured value was found to be:

$$\nu_S = 0{,}2985 \text{ [59]}. \tag{3.3}$$

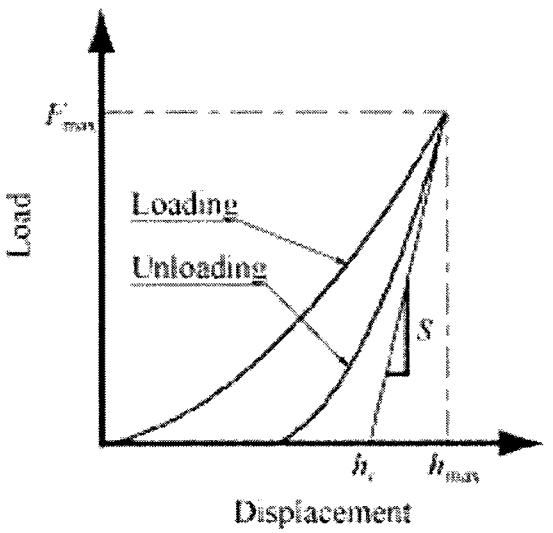

Figure 3.1 – Typical Load/Displacement curve [67].

The data was then processed using the Load/Displacement plots while correcting for thermal drift and hardware constants (frame compliance, transducer spring force and electrostatic force constants). Applying the Oliver and Pharr method [67], the

Load/Displacement plots were analyzed by fitting a power law relationship to the unloading curve:

$$F = A\left(h - h_f\right)^m \tag{3.4}$$

where, F is the indentation force in μm, h is the total displacement of the tip in nm and A, h_f and m are constants determined by a least squares fitting method expressed respectively in μN/nm^2 and nm, m is a dimensionless quantity.

The derivative of Equation 3.4 with respect to h is evaluated at the maximum load to determine the initial unloading stiffness S:

$$S = \frac{dF}{dh} \tag{3.5}$$

contact depth h_c is then calculated from,

$$h_c = h_{\max} - 0{,}75\frac{F_{\max}}{S} \tag{3.6}$$

where, h_c is the contact depth in nm, $h_{\max}$ is the maximum indentation depth nm, $F_{\max}$ is the maximum test force in μN, and S is the initial unloading contact stiffness in μN/nm.

Then, the hardness and the reduced Young's modulus are found by using Equations 3.7 and 3.8,

$$H_{IT} = \frac{F_{\max}}{A(h_c)} \tag{3.7}$$

$$E_r = S\frac{\sqrt{\pi}}{2\sqrt{A(h_c)}}. \tag{3.8}$$

Here, H_{IT} is the indentation hardness in GPa, $A(h_c)$ is the projected contact area at peak load in nm^2 and E_r is the reduced Young's modulus in GPa.

The projected contact area $A(h)$ is calculated from the area function of the tip that gives $A(h)$ evolution as a function of the contact depth of the tip h_c. The area function is set during the calibration process by performing series of indentation in a material of known reduced Young's modulus. In this study, calibration indentations were performed in quartz (E_r = 69,6 GPa).

3.3 SCANNING PROBE MICROSCOPY (SPM)

Because of the relative thinness of the studied white layers ($\tau \leq 20\mu m$ for most samples) we had to use AFM-like imagery to position the indenter properly over the samples and obtain reliable images of the studied regions. This imagery was done using the integrated scanning device of the Hysitron triboindentation system.

This AFM-like imaging is achieved by scanning a sharp tip, in a raster scan pattern, across the sample's surface and following the topography with a very high resolution. On our system, the positioning of the tip is controlled by a three-axis piezo positionner. Four main parameters are controlled while scanning the sample. These parameters are:

- The scan size which is also the image size.
- The tip velocity above sample's surface. A slow velocity will give the tip time to follow precisely the topography of the sample but will also substantially raise the measurement time. A high velocity will shorten the measurements but may lead to loss of contact between tip and the surface. In practice we used low velocities to obtain very precise images before and after indenting the samples and higher ones while performing the cross-sections.
- The setpoint is the amount of force applied by the tip to the sample during imaging. If the setpoint is to low then the tip may loose contact with the surface after meeting a sudden elevation or hole. However, too much force may damage the surface and reduce the time response of the tip to vertical solicitations.
- The integral gain which is a function of the vertical speed of the tip, determines how fast the tip reacts to changes in elevation of the sample. If the integral gain is set to high values, the tip may oscillate. On the other hand, a low gain may prevent the tip to react quickly enough to changes in the sample and wear may occur.

A good compromise between these parameters is to be found to ensure a good quality image. The surface roughness of the sample and the wear of the scanning tip are the main

factors influencing these parameters. During our study the parameters were set to the following values:

- Tip velocity: between 2 and 120 μm/s.
- Setpoint: between 2,0 and 2,5 μN.
- Integral gain: between 300 and 1000.

The tip used for this AFM-like imaging is a Berkovich tip as described previously. It is calibrated with a fused quartz sample of known reduced Young's modulus. After imaging a region of interest, indentations were performed perpendicularly to the Epoxy/Sample interface from the epoxy to the bulk and another image of the surface was made to locate the indentations on the studied region.

3.4 SCHEMATIC REPRESENTATION OF THE SAMPLES

The schematic representations of the samples are in Appendix 1. Samples are grouped according to the machining process. On each illustration, the investigated zones are represented by circles of different color (red for indentations in the bulk, blue for indentations made only in the white layer and yellow for indentations performed along the cross section of the sample). The illustrations are not to scale, but approximate distances between each indented zones are given. The studied zones are given numbers that are used in Chapter 4 and in other appendixes.

CHAPTER 4 – PROPERTIES OF WEL

In this chapter we present, describe and discuss the experimental results obtained for white etching layers (WEL) produced by different machining techniques (EDM and broaching) using multiple sets of machining parameters (refer to Chapter 3 for details on the samples).

4.1 EXPERIMENTAL RESULTS

4.1.1 SAMPLES MACHINED BY LSG (REFERENCE SAMPLES)

As previously mentioned, low-stress grinding (LSG) is used in this work as a reference for the two other machining techniques, namely electrical-discharge machining (EDM) and broaching. LSG is considered a much "softer" machining technique than EDM or broaching which produce heat and plastically deformed zones near the machined surface. Therefore, LSG is used to evaluate the mechanical properties of IN100 after machining without formation of a white layer.

In this study, half of the samples have undergone a fatigue test, used to characterize the response of the material to its operating conditions (refer to chapter 3). Therefore, one sample machined by LSG has undergone a fatigue test to characterize the influence of fatigue on the mechanical properties of IN100 nickel-based superalloy.

The hardness and Young's modulus before fatigue testing of IN100 machined by LSG where provided by Pratt & Whitney Canada. The highest values of hardness were obtained close to the machined surfaces (Table 4.2). The values after the fatigue tests were obtained by nanoindentation. We performed two sets of indentations along the cross-section of sample H3 (Table 4.1) in two different zones. As the values measured during each set of indentations were very similar (Table 4.2) only those of the first set are

presented below. One can find the mean values obtained after each set of indentation in Table 4.2 and the detailed values in Appendix 2.

Table 4.1 – Indentation zones and number of indentations for sample H3.

Sample	Zones	Location of the indentation zones	Number of indentations
H3 (Ref)	#1	Nickel alloy (near surface)	15
	#2	Nickel alloy (bulk)	3
	#3	Nickel alloy (near surface)	11
	#4	Nickel alloy (bulk)	5

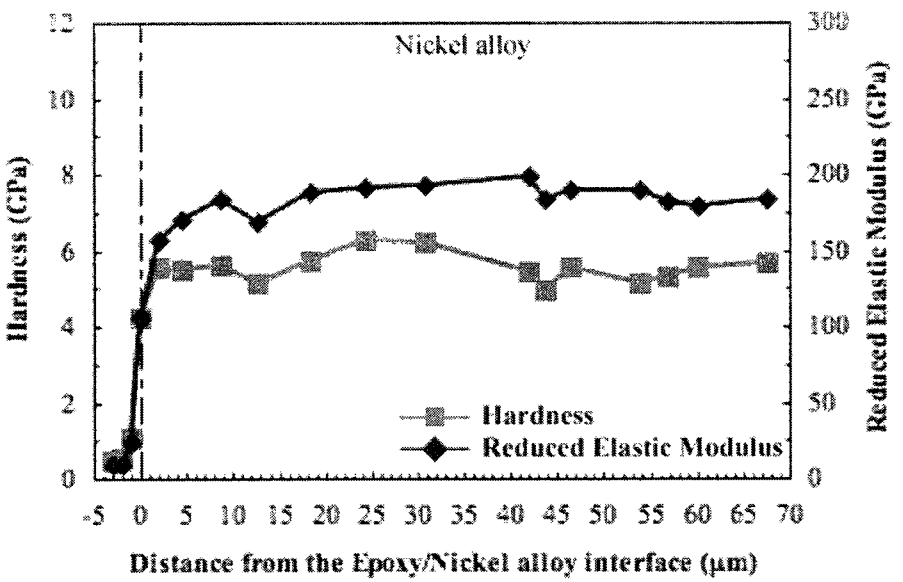

Figure 4.1 –Hardness and reduced Young's modulus as a function of the distance from the Epoxy/Nickel alloy interface for sample H3.

Three Load/Displacement curves obtained by nanoindentation and used to calculate the hardness and reduced Young's modulus of IN100 after fatigue testing are shown in Figure 4.2. Theses curves were obtained at different positions on sample H3 (Figure 4.3) and they document the uniformity of the material along its cross section. The uniformity of the mechanical properties is also clearly visible on Figure 4.1.

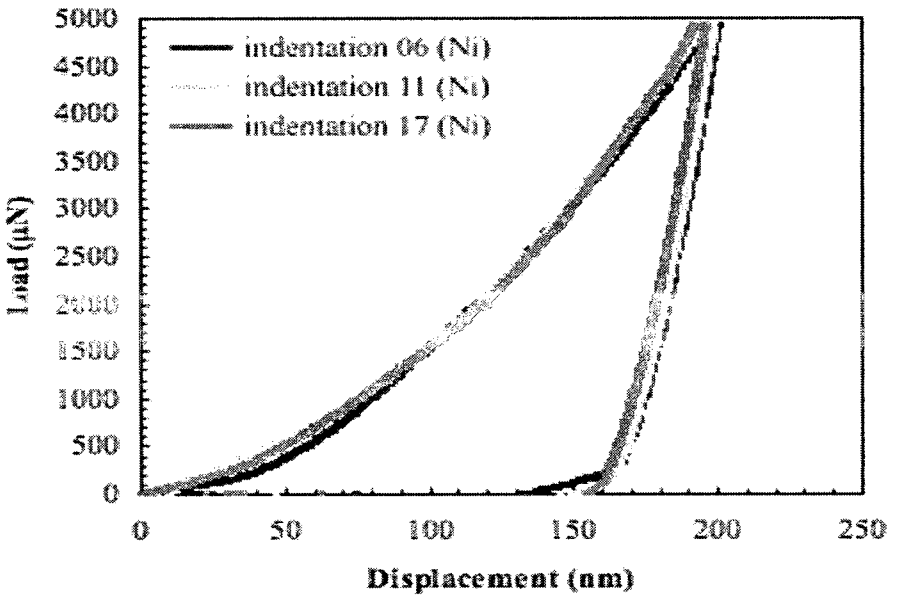

Figure 4.2 – Load/Displacement curves for sample H3 in the bulk.

An AFM image of the sample's surface is provided below (Figure 4.3) to show that the material was not deformed in the zone of indentation and that no WEL has formed at the surface of the sample. This picture also provides the localization of the indentations presented in Figure 4.2.

The results of this section are summarized in Table 4.2. All given values are average from the experimental values. The standard deviations are given in brackets. All theses values are considered to be reference values for the hardness and Young's modulus of IN100, before and after fatigue testing which will be described further in this chapter.

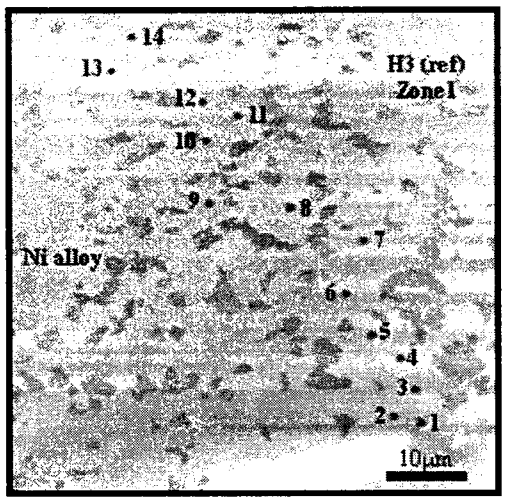

Figure 4.3 – Indentation positions with respect to the Epoxy/Ni alloy interface for sample H3.

Table 4.2 – Average hardness and Young's modulus of IN100 before and after fatigue testing.

Sample	H_{IT} (GPa)	E_r (GPa)	E_{IT} (GPa)	Number of indentations	Fatigue test
REF [60]	4,15 to 5	195	214	-	No
H3 (1st set) (fatigue)	5,6 (0,4)	183 (11)	198	13	Yes
H3 (2nd set) (fatigue)	5,7 (0,4)	180 (5)	195	10	Yes

4.1.2 SAMPLES MACHINED BY EDM

4.1.2.1 MECHANICAL TESTING BEFORE FATIGUE TESTING

We first investigated the samples machined by EDM before undergoing fatigue testing. For each sample, the number of indentations in each investigated zone (refer to Chapter 3 for a detailed description) is given in Table 4.3. Detailed values of the mechanical properties (H_{IT} and E_r) of the three samples presented here can be found in Appendices 3, 4 and 5.

Table 4.3 – Indentation zones and number of indentations for samples machined by EDM before fatigue testing.

Sample	Zones	Location of the indentation zones	Number of indentations
EDM-F (A)	#1	From white layer to nickel alloy	10
	#2	Nickel alloy (bulk)	5
EDM #35 (B)	#1	From white layer to nickel alloy	16
EDM-R (B)	#1	From white layer to nickel alloy	11

In this study, samples are grouped by machining parameters, these parameters can be found in Chapter 3. Sample EDM-F (machined using the set of machining parameters "A") is the first one to be presented below. Then, we present the results for samples EDM #35 and EDM-R, machined using the set of machining parameters "B".

Hardness and reduced Young's modulus values as a function of the distance from the Epoxy/White layer interface for sample EDM-F are presented in Figure 4.4. A clear change in the mechanical properties of the sample can be observed between the WEL and the bulk material. The hardness drops from $4{,}0 - 5{,}0$ GPa in the WEL to around $3{,}0$ GPa in the base material, which represents a hardness value lower than that of the IN100

nickel-based superalloy machined by LSG (Table 4.2). This difference is attributed to the presence of a heat affected zone under the WEL. On the other hand, the reduced Young's modulus increases from around 190 to 250 GPa. This rise occurs on a very short distance with no noticeable transition between the WEL and the bulk material. The WEL average thickness for sample EDM-F is around 5,0 μm.

The difference of mechanical properties between the WEL and the base material is also visible on Figure 4.5 which presents Load/Displacement curves obtained on the WEL and on the bulk material.

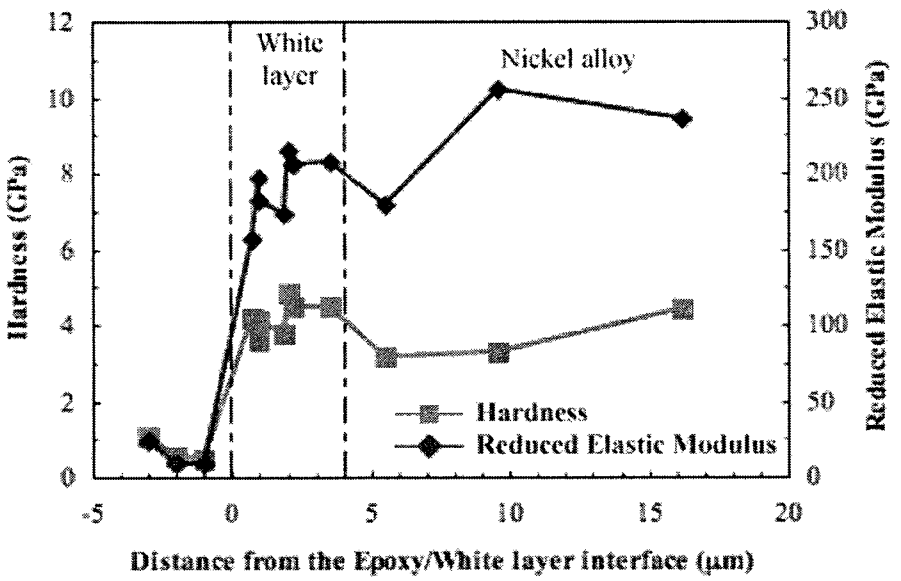

Figure 4.4 – Hardness and reduced Young's modulus as a function of the distance from the Epoxy/White layer interface for sample EDM-F.

The exact locations of the indentations presented in Figures 4.4 and 4.5 are shown in Figure 4.6. An AFM image of sample EDM-F as well as a 3D image are provided. These images offer a good perspective of the microstructural differences existing between the white layer and the bulk material. The γ' phase (dark brown inclusions in the bulk material) has melted and is not observed in the WEL.

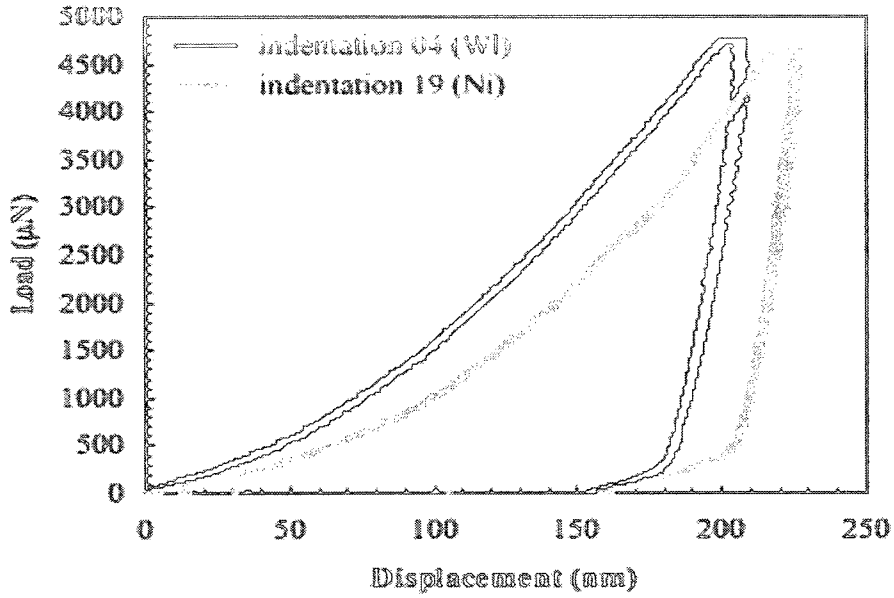

Figure 4.5 – Load/Displacement curves for sample EDM-F in the WEL and in the bulk.

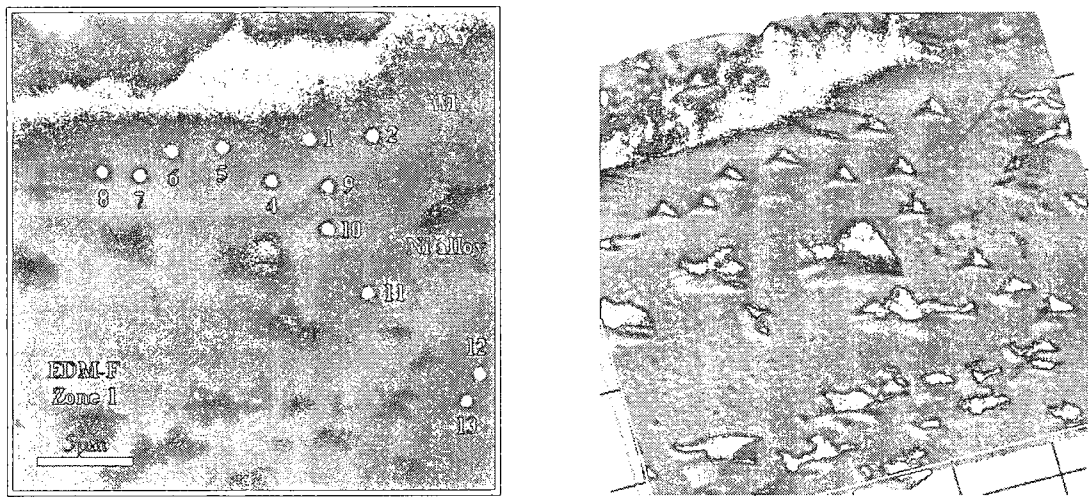

(a) (b)

Figure 4.6 – Indentation positions with respect to the Epoxy/WEL interface for sample EDM-F.

Hardness and reduced Young's modulus values as a function of the distance from the Epoxy/White layer interface for samples EDM #35 and EDM-R are shown in Figures 4.7 and 4.8. Similarly to sample EDM-F, we observe a harder WEL at the surface of the samples and an increase of the reduced Young's modulus when passing from the WEL to the nickel-based superalloy.

On sample EDM #35, the measured hardness for the WEL is of 5,3 GPa and the reduced Young's modulus is of 190 GPa. These values change to 3,0 GPa for the hardness and 200 GPa for the reduced Young's modulus once in the base material.

On sample EDM-R, we measured a hardness of a little less than 5,0 GPa and a reduced Young's modulus of 180 GPa for the WEL. These values are found to be equal to 4,5 GPa for the hardness and 225 GPa for the reduced Young's modulus in the base material.

Load/Displacement curves of indentations made on samples EDM #35 and EDM-R are presented in Figures 4.9 and 4.10. As for sample EDM-F, we recorded a higher maximum displacement in the bulk material than in the WEL confirming a higher hardness of the recast layer compared to the one of the bulk material.

The mean value of WEL thicknesses on samples EDM #35 and EDM-R are equal to 15,0 μm and 8,0 μm.

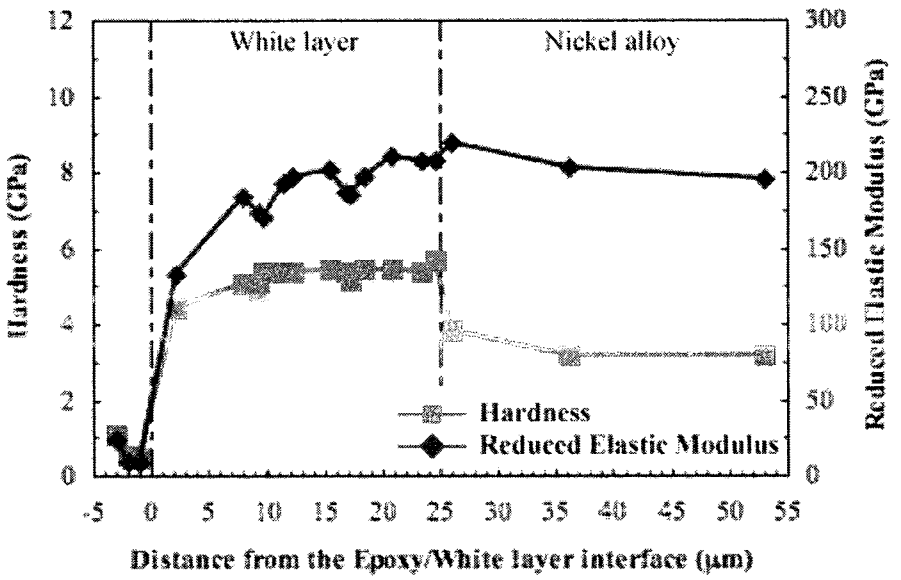

Figure 4.7 – Hardness and reduced Young's modulus as a function of the distance from the Epoxy/White layer interface for sample EDM #35.

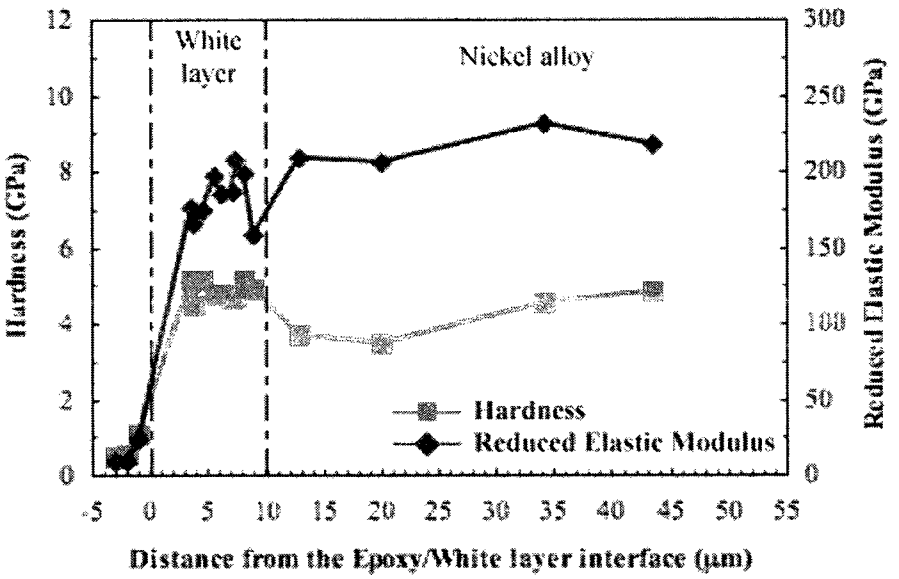

Figure 4.8 – Hardness and reduced Young's modulus as a function of the distance from the Epoxy/White layer interface for sample EDM-R.

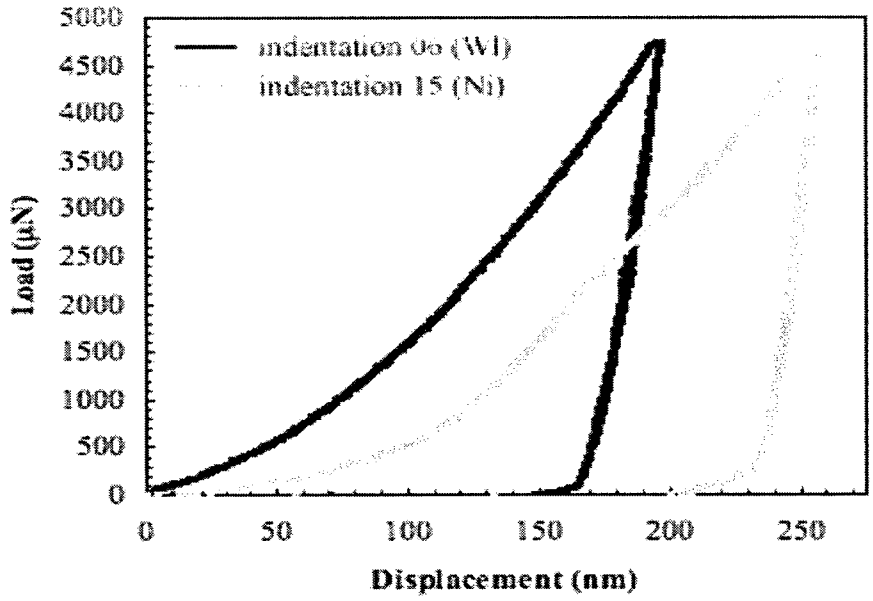

Figure 4.9 – Load/Displacement curves for sample EDM #35 in the WEL and in the bulk.

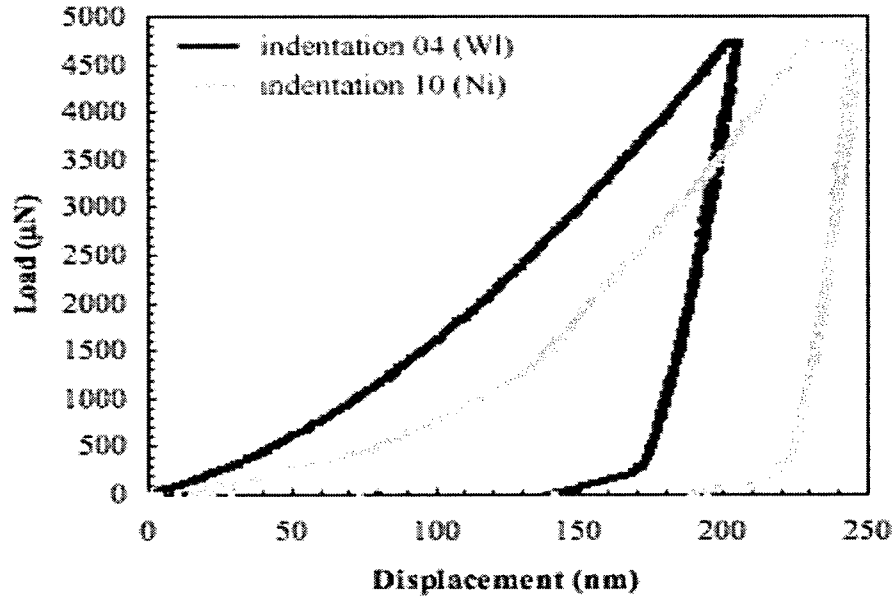

Figure 4.10 – Load/Displacement curves for sample EDM-R in the WEL and in the bulk.

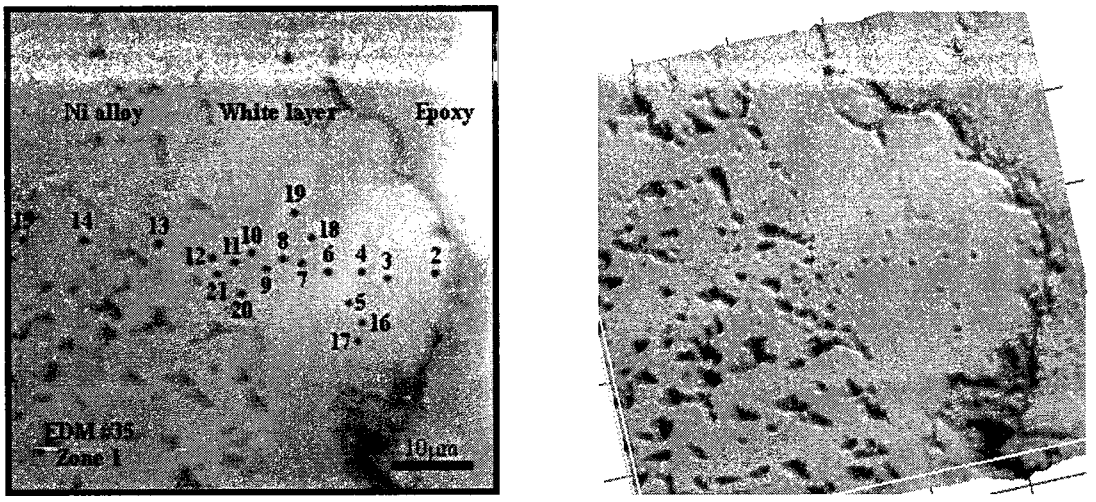

(a) (b)

Figure 4.11 – Indentation positions with respect to the Epoxy/WEL interface for sample EDM #35.

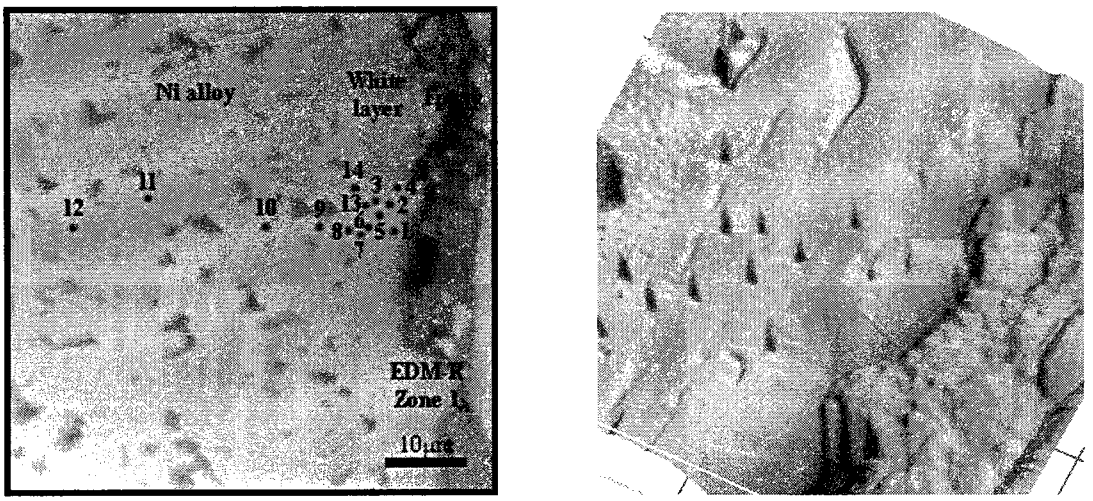

(a) (b)

Figure 4.12 – Indentation positions with respect to the Epoxy/WEL interface for sample EDM-R.

Figures 4.11 and 4.12 present AFM images of the indentation zones on samples EDM #35 and EDM-R. Like for sample EDM-F, a clear change of microstructure is observed

between the white layer and the nickel-based superalloy with the disappearance of the γ' phase. On these images "liquid drop" patterns are also visible. This phenomenon is well known for steels and is caused by a high pulse current (see Chapter 2). IN100 seems to behave in a similar fashion as steels under these conditions.

The results obtained for the mechanical properties of WEL formed by EDM before fatigue testing are summarized in Table 4.4. All values represent averages of the results we obtained. The standard deviation is given in brackets. The set of machining parameters is given with the sample name. All detailed results can be found in Appendices 3, 4 and 5.

Table 4.4 – Average values of WEL properties formed by EDM before fatigue testing.

Sample	H_{IT} (GPa)	E_r (GPa)	E_{IT} (GPa)	WEL thickness (μm)	Number of indentations
EDM-F (A)	4,2 (0,4)	191 (21)	209	5,0	7
EDM #35 (B)	5,3 (0,3)	188 (21)	205	15,0	13
EDM-R (B)	4,8 (0,2)	183 (16)	198	8,0	9
Bulk (Ni alloy)	3,7 (0,3)	219 (18)	247	-	12

4.1.2.2 MECHANICAL TESTING AFTER FATIGUE TESTING

In this section we present the results obtained for samples machined by EDM (produced with the same sets of machining parameters as in the previous section) after undergoing fatigue testing. The number of indentations performed on every sample is given in Table 4.5. Details on the machining conditions of the samples can be found in Chapter 3. All the detailed results of this section are in Appendices 6, 7, 8 and 9.

Samples J7, H7 and H11 were machined using set of machining parameters "A" and sample H14 using set "B". Also, sample H11 was shot peened prior to fatigue tests.

Table 4.5 – Indentation zones and number of indentations for samples machined by EDM after fatigue testing.

Sample	Zones	Location of the indentation zones	Number of indentations
J7 (A)	#1	From white layer to nickel alloy	17
	#2	Nickel alloy (bulk)	3
H7 (B)	#1	From white layer to nickel alloy	17
	#2	Nickel alloy (bulk)	3
H11 (B, SP)	#1	From white layer to nickel alloy	18
	#2	Nickel alloy (bulk)	3
H14 (B)	#1	From white layer to nickel alloy	26
	#2	Nickel alloy (bulk)	3

In Figures 4.13 and 4.14 we present the hardness and reduced Young's modulus values as a function of the distance from the Epoxy/White layer interface of samples J7 and H7. Similarly to sample EDM-F, we observe a drop of the hardness and an increase of the reduced Young's modulus at the interface between the WEL and bulk material.

The WEL formed on samples J7 and H7 exhibits a hardness of 8,0 GPa and a reduced Young's modulus of 185 GPa. This value is much higher than the one obtained for sample EDM-F (Table 4.4). For both samples the hardness value drops to 5,0 – 6,0 GPa in the bulk material and the reduced Young's modulus rises to around 200 GPa. The thicknesses of these two WEL are respectively 7,0 μm and 8,0 μm.

The obtained values are different than those observed on sample EDM-F, leading to the conclusion that the fatigue test has an influence on the mechanical properties of the WEL. This point is discussed in more detail in the second section of this chapter.

The indentations made far from the surface (indentation zones #2) gave hardnesses of 5,0 GPa for sample J7 and 6,0 GPa for sample H7. The reduced Young's modulus were found to be around 200 GPa.

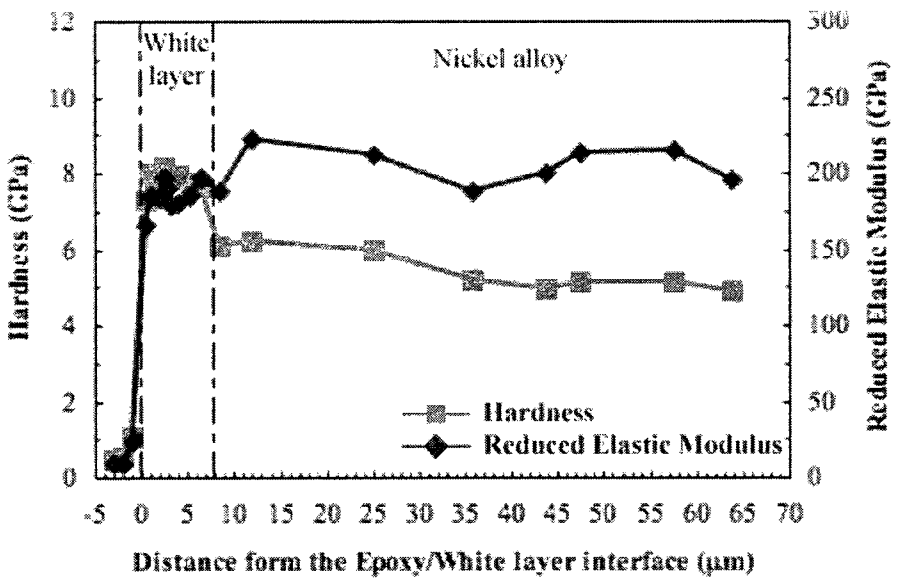

Figure 4.13 – Hardness and reduced Young's modulus as a function of the distance from the Epoxy/White layer interface for sample J7.

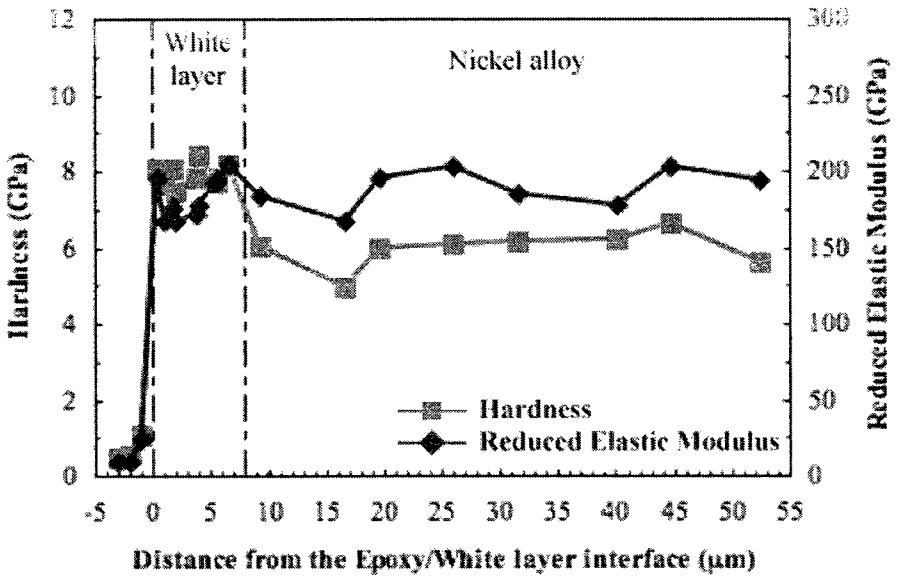

Figure 4.14 – Hardness and reduced Young's modulus as a function of the distance from the Epoxy/White layer interface for sample H7.

Load/Displacement curves obtained on the WEL and nickel-based superalloy of samples J7 and H7 are shown in Figures 4.15 and 4.16. Like the results for samples EDM-F and EDM #35 we can see a clear difference of maximum indentation depth between indentations made in the WEL and those made in the bulk material.

The "steps" visible on the curves of Figure 4.15 where caused by an oxidized contact on one of the acquisition boards of the indentation system. After analysis, it was found that the number of affected points was not sufficient to influence the result of the performed fit. This conclusion stands for all other Load/Displacement curves that present this pattern.

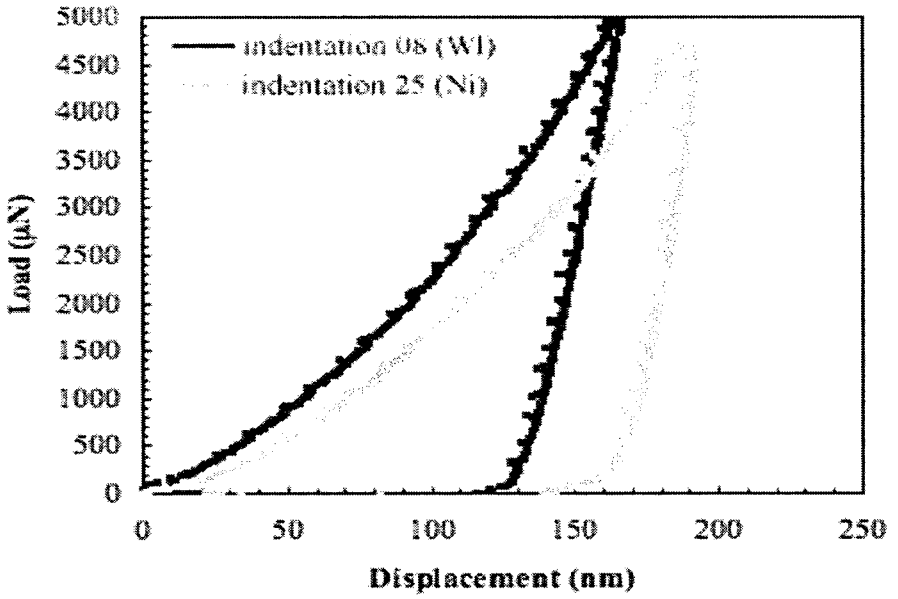

Figure 4.15 – Load/Displacement curves for sample J7 in the WEL and in the bulk.

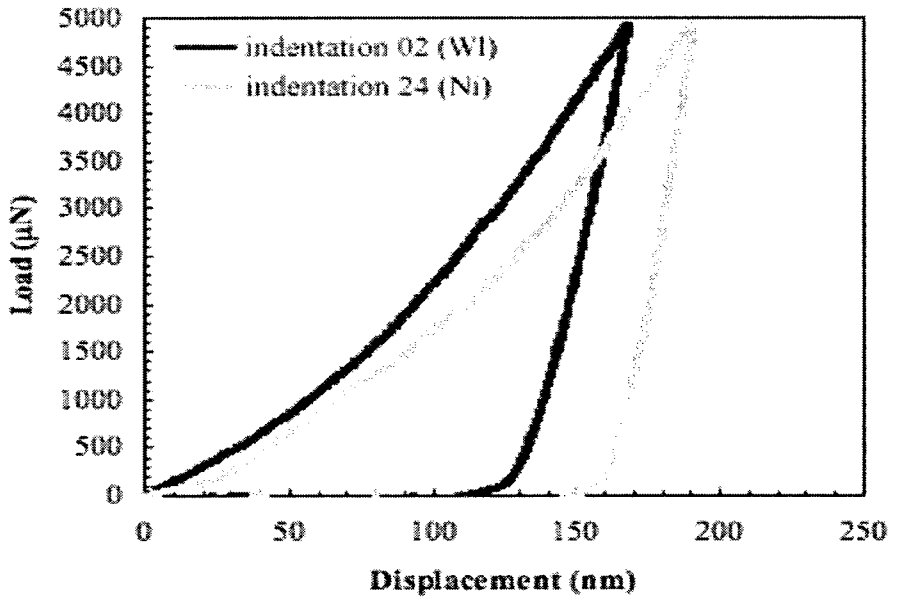

Figure 4.16 – Load/Displacement curves for sample H7 in the WEL and in the bulk.

AFM images of samples J7 and H7 are presented in Figure 4.17 below. They provide information on the localization of the indentations made and on the structure of the WEL and the base material beneath it.

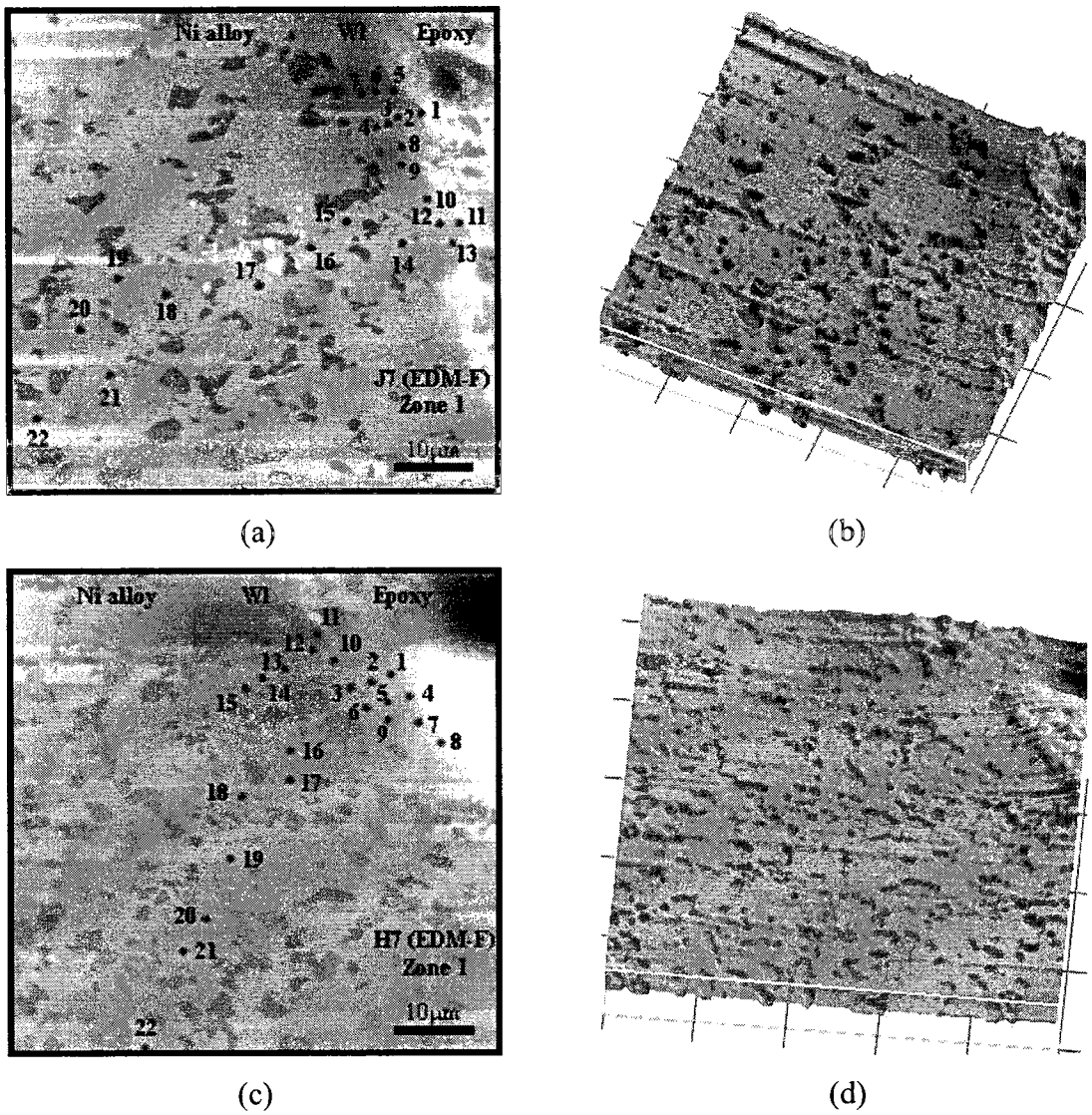

Figure 4.17 – Indentation positions with respect to the Epoxy/WEL interface for samples J7 ((a) and (b)) and H7 ((c) and (d)).

Machined using the same machining parameters as samples J7 and H7, sample H11 was shot peened before being tested under fatigue. Hardness and reduced Young's modulus values are given in Figure 4.18. Shot peening has equalized the thickness of the WEL to 5 μm. In fact, the "liquid drop" patterns have disappeared. This low thickness made the nanoindentation process difficult by causing problems in positioning the tip onto the WEL and by having the tip sliding into the gap between the WEL and epoxy. Once again, we found that the WEL is harder than the base material.

The WEL hardness is 7,5 GPa and its reduced Young's modulus is equal to 181 GPa. In the bulk, the hardness then drops to 6,5 GPa and the reduced Young's modulus raises to around 200 GPa. The indentations made far from the surface (indentation zone #2) gave a hardness of 6,2 GPa and a reduced Young's modulus of 205 GPa.

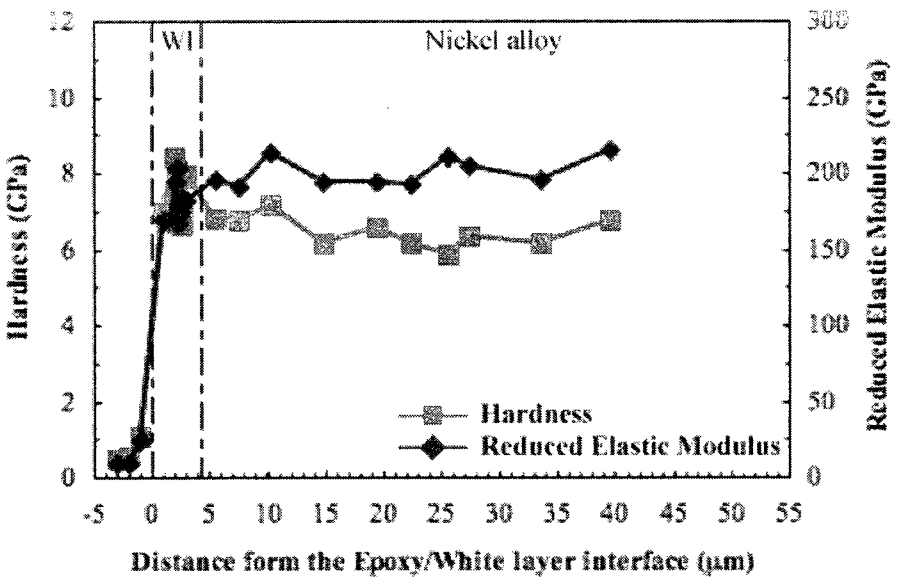

Figure 4.18 – Hardness and reduced Young's modulus as a function of the distance from the Epoxy/White layer interface for sample H11.

The Load/Displacement curves presented below show different mechanical properties between the WEL and the base material. However, the difference of maximum indentation depth is much lower than for samples J7 and H7 (Figures 4.15 and 4.16).

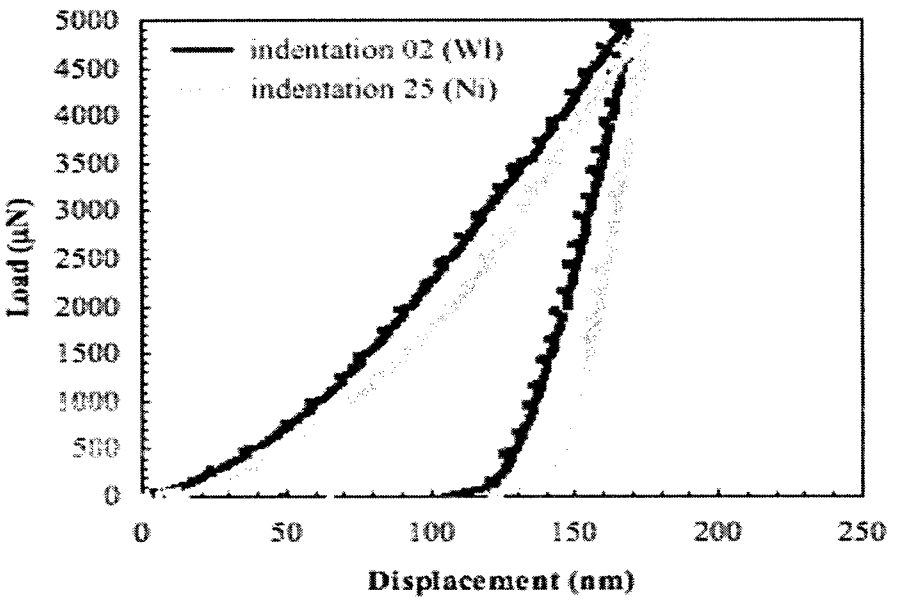

Figure 4.19 – Load/Displacement curves for sample H11 in the WEL and in the bulk.

The images presented in Figure 4.20 show the extreme thinness of the WEL on sample H11. Measurements on the WEL were performed parallel to the surface because there was no room for a cross-sectional measurement. Like for samples J7 and H7, these images don't reveal any microstructural evolution after the fatigue test.

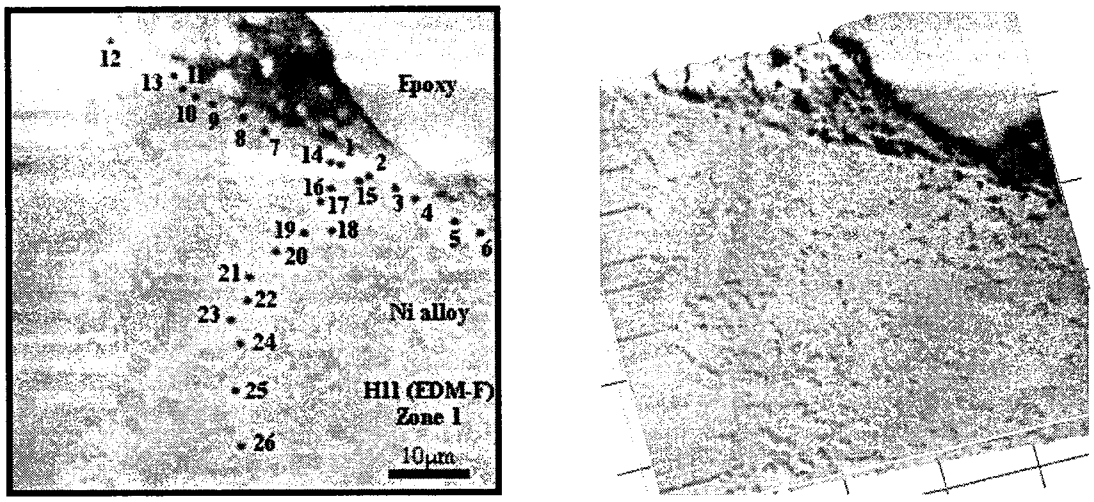

(a) (b)

Figure 4.20 – Indentation positions with respect to the Epoxy/WEL interface for sample H11.

Sample H14 was machined in the same conditions as samples EDM #35 and EDM-R before undergoing a fatigue test but without being shot peened. Its fatigue performance was very poor (Table 3.1) and the surface roughness (presence of "liquid drop" patterns) of the sample is thought to have played a key role here. A rougher sample means peaks and depressions at the surface introducing stress concentration points leading to a rapid failure under cyclic-stress solicitation. Also, the presence of micro-cracks produced during the machining process in the WEL could explain this poor fatigue resistance.

Similarly to when comparing samples EDM #35 and EDM-R to sample EDM-F, sample H14 presents on average a thicker white layer than samples J7, H7 and H11. This difference is attributed to different machining parameters. WEL thickness is a function of the heat produced during the machining and therefore of the pulse conditions (peak current, duration, electrode material). In the case of sample H14 we measured an average thickness of around 20,0 µm.

Hardness and reduced Young's modulus variations as a function of the distance from the Epoxy/White layer interface are given in Figure 4.21. Like the other samples already presented, the WEL is harder than the nickel-based superalloy beneath it. From a distance

of 0 to 13,0 μm from the Epoxy/White layer interface, the reduced Young's modulus increases regularly. This behavior was not present for the other samples and can be explained by a change in the leveling of the sample.

For sample H14 the WEL hardness was measured at 6,9 GPa and the reduced Young's modulus at 179 GPa. Measurements performed far from the surface of the sample gave values of 6,4 GPa for the hardness and 209 GPa for the reduced Young's modulus.

Load/Displacement curves and AFM images obtained on sample H14 are presented below in Figures 4.22 and 4.23.

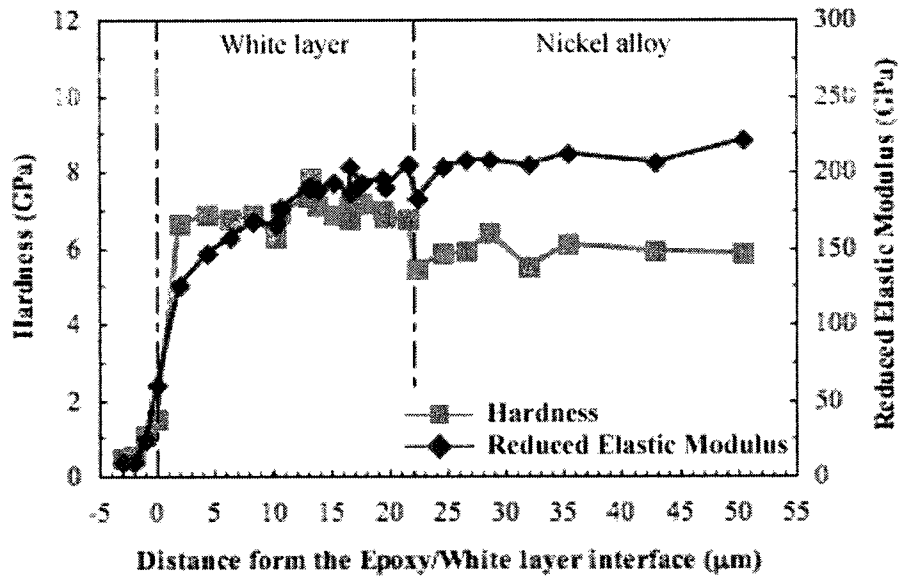

Figure 4.21 – Hardness and reduced Young's modulus as a function of the distance from the Epoxy/White layer interface for sample H14.

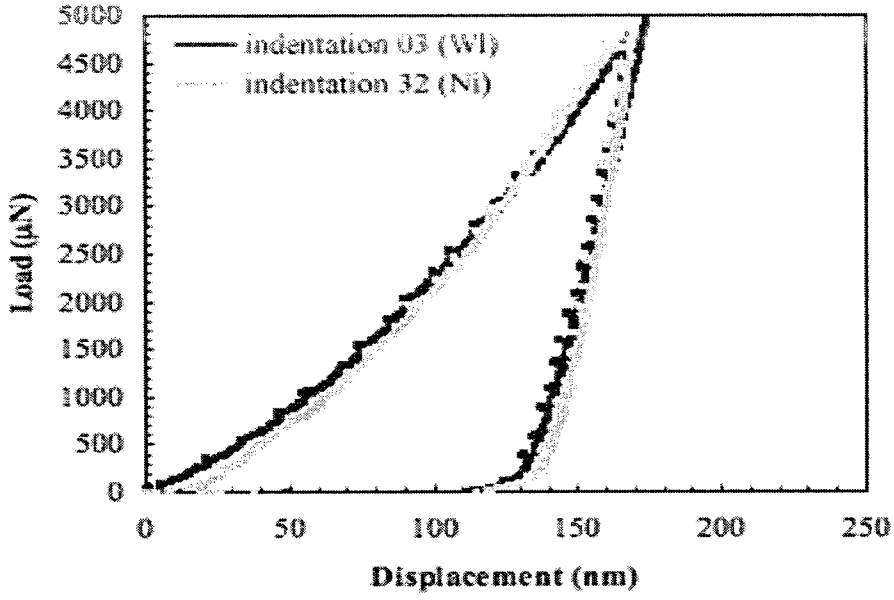

Figure 4.22 – Load/Displacement curves for sample H14 in the WEL and in the bulk.

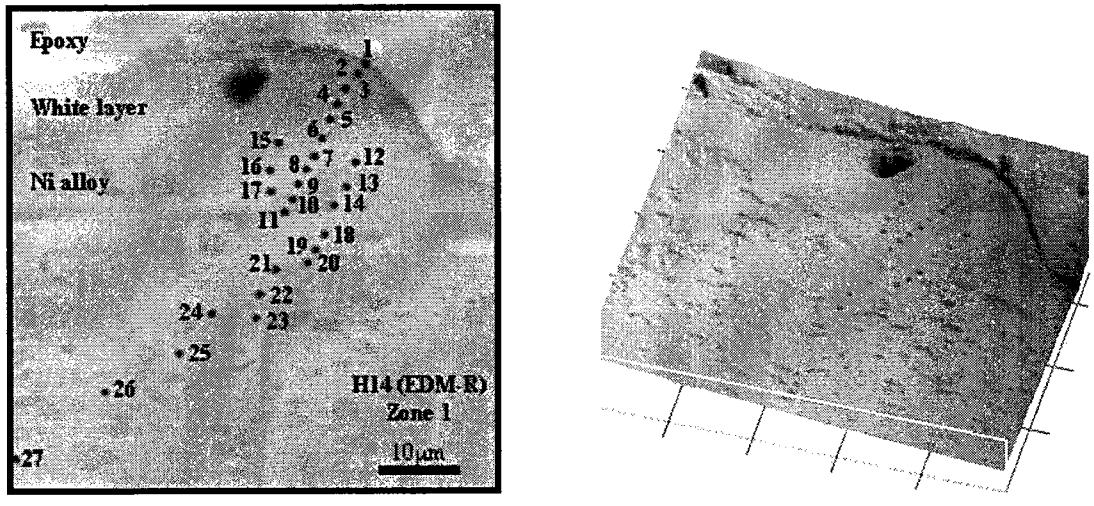

(a) (b)

Figure 4.23 – Indentation positions with respect to the Epoxy/WEL interface for sample H14.

The following table summarizes the mechanical properties of WEL formed by EDM on IN100 after fatigue testing. The presented values represent averages of the results we obtained. The standard deviation is given in brackets. Machining sets of parameters are given along samples names. All the detailed results can be found in Appendices 6, 7, 8 and 9.

Table 4.6 – Average values of WEL properties formed by EDM after fatigue testing.

Sample	H_{IT} (GPa)	E_r (GPa)	E_{IT} (GPa)	WEL thickness (μm)	Number of indentations
J7 (A)	7,8 (0,2)	185 (10)	201	7,0	9
H7 (A)	7,9 (0,3)	183 (14)	198	8,0	9
H11 (A, SP)	7,5 (0,6)	181 (12)	196	4,9	11
H14 (B)	6,9 (0,3)	179 (22)	193	20,0	16
Bulk (Ni alloy)	5,7 (0,3)	203 (27)	225	-	12

4.1.3 SAMPLES MACHINED BY BROACHING

The second machining process studied here is broaching. Samples machined by broaching vary from those machined by EDM. In the case of EDM melting followed by a rapid cooling causes a phase transformation that produces a WEL. In broaching, this transformation occurs because the sample's surface undergoes a severe plastic deformation. This plastic deformation leads to the apparition of a WEL but also of a plastically deformed layer that is not present in EDM samples. Therefore, we will not only be analyzing mechanical properties of the WEL and bulk material but also of this deformed layer (DL).

As presented in Chapter 3 and as for EDM samples in the previous section, we will first present the results obtained on samples that didn't undergo fatigue testing and then those obtained on similar samples after fatigue testing.

4.1.3.1 MECHANICAL TESTING BEFORE FATIGUE TESTING

Samples studied in this section were machined using three different sets of machining parameters. As presented in Chapter 3, sample Broaching #2 was machined using the set of parameters "C", sample Broaching #4 using set "D" and samples Broaching #41 and Broaching #X2 using set "E".

The number of indentations performed on every samples and a brief description of the indentation zones are given in Table 4.7 below. All the detailed results of the measurements performed on broached samples before fatigue tests can be found in Appendices 10, 11, 12 and 13.

Table 4.7 – Indentation zones and number of indentations for samples machined by broaching before fatigue testing.

Sample	Zones	Location of the zones	Number of indentations
Broaching #2	#1	From white layer to nickel alloy	18
(C)	#2	Nickel alloy (bulk)	5
	#1	From white layer to DL	10
Broaching #4	#2	White layer	7
(D)	#3	From white layer to DL	18
	#4	Nickel alloy (bulk)	3
Broaching #41	#1	From white layer to nickel alloy	25
(D)	#2	Nickel alloy (bulk)	4
Broaching #X2	#1	From white layer to nickel alloy	19
(E)	#2	Nickel alloy (bulk)	6

Hardness and reduced Young's modulus values as a function of the distance from the Epoxy/White layer interface are presented in Figure 4.24 for sample Broaching #2. We observe the same general behavior as for samples machined by EDM. A harder WEL than the bulk material (6,1 GPa compared to around 5,0 GPa) and an increase of the Young's modulus from the WEL to the bulk (from 140 GPa to 225 – 250 GPa). The measurements performed far form the surface (indentation zone #2) gave a hardness of 4,0 GPa and a reduced Young's modulus of 208 GPa. For this sample, the WEL thickness is less than 5,0 μm.

The DL on sample Broaching #2 is about 3,0 μm thick and exhibit a hardness of 3,5 GPa and a reduced Young's modulus of around 160 GPa.

Load/Displacement curves obtained on the WEL, DL and nickel-based superalloy of sample Broaching #2 are shown in Figure 4.25. We notice a clear difference of maximum indentation depth between the indentations made in the WEL, the DL and in the bulk material.

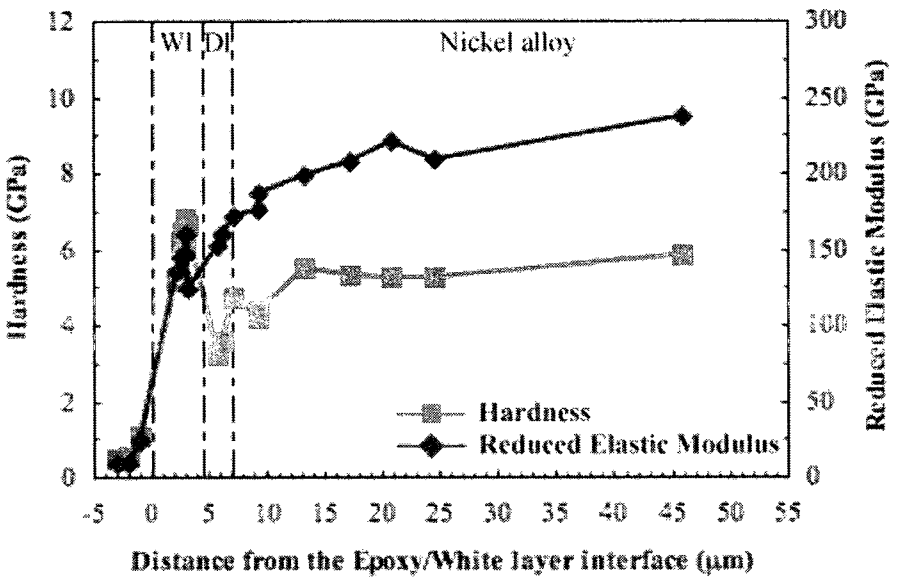

Figure 4.24 – Hardness and reduced Young's modulus as a function of the distance from the Epoxy/White layer interface for sample Broaching #2.

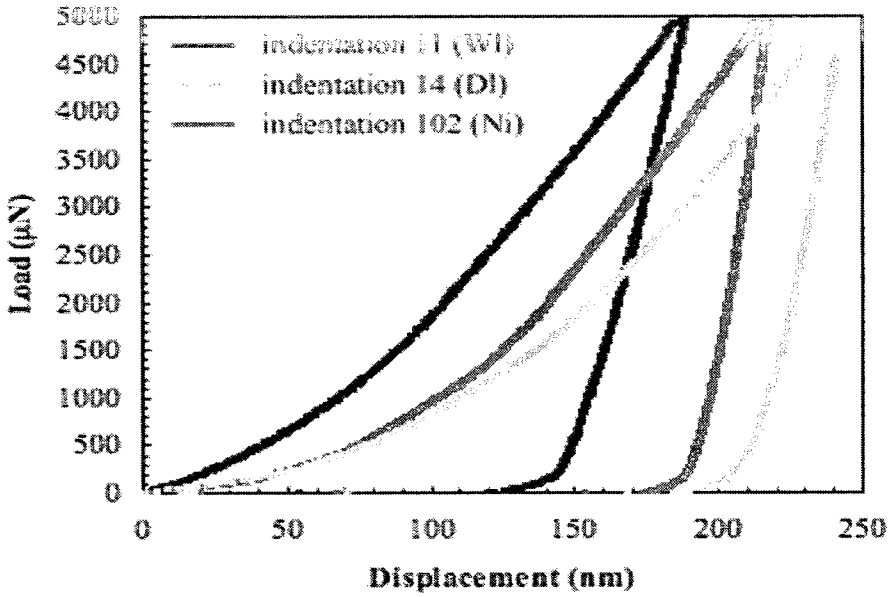

Figure 4.25 – Load/Displacement curves for sample Broaching #2 in the WEL and in the bulk.

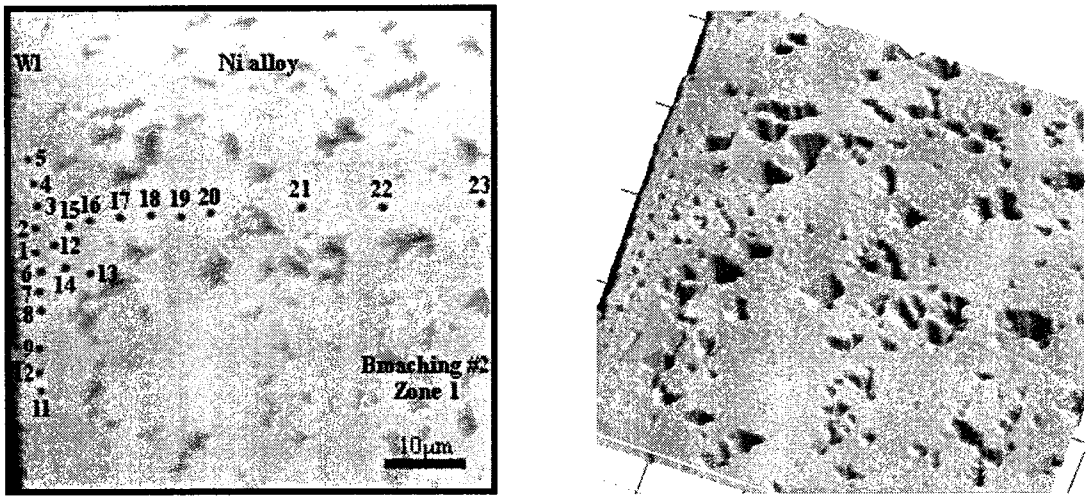

(a) (b)

Figure 4.26 – Indentation positions with respect to the Epoxy/WEL interface for sample Broaching #2.

The AFM images presented on Figure 4.26 show the same microstructural differences between the WEL and the base material as for sample machined by EDM. The γ' phase is not visible in the WEL because it has been completely transformed by the action of the broach. The DL in the near surface region of the sample is barely visible.

Sample Broaching #4 was investigated twice. We first focused (Figures 4.27 and 4.28) on the WEL properties (indentation zones #1 and #2) and then on the properties of the DL (Figure 4.30) present on this sample (indentation zone #3).

The hardness and reduced Young's modulus as a function of the distance from the Epoxy/White layer interface for the first and second indentation zones for sample Broaching #4 are given in Figures 4.27 and 4.28. We observe a harder WEL than DL.

Mechanical properties of the WEL have similar values in zones #1 and #2. In both cases, we obtained a hardness of 6,5 GPa and a reduced Young's modulus of 187 GPa. The WEL's thickness is of 5,0 μm for this sample. The DL has a hardness of around 3,5 GPa and a reduced Young's modulus of 180 GPa on average.

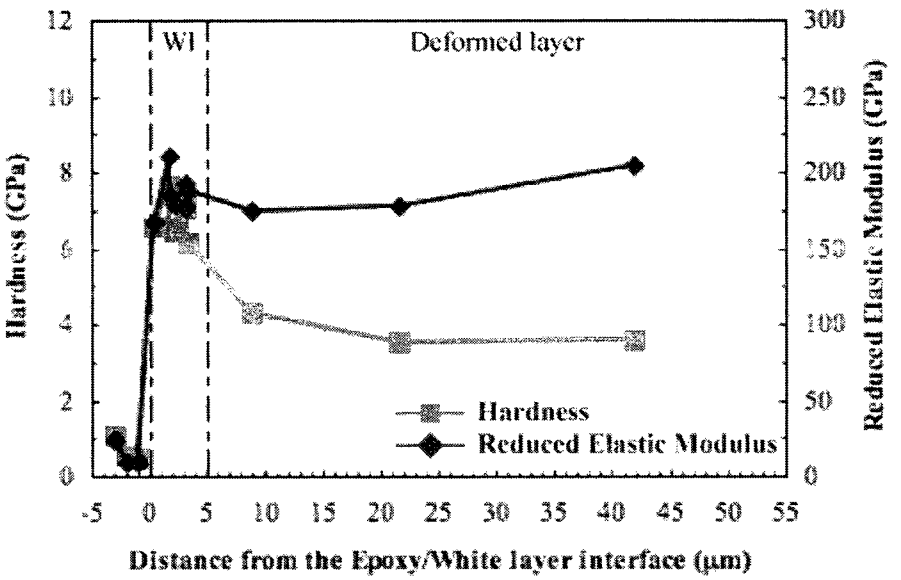

Figure 4.27 – Hardness and reduced Young's modulus as a function of the distance from the Epoxy/White layer interface for sample Broaching #4 (indentation zone #1).

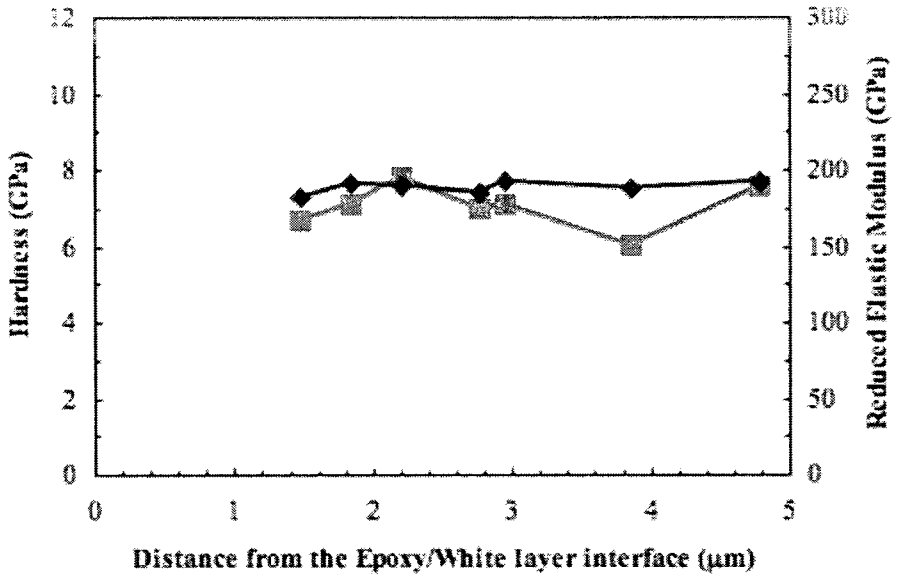

Figure 4.28 – Hardness and reduced Young's modulus as a function of the distance from the Epoxy/White layer interface for sample Broaching #4 (indentation zone #2).

On this sample, the DL is clearly visible on the AFM images (Figure 4.29). An elongation of the γ' phase is visible in the near surface regions of the material and some traces of the inclusions are still visible in the WEL on Figure 4.29 (d). This indicates that the γ' phase has not completely transformed during the machining process.

The thickness of the WEL for this sample and the lack of indentations in the first two indentation zones (#1 and #2) led to the a more careful study of the DL mechanical properties (Figure 4.30). This second set of measurements confirmed the first values presented on Figure 4.27. The hardness of the WEL was found equal to a little more than 6,0 GPa with a reduced Young's modulus of 190 GPa. The DL presented a hardness of 3,5 GPa with a reduced Young's modulus increasing from 175 GPa to 250 GPa. This change is though to result from a decrease in plastic deformation of the DL as we get further from the sample's surface. The Load/Displacement curves obtained for sample Broaching #4 (Figure 4.31) show the differences of mechanical properties found between the WEL, the DL and the bulk material. On the AFM images of the sample (Figure 4.32)

it is clearly visible that the γ' phase is deformed and that this deformation reduces with the distance from sample's surface. The DL thickness was found to be more than 50,0 μm (Figure 4.32).

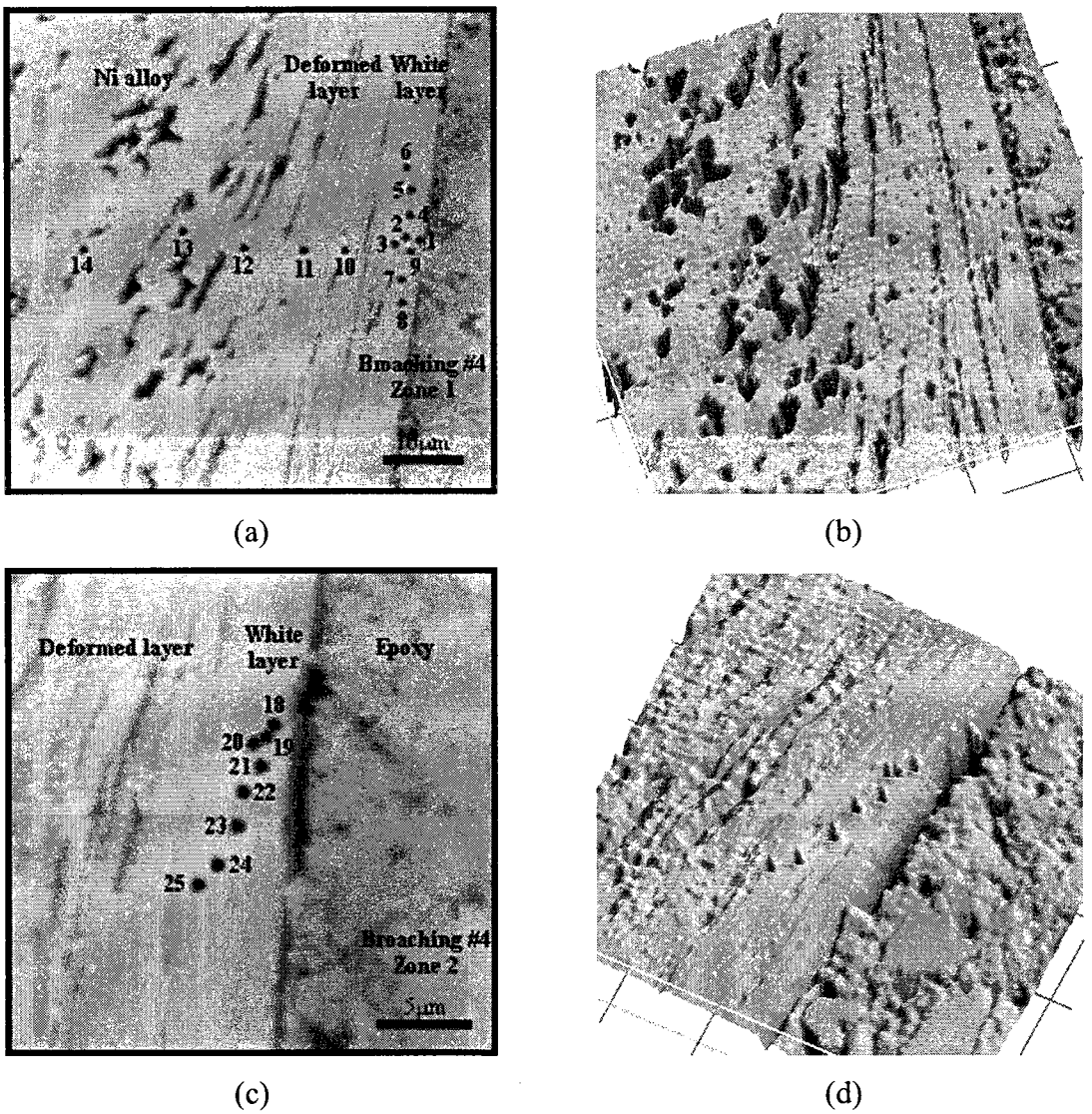

Figure 4.29 – Indentation positions with respect to the Epoxy/WEL interface for sample Broaching #4 indentation zone #1 ((a), (b)) and indentation zone #2 ((c), (d)).

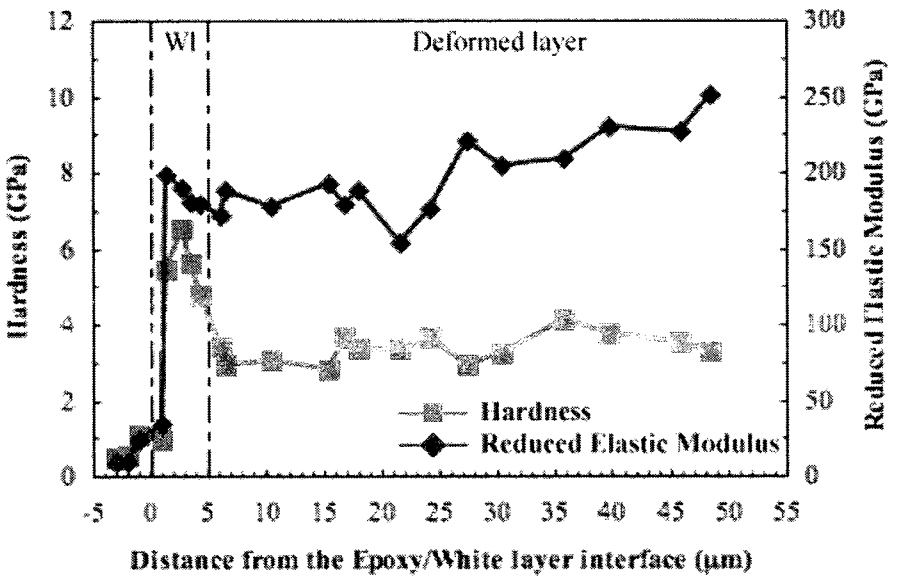

Figure 4.30 – Hardness and reduced Young's modulus as a function of the distance from the Epoxy/White layer interface for sample Broaching #4 (DL study).

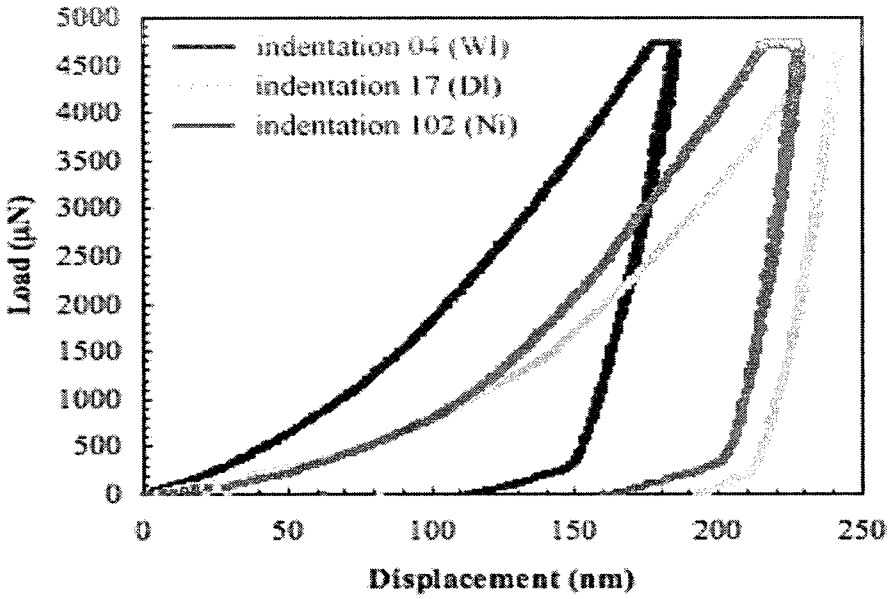

Figure 4.31 – Load/Displacement curves for sample Broaching #4 in the WEL and in the bulk.

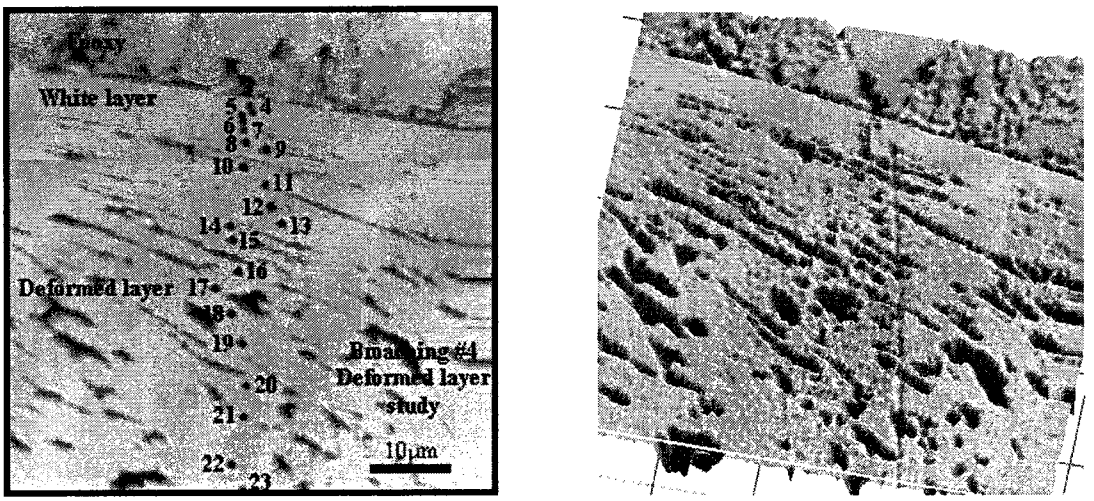

(a) (b)

Figure 4.32 – Indentation positions with respect to the Epoxy/WEL interface for sample Broaching #4 (DL study).

Sample Broaching #41 was machined using the same set of machining parameters as sample Broaching #4. As we obtained very different properties for these two samples, we decided not to present the results for these samples together.

Figure 4.33 shows a very similar "structure" than that of sample Broaching #4 (Figures 4.27, 4.28 and 4.30). We observe a WEL of 8,0 μm and a DL of 42,0 μm which are similar values than those of sample Broaching #4. However, the values found for the hardness and the reduced Young's modulus are very different. For sample Broaching #41 we found a hardness of 9,0 GPa for the WEL and 6,7 GPa for the DL. These values are much higher than those we found for sample Broaching #4. The reduced Young's modulus values are 151 GPa for the WEL and 165 GPa for the DL. These values are much lower than those found on sample Broaching #4.

These differences result from different strain rates during the machining process. This point will be discussed in the second section of this chapter.

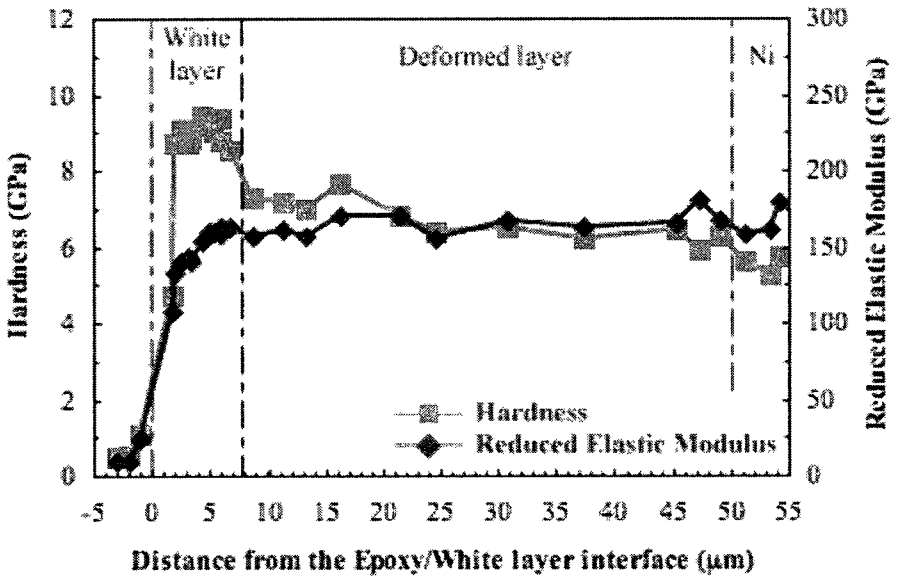

Figure 4.33 – Hardness and reduced Young's modulus as a function of the distance from the Epoxy/White layer interface for sample Broaching #41.

Load/Displacement curves of sample Broaching #41 are provided in Figure 4.34. These show the difference of maximum indentation depths recorded during the measurements. As exposed in Chapter 3, this difference comes from variations of the hardness in the different indented regions.

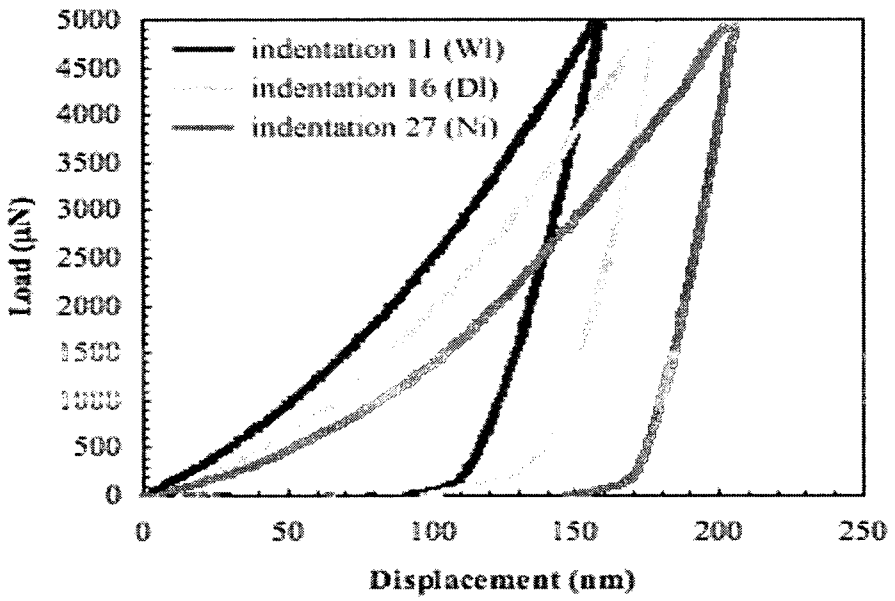

Figure 4.34 – Load/Displacement curves for sample Broaching #41 in the WEL and in the bulk.

Figure 4.35 below shows the typical microstructure of a broached sample with a WEL accompanied by a DL underneath. It is hard to conclude on the presence of the γ' phase in the WEL.

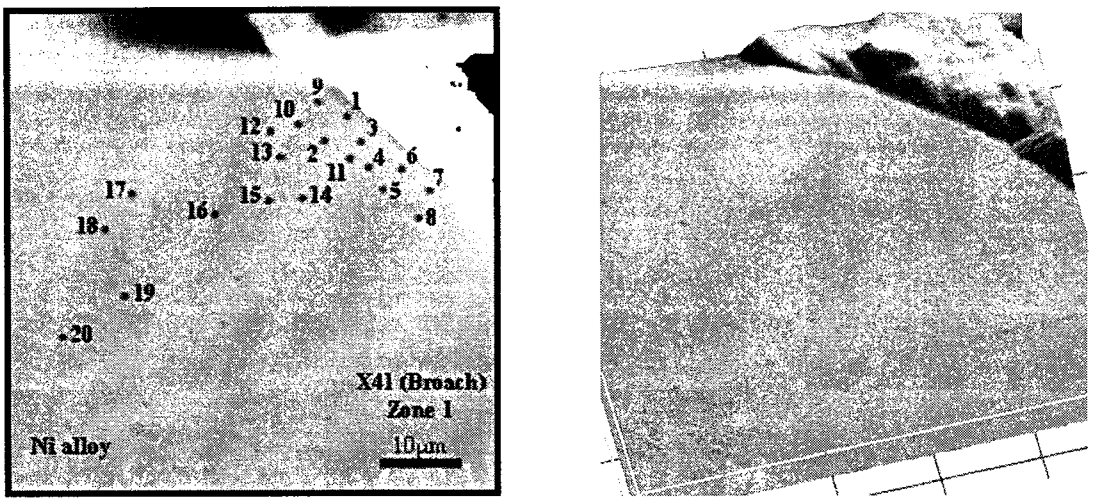

(a) (b)

Figure 4.35 – Indentation positions with respect to the Epoxy/WEL interface for sample Broaching #41.

Sample Broaching #X2 was machined using set of parameters "E". It is the only sample that was machined in this way in our study. This set of parameters corresponds to the "softest" way to broach IN100.

On Figures 4.36 and 4.38 we can't observe any WEL could be found on this sample. Only a DL was found in the near surface region. In Figure 4.36, we see that the sample exhibits mechanical properties that are relatively close to those of sample REF (Table 4.2), meaning that the machining process didn't have a great impact on the sample.

This sample proves that no WEL forms at the surface of metallic workpieces if a critical energy (resulting from a high deformation and temperatures) is not reached during the machining. Therefore, the set of machining parameters "E" should be considered as ideal as it does not produce a WEL. However, it is to slow and not compatible with the production process.

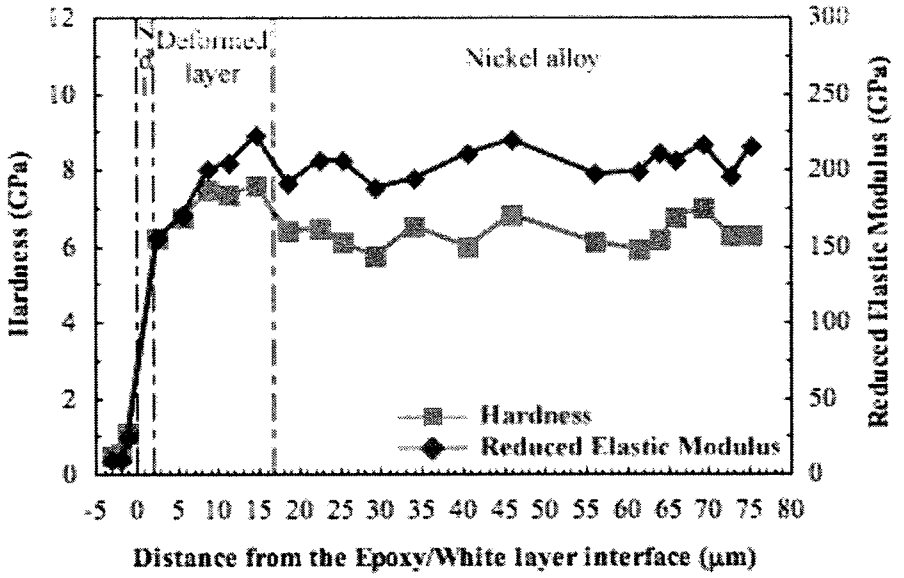

Figure 4.36 – Hardness and reduced Young's modulus as a function of the distance from the Epoxy/White layer interface for sample Broaching #X2.

Load/Displacement curves for sample Broaching #X2 are provided in Figure 4.37. Except for indentation 02 which was made in the severely deformed layer very close to the surface of the sample (Figure 4.38), we can see that the curves have very similar shapes indicating stable mechanical properties as a function of distance to the surface.

AFM images of the sample are also provided (Figure 4.38). On these images, no WEL can be seen and the DL is barely noticeable. This microstructure is very close to the one found on sample H3 after fatigue testing (Figure 4.3).

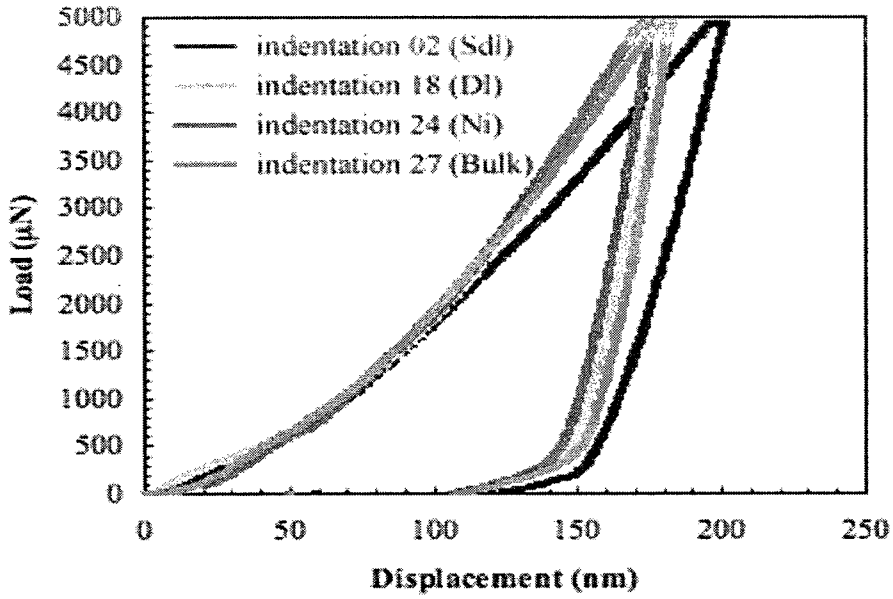

Figure 4.37 – Load/Displacement curves for sample Broaching #X2 in the WEL and in the bulk.

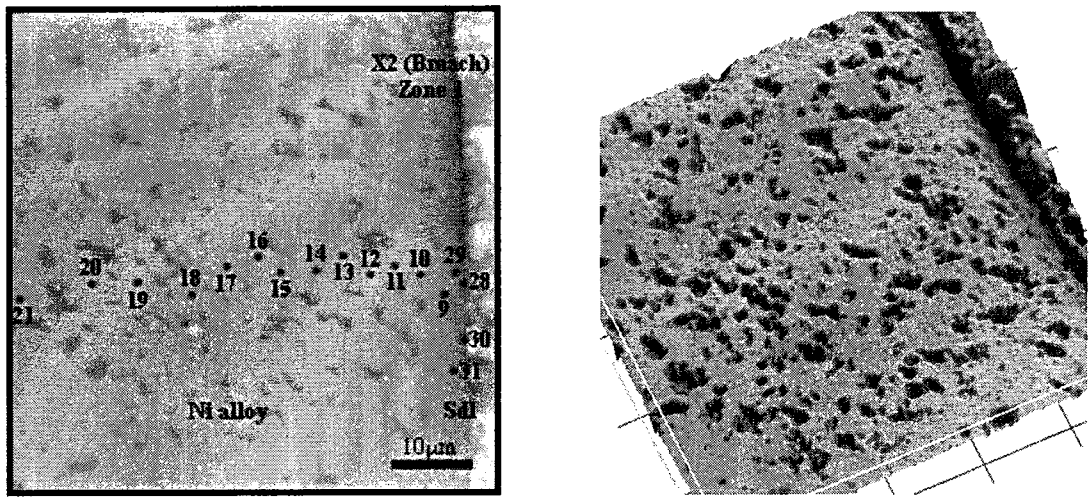

(a) (b)

Figure 4.38 – Indentation positions with respect to the Epoxy/WEL interface for sample Broaching #X2.

The following table summarizes the results presented in this section. These are average values and the standard deviation is given in brackets. The detailed results can be found in Appendices 10 ,11, 12, 13.

Table 4.8 – Average values of WEL and DL properties formed by broaching before fatigue testing.

Sample	H_{IT} (GPa)	E_r (GPa)	E_{IT} (GPa)	Thickness (μm)	Number of indentations
Broaching #2 (WEL) (C)	6,1 (0,7)	143 (11)	149	4,5	7
Broaching #2 (DL) (C)	3,4 (0,3)	156 (5)	165	3,0	2
Broaching #4 (WEL) (D)	6,5 (0,5)	187 (13)	203	5,0	18
Broaching #4 (DL) (D)	3,5 (0,5)	195 (25)	214	55,0	18
Broaching #41 (WEL) (D)	9,0 (0,3)	151 (11)	159	8,0	10
Broaching #41 (DL) (D)	6,7 (0,5)	165 (7)	176	42,0	11
Broaching #X2 (DL) (E)	7,3 (0,4)	199 (21)	219	15,0	4
Bulk (Ni alloy)	5,4 (0,3)	202 (20)	223	-	20

4.1.3.2 MECHANICAL TESTING AFTER FATIGUE TESTING

The number of indentations performed on every studied sample is given in Table 4.9. Details on the sample machining conditions can be found in Chapter 3. All the detailed results of this section can be found in Appendices 14, 15 and 16.

Table 4.9 – Indentation zones and number of indentations for samples machined by broaching after fatigue testing.

Sample	Zones	Location of the zones	Number of indentations
H18 (C)	#1	From white layer to nickel alloy	25
	#2	Nickel alloy (bulk)	5
J5 (C)	#1	From white layer to nickel alloy	43
	#2	White layer	4
	#3	White layer	6
	#4	Nickel alloy (bulk)	3
H22 (C, SP)	#1	From white layer to nickel alloy	28
	#2	Nickel alloy (bulk)	3
	#3	White layer	9
	#4	From white layer to nickel alloy	15
	#5	Nickel alloy (bulk)	5

Samples H18 and J5 were machined using the same set of machining parameters. Therefore, the results obtained on these samples are presented together in this section. The sample J5 was investigated near a crack produced during the fatigue test (indentation zones #1 and #2). A third set of measurements (indentation zone #3) was performed far from the crack to confirm the obtained results. Only the detailed results obtained on indentation zone #1 are presented below.

These two samples present similar values of hardness for the WEL (Figures 4.39 and 4.40). This value is 10,3 GPa for sample H18 and 10,4 GPa for sample J5 on average. However, in sample J5 (Figure 4.40) two different zones are observed (between 0 μm and 22,0 μm and between 22,0 μm and 50,0 μm). The hardness shows a little drop. This means that beneath 22,0 μm, the transformation into a WEL of the nickel-based superalloy is not fully achieved. On sample H18 such behavior can't be seen. The reduced Young's modulus is equal to 183 GPa for sample H18 and 202 GPa for sample J5. The thickness of the WEL was found to be equal to 5,0 μm for sample H18 and 50,0 μm for sample J5. Although machined using the same parameters, samples H18 and J5 present very different WEL thicknesses. Like for samples Broaching #4 and Broaching #41, this difference can be explained by different strain rates. This also explains the difference in the thicknesses of the two DL. For sample H18 the DL was found to be 35,0 μm thick where as for sample J5 it is equal to 70,0 μm. On both samples the DL has a hardness of 8,9 GPa. The reduced Young's modulus of sample H18 is equal to 191 GPa and for sample J5 it is equal to 211 GPa.

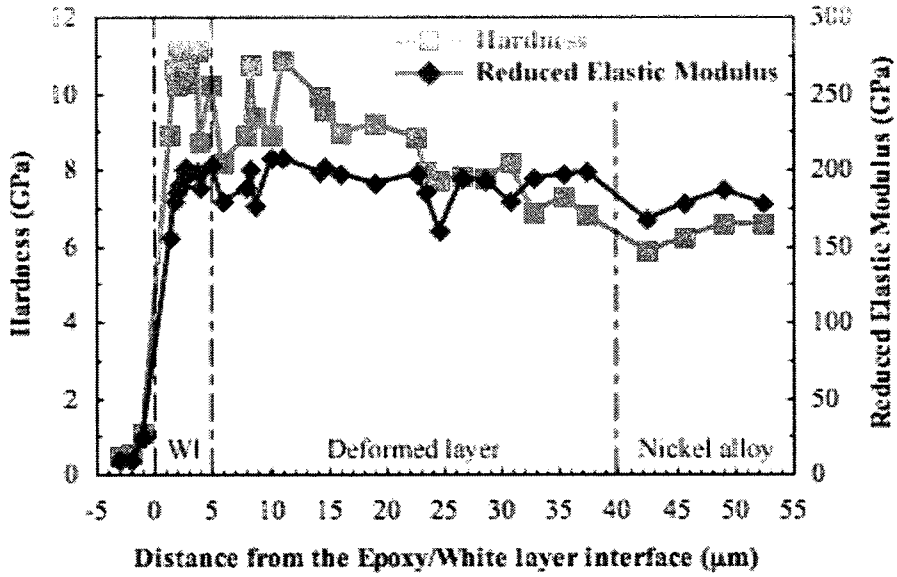

Figure 4.39 – Hardness and reduced Young's modulus as a function of the distance from the Epoxy/White layer interface for sample H18.

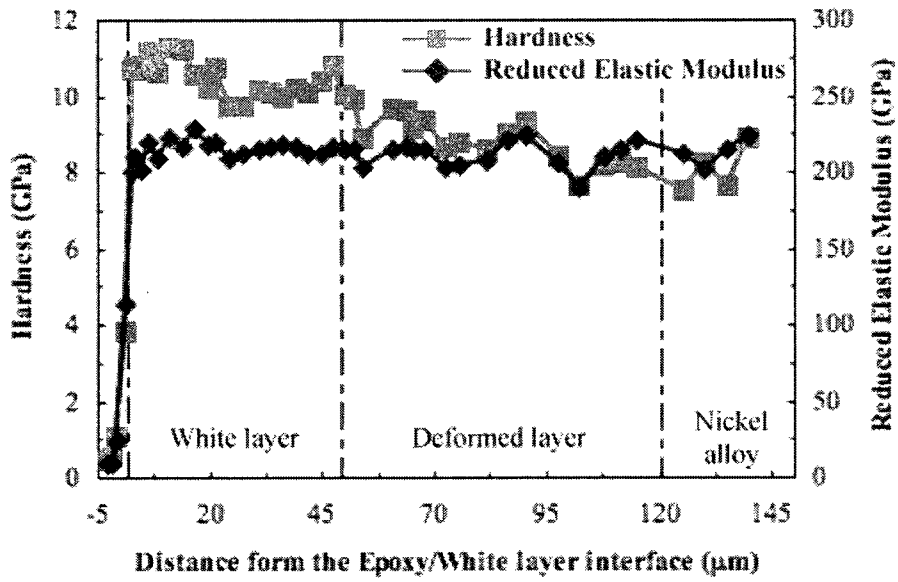

Figure 4.40 – Hardness and reduced Young's modulus as a function of the distance from the Epoxy/White layer interface for sample J5 (indentation zone #1).

Load/Displacement curves for samples H18 and J5 are presented below in Figures 4.41 and 4.42. Like for all the other samples, different behavior can be observed depending on the indentation's location.

AFM images obtained on samples H18 and J5 are presented on Figures 4.43 and 4.44. These pictures clearly show the difference of microstructure between the WEL, the DL and the base material.

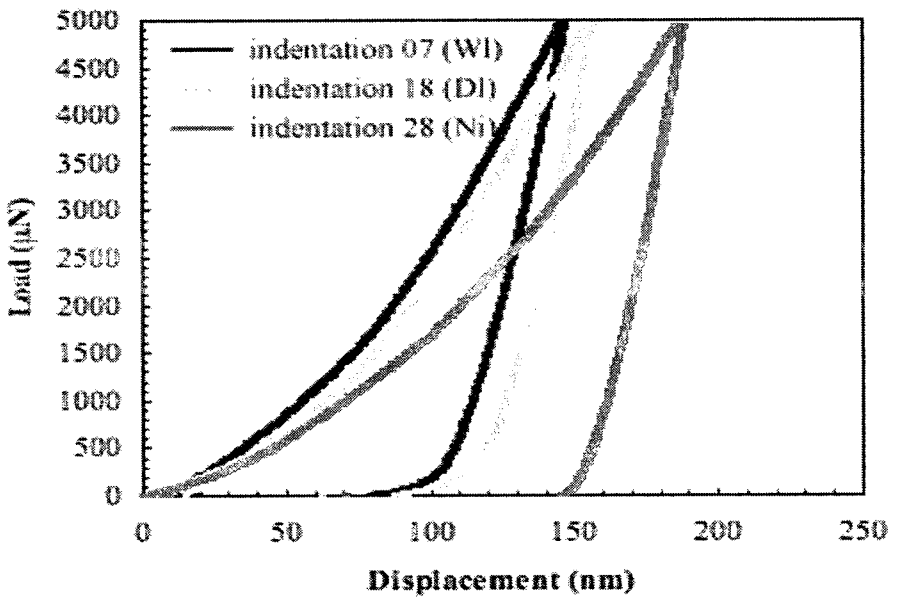

Figure 4.41 – Load/Displacement curves for sample H18 in the WEL and in the bulk.

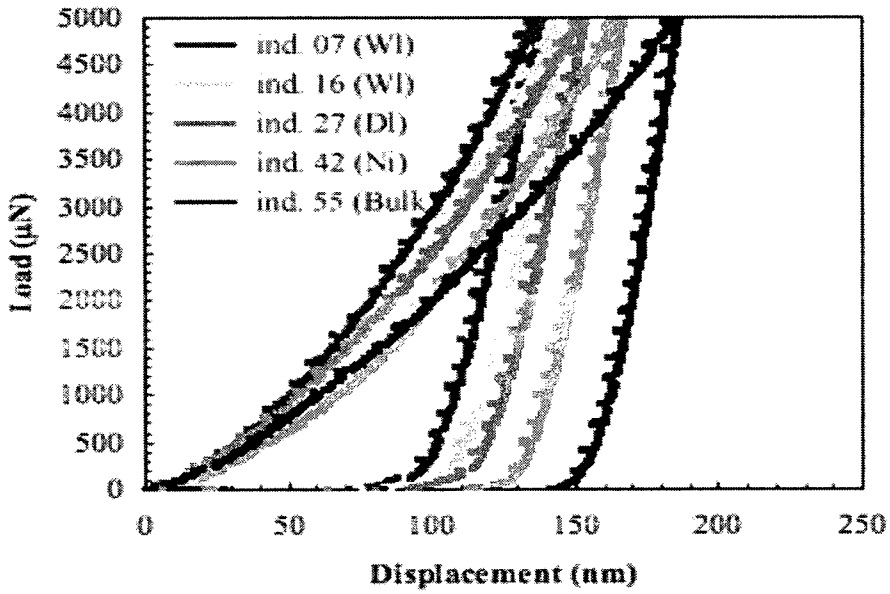

Figure 4.42 – Load/Displacement curves for sample J5 at various locations along the cross-section.

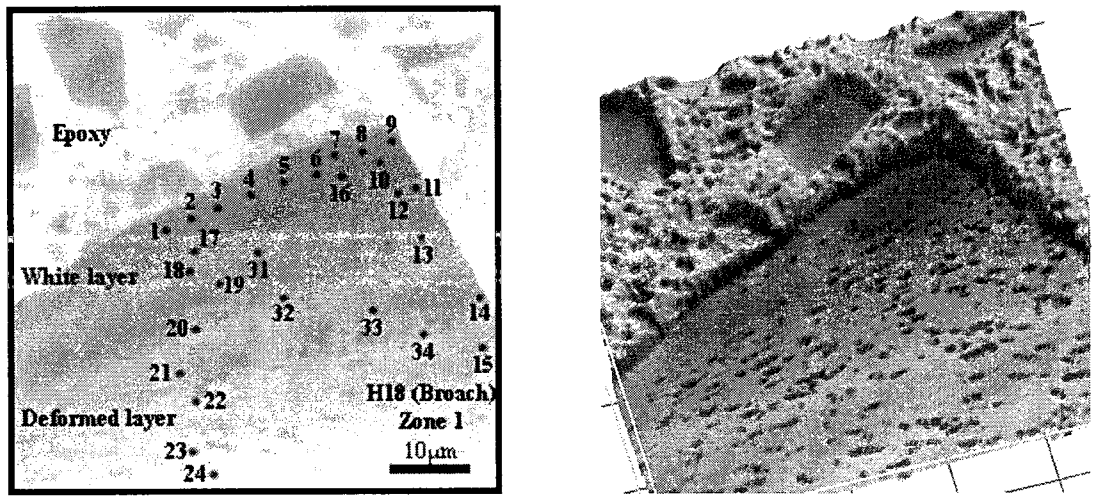

(a) (b)

Figure 4.43 – Indentation positions with respect to the Epoxy/WEL interface for sample H18.

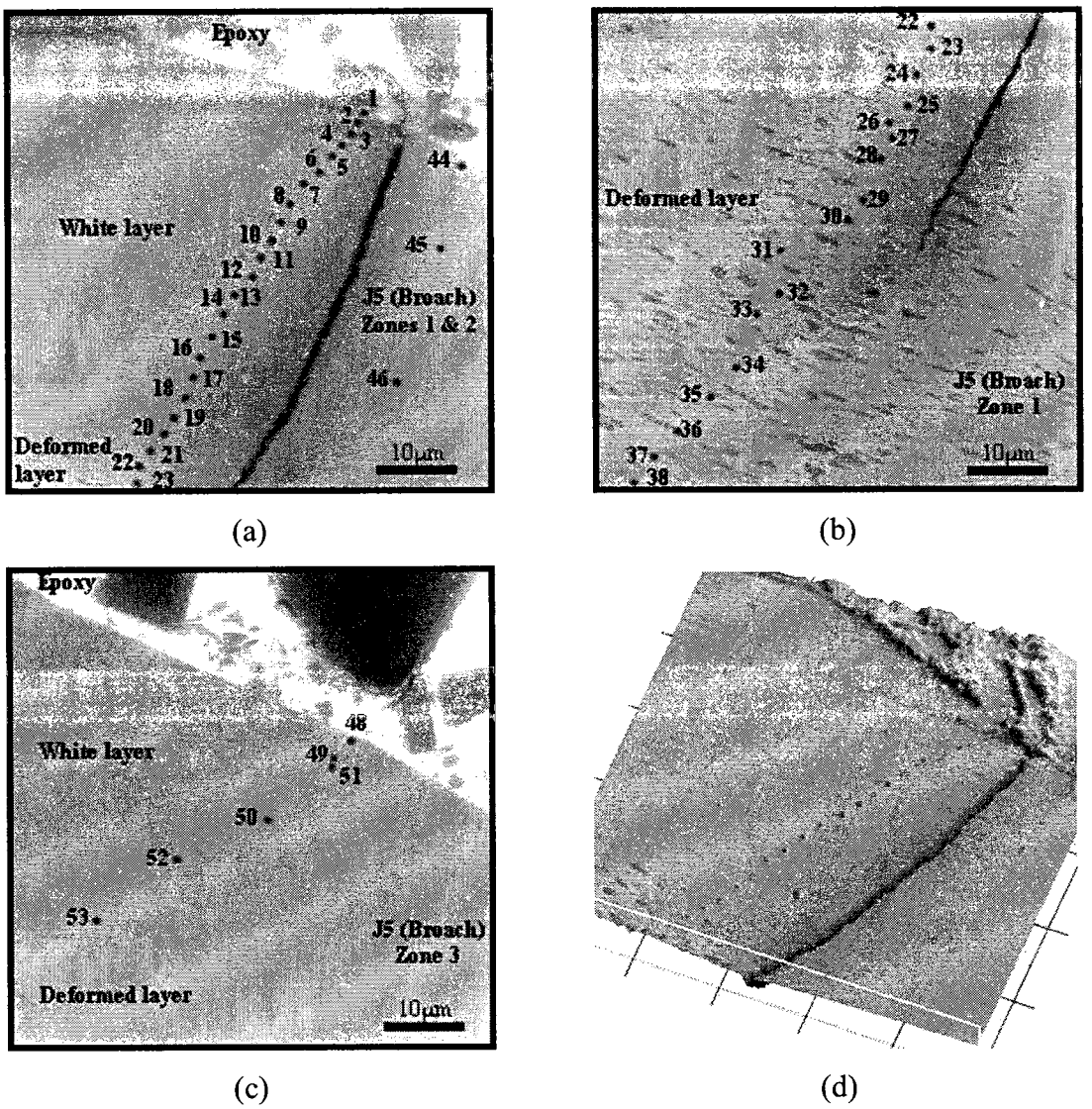

Figure 4.44 – Indentation positions with respect to the Epoxy/WEL interface for sample J5 ((a) indentation zones #1 & #2, (b) indentation zone #1, (c) indentation zone #3 and (d) indentation zones #1 & #2).

The last sample investigated in this work, sample H22 was machined using the same set of machining parameters than samples H18 and J5 but it was shot peened prior to fatigue testing. This sample was investigated twice (indentation zone #1 and indentation zones #3 and #4) to confirm the results of the first set of measurements which gave low values of hardness compared to samples H18 and J5. As the results found for indentation

zones #3 and #4 are very close (Table 4.10), only these two are considered below. The detailed results for the indentation zone #1 can be found in Appendix 16.

Sample H22 presents a WEL of 13 μm in thickness. The hardness of the WEL is 11,0 GPa on average. Its reduced Young's modulus is 201 GPa. The DL has a hardness of 8,7 GPa and a reduced Young's modulus of 201 GPa. Its thickness is of 44,0 μm (Figure 4.45).

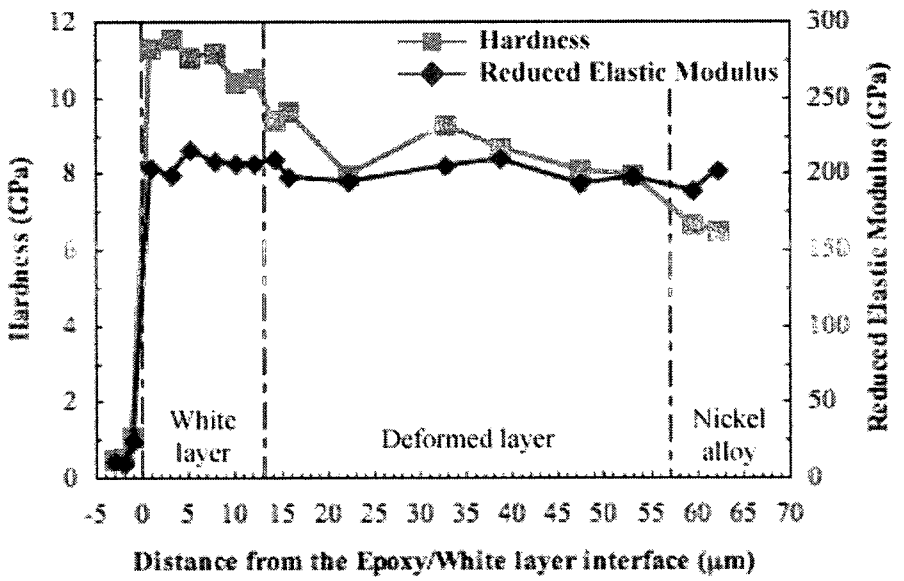

Figure 4.45 – Hardness and reduced Young's modulus as a function of the distance from the Epoxy/White layer interface for sample H22 (indentation zone #4).

Load/Displacement curves are given in Figure 4.46. The maximum indentation depth is different for indentations made in the WEL, the DL or the bulk material. This confirms that the hardness of the different zones is different.

In Figure 4.47 we present the AFM images obtained for sample H22. As for all other samples, these images show the difference of microstructure between the WEL, the DL and the base material. However, it is not possible to see the influence of the fatigue test on these images.

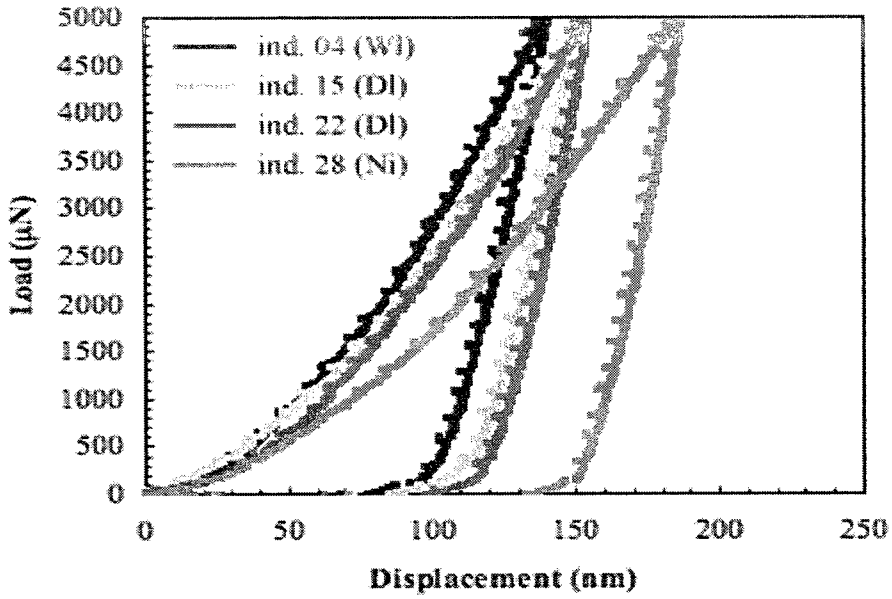

Figure 4.46 - Load/Displacement curves for sample H22 at various locations along the cross-section.

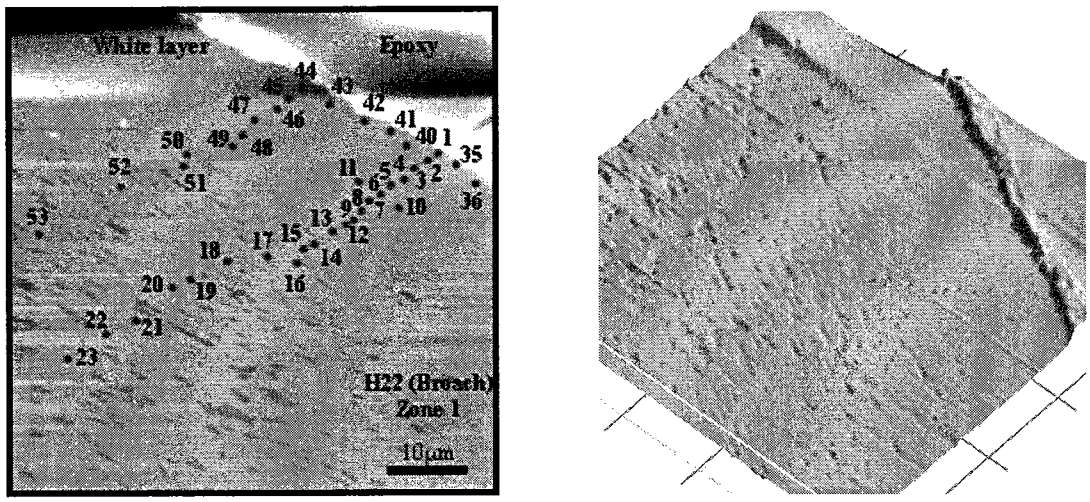

(a) (b)

Figure 4.47 – Indentation positions with respect to the Epoxy/WEL interface for sample H22.

The following table summarizes the results presented in this section. These are average values and the standard deviation is given in brackets. The detailed results can be found in Appendices 14, 15 and 16.

Table 4.10 – Average values of WEL and DL properties formed by broaching after fatigue testing.

Sample	H_{IT} (GPa)	E_r (GPa)	E_{IT} (GPa)	Thickness (μm)	Number of indentations
H18 (WEL) (C)	10,3 (1,1)	183 (13)	199	5,0	10
H18 (DL) (C)	8,9 (1,0)	191 (13)	209	35,0	18
J5 (WEL zone #1) (C)	10,5 (0,5)	214 (7)	240	50,0	16
J5 (WEL zone #2) (C)	10,1 (0,9)	186 (13)	202	50,0	4
J5 (WEL zone #3) (C)	10,7 (0,5)	207 (12)	230	50,0	6
J5 (DL zone #1) (C)	8,9 (0,6)	211 (8)	236	70,0	15
H22 (WEL zone #1) (D, SP)	9,4 (0,5)	200 (9)	221	14,0	11
H22 (WEL zone #3) (D, SP)	10,9 (0,6)	188 (12)	205	14,0	9
H22 (WEL zone #4) (D, SP)	11,0 (0,4)	207 (5)	230	14,0	6
H22 (DL zone #1) (D, SP)	7,8 (0,8)	203 (7)	225	44,0	12
H22 (DL zone #4) (D, SP)	8,7 (0,7)	201 (7)	222	44,0	7
Bulk (Ni alloy)	6,2 (0,4)	200 (10)	219	-	16

4.2 DISCUSSION

In the first section of this chapter, we presented results for the mechanical properties of WEL on IN100 machined by EDM and broaching using different sets of machining parameters. These results exhibited significant differences and the effects of low-cycle fatigue and shot peening on the mechanical and microstructural properties of the studied WEL were also evaluated. The main values obtained during our experiments are summarized below in Table 4.11.

Table 4.11 – Properties of IN100 and WEL.

Type of machining	Region	H_{IT} (GPa)	E_r (GPa)	E_{IT} (GPa)	Thickness (μm)
LSG Before fatigue	Bulk	4,15 to 5,0	195	214	-
LSG After fatigue	Bulk	5,6 to 5,7	180 to 183	195 to 198	-
EDM Before fatigue	WEL	4,2 to 5,3	170 to 191	182 to 209	5,0 to 15,0
	Bulk	3,2 to 4,1	199 to 239	219 to 275	-
EDM After fatigue	WEL	6,9 to 7,9	179 to 185	193 to 201	4,9 to 20,0
	WEL (SP)	7,5	181	196	4,9
	Bulk	5,0 to 6,4	197 to 209	217 to 233	-
Broaching Before fatigue	WEL	6,1 to 9,0	143 to 187	149 to 203	4,5 to 8,0
	DL	3,4 to 6,7	156 to 195	165 to 214	3,0 to 55,0
	Bulk	4 to 6.7	183 to 220	198 to 248	-
Broaching After fatigue	WEL	10,1 to 11,0	183 to 214	199 to 240	5,0 to 50,0
	WEL (SP)	11,0	195	215	14,0
	DL	7,8 to 8,9	191 to 211	209 to 236	35,0 to 70,0
	Bulk	5,9 to 6.4	186 to 214	202 to 240	-

In this work, a methodology was also developed to investigate the mechanical and microstructural properties of WEL formed on IN100 nickel-based superalloy by nanoindentation and AFM-like imagery. Sets of experimental parameters were assessed in order to obtain good AFM images of sample surfaces. It should be noted that this methodology could be applied to any Metal/WEL system.

It is a commonly accepted fact that a WEL is harder than the material on which it forms. However, no study had ever been performed on WEL formed on nickel-based superalloys. For both machining techniques we noticed clear variations in the hardness between the WEL and the bulk material but the WEL produced by broaching was found to be harder than the one produced by EDM. We also found differences in the microstructure between the IN100 and the WEL. Figure 4.48 shows a schematic representation of the microstructure obtained on samples machined by LSG, EDM and broaching. The temperature and deformation scales are also indicated. The WEL and DL shown in Figure 4.48 (b) and (c) are not to scale.

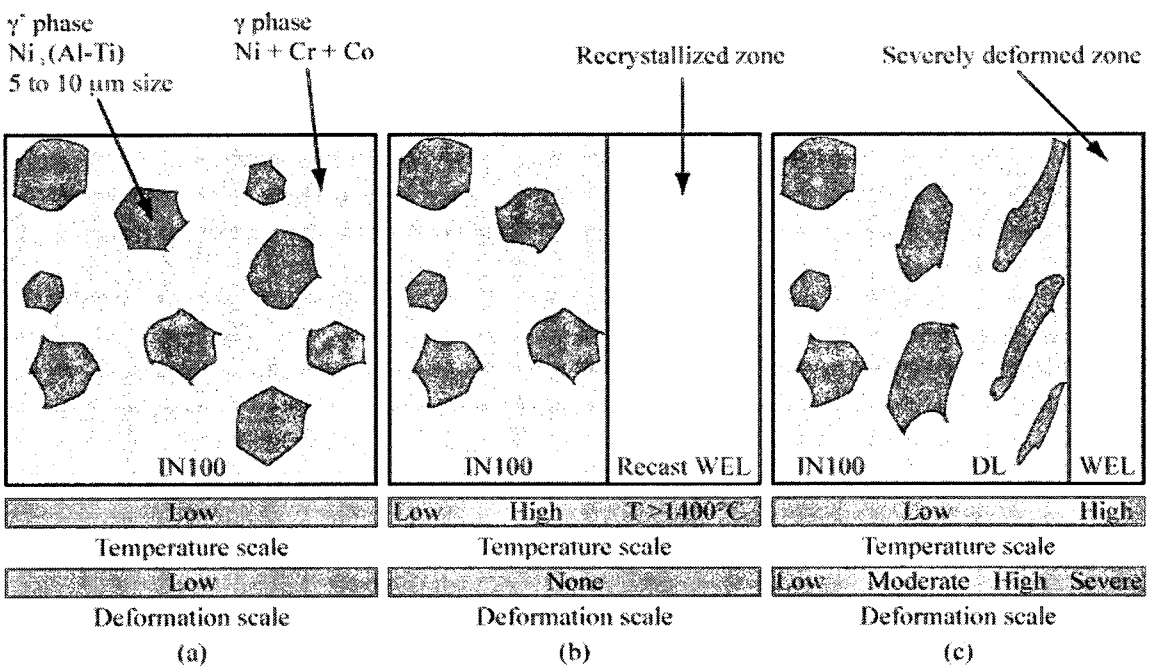

Figure 4.48 – Microstructure of IN100 machined by (a) LSG; (b) EDM and (c) broaching with respect to the temperature and the deformation during machining.

For samples that didn't undergo fatigue testing, we found that the bulk material located directly beneath the WEL (deformed layers for broached samples and heat affected zones for the samples machined by EDM) always exhibit a lower hardness than the WEL or even the bulk material itself. Near-surface regions of samples machined by EDM have a hardness equal to 75% (EDM-R and EDM-F) and 60% (EDM #35) of the WEL hardness. In the case of broaching, the values are of 55% in the case of the Broaching #2 and Broaching #4 samples, and 75% in the case of sample Broaching #41. This variation is thought to result from the formation process of the WEL.

Although very different, EDM and broaching processes both produce an amount of energy that is responsible for the phase change of the bulk material (since the machining parameters are not known, it is not possible to give precise values here). In fact, the near surface regions of the machined material which do not transform into a WEL are modified (deformed or heat-affected) by the energy they receive during the machining process (Figure 4.48).

EDM operates by fusion and the machining temperatures can reach more than 1400 °C. Therefore, heat-affected regions of lower hardness correspond to the intermediate condition of the nickel-based IN100 superalloy between its normal state and the WEL.

AFM images provided in the previous section of this chapter show that the WEL has a different microstructure than the one of the bulk material: the γ' phase was not present in the WEL (Figure 4.48). This absence of the γ' phase is the result of the WEL formation mechanism which involves fusion in the case of EDM and a high plastic deformation along with local heating in the case of broaching. Still, some differences can be observed.

For broached samples, when there is direct contact with the cutting tool the region directly beneath the WEL are deformed in the direction of the tool movement (Figure 4.48). These zones can be easily identified due to the presence of altered (or deformed) γ' phase. We found that the amount of deformation of the γ' phase is not the same for every sample and it is probably due to the different energetic conditions during machining. AFM images of sample Broaching #4 show traces of the γ' phase in the WEL. This is not

the case for other samples because generally the energy produced by the machining process induces homogenization of the γ matrix and γ' phase. When this energy is not sufficient, a deformed γ'-like phase can still be observed in the WEL. It was impossible to conclude on the influence of the machining process for samples machined by EDM since the phase transformation occurs by fusion and does not produce any visible differences in the AFM images.

After characterizing the fatigue tested samples we found that the bulk's hardness had increased. This is due to strain hardening provoked by the cyclic solicitations of the fatigue test. Strain hardening is a very common phenomenon that can be observed on ductile materials. In nickel-based superalloys, this phenomenon is explained by characteristic dislocation behavior. Dislocations tend to accumulate around the γ' phase because the sliding planes of this phase differ from those of the γ matrix at high temperature. During this work, we found that after fatigue testing, the regions underneath the WEL have higher hardnesses than the one of the bulk material. Sliding planes of the γ' phase only differ from those of the γ matrix at high temperature.

The fatigue tests where conducted in an oven at high temperature (above 600 °C). Due to the poor thermal conductivity of nickel-based superalloys, the change of sliding planes in the γ' phase could only take place in the near surface regions of the samples. This could explain why, after fatigue testing, the samples machined by EDM present hardened layers under the WEL. In the case of broached samples, this process is assisted by the fact that the deformed γ' phase prevents dislocations from moving.

The unexpected result of the fatigue test is that the WEL also underwent strain hardening. So far, the WEL had been reported to be brittle but a strain hardening process can only be observed on ductile materials. Therefore, we must conclude that in the case of IN100 nickel-based superalloy, the formed WEL are ductile in nature.

The fatigue testing results presented in Chapter 3 proved that both the machining process and the machining parameters have a great influence on the fatigue behavior of the samples. Sample H3 exhibited the best fatigue behavior because the LSG process produced very little stress in the material.

It appears that the WEL mechanical properties and thickness are linked to the "aggressiveness" of the machining process. Samples EDM #35 and EDM-R were machined the same way and exhibit a thicker WEL than sample EDM-F that was machined using a "softer" set of machining parameters. They also exhibit a harder WEL and no "liquid drop" patterns could be observed on sample EDM-F. In addition, we found that samples machined by EDM with the same set of machining parameters have a very similar hardness and Young's modulus. However, differences can be noted in the fatigue behavior. Sample H14 was machined using a more "aggressive" set of parameters and exhibited the poorest performance in fatigue. This is related to the presence of micro-cracks in the WEL which are produced during rapid quenching of the WEL.

Samples Broaching #4 and Broaching #41 were broached using the same machining parameters but the WEL formed on sample Broaching #41 is much harder than the one formed on sample Broaching #4. This difference comes from a variation in the strain rate applied to the machined surface at the passage of the broach. In machining, some parameters (cutting speed, feed, rake angle, ...) are set and controlled during all the process. Other parameters such as the wear of the tool can't be controlled. In broaching it is impossible to control the quantity of material that each tooth of the broach will face. Therefore, some spikes in the strain rate can be generated leading to higher deformations and resulting in the formation of a WEL. The thickness of this WEL is directly related to the strain rate. In fact, it is not possible to conclude that two cuts performed by broaching using the same set of machining parameters will result in the formation of two identical WEL.

Finally, two samples were shot peened prior to fatigue testing in order to evaluate the impact of a compressive layer on the propagation of cracks in the WEL. In the case of EDM, we can conclude that shot peening has an effect on the "liquid drop" patterns. These patterns could be observed on samples J7 and H7 but not on sample H11 which was shot peened. Therefore, the WEL thickness was homogenized. In broaching, shot peening didn't have any visible impact on the fatigue behavior of the sample.

CHAPTER 5 – CONCLUSION

In this work we have studied the mechanical and microstructural properties of WEL formed on IN100 nickel-based superalloy by two different machining techniques, EDM and broaching. The main results of this work can be summarized as follows:

- We demonstrated that nanoindentation can be used to determine the mechanical properties of WEL formed on superalloys. The use of a nanoindentation system equipped with imaging capabilities allows for very precise measurements to be performed along the cross-sections of the samples. The imaging parameters enabling the acquisition of high resolution images of the studied sample surfaces were also defined.
- The AFM images produced during this study have also made it possible to investigate in more detail the formation mechanisms of the WEL on IN100.
- We proved that both the machining process and the set of machining parameters employed during the production of IN100 workpieces have a direct influence on the mechanical properties (hardness and Young's modulus) of the resulting WEL. WEL formed by EDM and broaching have hardness of 4,2 to 5,3 GPa and 6,1 to 9,0 GPa respectively compared with 3,2 to 6,7 GPa for nickel-based superalloy. Reduced Young's modulus are comprised between 170 and 191 GPa for WEL formed by EDM. These values are 143 and 187 GPa for WEL formed by broaching and 183 and 239 GPa.
- It was hard to conclude on the influence of the machining parameters on the microstructural properties of the samples machined by EDM. However, some relations could be found in the case of broached samples.
- We evaluated the influence of fatigue testing on the mechanical properties of WEL and of the base material. We found that the WEL formed on IN100 by EDM and broaching are ductile and can be strain hardened. Hardnesses of 4,2 to 9,0 GPa were found before fatigue. These values raised to 6,9 to 11,0 GPa.

This thesis represents a systematic work on the characterization of the mechanical and microstructural properties of WEL formed on IN100 nickel-based superalloy by broaching and EDM. Due to their excellent mechanical properties and good corrosion resistance at high temperatures, superalloys are very attractive for applications in the field of jet engines. Unfortunately, theses alloys are hard to machine and produce defects (WEL) during abusive machining. This work has established a basis for the characterization of WEL produced on nickel-based superalloys but has also offered new research perspectives.

Therefore, if the mechanical properties of WEL formed on IN100 are now well known, the influence of this WEL on the operational life was not assessed. More extensive work should be done in analyzing fracture conditions of mechanical components exhibiting a WEL at their surface in order to determine the fracture mechanisms of the WEL and its influence on the failure of the part.

Consequently, this fracture study should lead to the study of the impact of fretting wear on the WEL. This type of wear is very present in turbine fixings of jet engines and therefore, the influence of a WEL on the mechanisms governing the fretting wear should be assessed.

Finally, formation mechanisms of WEL are still to be investigated. In broaching, thermal and plastic flow processes are involved. However, it is yet to be demonstrated what is their relative influence on the mechanical properties and the microstructure of the resulting WEL.

REFERENCES

[1] S. Dalton, «The Miracle of Flight», Firefly books, 1999.

[2] W.J. Boyne, «The Smithsonian Book of Flight», Smithsonian books, 1987.

[3] I.G. Edmonds, «Jet and Rocket Engines: How They Work», Putnam's sons, 1973.

[4] K. Hunecke, «Jet Engines: Fundamentals of Theory, Design and Operation», Motorbook international, 1997.

[5] J. Bennett, M. Hussey, «New Jet Engines, New Materials», Seventh annual Freshman conference, 2007.

[6] S.L. Jone, «NASA's Shift to Carbon Signals Trend Toward Lighter Materials», American Metal Market, 1987.

[7] R.T. Holt, A.K. Koul, L. Zhao, W. Wallace, J.C. Beddoes, J.P. Immarigeon, «Lightweight Materials for Aircraft Applications», Material Characterization, vol. 35, 1995, p. 41-67.

[8] «Airplane Flying Handbook» , U.S. Government Printing office, 2004.

[9] «Proceedings of the International Symposium on Superalloys IX», Warrendale, 2000.

[10] G. Geschler, «Powder Metallurgy of Superalloys», Butterworth, London, 1986.

[11] www.swedm.com.

[12] M. A. Wusatowska-Sarnek, M.J. Blackburn, M. Aindow, «Techniques for Microstructural Characterization of Powder-Processed Nickel-Based Superalloys», Materials Science and Engineering, vol. A360, 2003, p. 390-395.

[13] D.A. Axinte, P. Andrews, W. Li, N. Gindy, P.J. Withers, «Turning of Advanced Ni Based Alloys Obtained Via Powder Metallurgy Route», Annals of the CIRP, vol. 55/1/2006, 2006, p. 117-120.

[14] A.R.C. Sharman, J.I. Hughes, K. Ridgway, «An Analysis of the Residual Stresses Generated in Inconel 718 When Turning», Journal of Materials Processing Technology, vol. 173, 2006, p. 359-367.

[15] T. Connolley , P.A.S. Reed, M.J. Starink, «Short Crack Initiation and Growth at 600°C in Notched Specimens of Inconel 718», Material Science and Engineering, vol. A340, 2003, p. 139-154.

[16] T. Connolley, M.J. Starink, P.A.S Reed, «Effect of Broaching on High-Temperature Fatigue Behavior in Notched Specimens of Inconel 718», Metallurgical and Materials Transactions, vol. 35A, 2004, p. 771-783.

[17] E.C. Jameson, «Electrical Discharge Machining: Tooling, Methods and Applications», Dearbern, Michigan, 1983.

[18] B.J. Griffiths, «Mechanisms of White Layer Generation with Reference to Machining and Deformation Processes», Journal of Tribology, vol. 109, 1987, p. 525-530.

[19] S. Akcan, S. Shah, S.P. Moylan, P.N. Chhabra, S. Chandrasekar, H.T.Y. Yang, «Formation of White Layers in Steels by Machining and their Characteristics», Metallurgical and Materials Transactions, vol. 33A, 2002, p. 1245-1254.

[20] A.W. Warren, Y.B. Guo, «Numerical Investigation on the Effects of Machining-Induced White Layer During Rolling Contact», Tribology Transactions, vol. 48, 2005, p. 436-441.

[21] J.W. Stead, «Micro-Metallography & its Practical Application», J. West. Scot. Iron & Steel Inst., vol. 19, 1912, p. 169-204.

[22] M. Field, W.P. Koster, J.B. Kohls, R.E. Snider, J. Maranchik, «Machining of High Strength Steels With Emphasis on Surface Integrity of Machined Components», Air Force Machinability Data Center Report No. AFMDC-70-1, 1970.

[23] Y.B. Guo, G.M. Janowski, «Microstructural Characterization of White Layers Formed During Hard Turning and Grinding», Transactions of NAMRI/SME, vol. 32, 2004, p. 367-374.

[24] Y.B. Guo, J. Sahni, «A Comparative Study of Hard Turned and Cylindrically Ground White Layers», International Journal of Machine Tools & Manufacture, vol. 44, 2004, p. 135-145.

[25] B. Ekmekci, «Residual Stresses and White Layer in Electric Discharge Machining (EDM)», Applied Surface Science, vol. 253, 2007, p. 9234-9240.

[26] M. Wojdyr, S. Gierlotka, Y. Ivanisenko, W. Lojkowski, H.J. Fecht, «X-ray Investigations of the Natural and Artificial White Etching Layer», Solid State Phenomena, vols. 101-102, 2005, p. 97-100.

[27] J. Jones, D.J.C. MacKay, H.K.D.H Bhadeshia, «The Strength of Ni-base Superalloys», Proceedings of the 5th International Symposium on Advanced Materials, 1995.

[28] «Mechanical Testing and Evaluation», ASM handbook, vol. 8, 2000.

[29] M. Durand-Charre, «The Microstructure of Superalloys», Gordon and Breach Science Publishers, 1997.

[30] A.M. Wusatowska-Sarnek, M.J. Blackburn, M. Aindow, « γ' Precipitation Kinetics in P/M IN100», Int, Conference Processing & Manufacturing of Advanced Materials, 2003.

[31] A.W. Warren, Y.B. Guo, M.L. Weaver, «The Influence of Machining Induced Residual Stress and Phase Transformation on the Measurement of Subsurface Mechanical Behavior Using Nanoindentation», Surface & Coatings Technology, vol. 200, p. 3459-3467.

[32] D.A. Stephenson, J.S. Agapiou, «Metal Cutting Theory and Practice», Dekker, 2006.

[33] M.C. Shaw, «Metal Cutting Principles», New York: Oxford university press, 2005.

[34] S. Akcan, S. Shah, S.P. Moylan, P.N. Chhabra, S. Chandrasekar, T.N. Farris, «Characteristics of White Layers Formed in Steels by Machining», Manufacturing Science and Engineering, vol. 10, 1999, p. 789-794.

[35] A. Ramesh, S.N. Melkote, L.F. Allard, L. Riester, T.R. Watkins, «Analysis of White Layers Formed in Hard Turning of AISI 52100 Steel», Materials Science and Engineering, vol. A390, 2005, p. 88-97.

[36] Y.B. Guo, A.W. Warren, «Microscale Mechanical Behavior of the Subsurface by Finishing Processes», Journal of Manufacturing Science and Engineering, vol. 127, 2005, p. 333-338.

[37] H.K. Tönshoff, C. Arendt, R. Ben Amor, «Cutting Hardened Steel», Annals of the CIRP, vol. 49, 2000, p. 1-19.

[38] M. Field, W.P. Koster, J.B. Kohls, R.E. Snider, J. Maranchik Jr., «Machining of High Strength Steels with Emphasis on Surface Integrity», Air Force Machinability Data Center Report No. AFMDC-70-1, 1970.

[39] «Machining Data Handbook», 3rd edition, Air Force Machinability Data Center, 1980.

[40] M. Field, J.F. Kahles, «Review of Surface Integrity of Machined Components», Annals of the CIRP, vol. 20/2, 1971, p.153-162.

[41] M. Field, J.F. Kahles, «The Surface Integrity of Machined & Ground High Strength Steels», Defense Metals Information Center Report, DMIC 210, 1964.

[42] G.R. Dickinson, «Effects of Machining on Ultra-High Strength Steels», Proc. Instn. Mech. Engrs., vol. 182, Part 3, p.148-151.

[43] C. Guo, Z. Shi, H. Attia, D. McIntosh, «Power and Wheel Wear for Grinding Nickel Alloy with Plated CBN Wheels», Annals of the CIRP, vol. 56, 2007, p. 343-346.

[44] W. Österle, P.X. Li, G. Nolze, «Influence of Surface Finishing on Residual Stress Depth Profiles of a Coarse-Grained Nickel-Base Superalloy», Materials Science and Engineering, vol. A262, 1999, p. 308-311.

[45] W. Österle, P.X. Li, «Mechanical and Thermal Response of a Nickel-base Superalloy upon Grinding with High Removal Rates», Materials Science and Engineering, vol. A238, 1997, p. 357-366.

[46] Y.B. Guo, D.W. Schwach, «An Experimental Investigation of White Layer on Rolling Contact Fatigue using Acoustic Emission Technique», International Journal of Fatigue, vol. 27, 2005, p. 1051-1061.

[47] H.T. Lee, T.Y. Tai, «Relationship Between EDM Parameters and Surface Crack Formation», Journal of Materials Processing Technology, vol. 142, 2003, p. 676-683.

[48] J. Brown, «Advanced Machining Technology Handbook», McGraw-Hill 1998.

[49] H. Ramasawmy, L. Blunt, K.P. Rajurkar, «Investigation of the Relationship Between the White Layer Thickness and 3D Surface Texture Parameters in the Die Sinking EDM Process», Precision Engineering, vol. 29, 2005, p. 479-490.

[50] G. Cusanelli, A. Hessler-Wyser, F. Bobard, R. Demellayer, R. Perez, R. Flükiger, «Microstructure at Submicron Scale of the White Layer Produced by EDM Technique», Journal of Materials Processing Technology, vol. 149, 2004, p. 289-295.

[51] D.K. Aspinwall, M.L.H. Wise, K.J. Stout, T.H.A. Goh, F.L. Zhao, M.F. El-Menshawy, «Electrical Discharge Texturing», Int. J. Mach. Tools Manufact., vol. 32, 1992, p. 183-193.

[52] A.R.C Sharman, J.I. Hughes, K. Ridgway, «An Analysis of the Residual Stresses Generated in Inconel718 when Turning», Journal of Materials Processing Technology, vol. 173, 2006, p. 359-367.

[53] J. Vigneau, «Usinage des matériaux aéronautiques à faible usinabilité», Techniques de l'ingénieur, traité Génie mécanique, BM 7 285, 1999, p. 1-9.

[54] P. Blanchard, «Alliages de nickel résistant à la corrosion humide», Techniques de l'ingénieur, traité Matériaux métalliques, M500, 1996.

[55] G. Gladel, J.L. Tous, D. Gourdet, «Matériaux pour outils de coupe», Techniques de l'ingénieur, B 7 080, 1992.

[56] Private communication with Professor Marek Balazinski.

[57] J.B. Vidal, «L'usinage à grande vitesse : principes, conséquences sur la conception des pièces», Techniques de l'ingénieur, 2003.

[58] B. Kramer, J.F. Huet, «The Wear of Ceramic Tools», Proceeding of NMARC, May 1982.

[59] Private communication with Dr. Nihad Ben-Salah.

[60] D.M. Turley, «Deformed Layers Produced by Machining 70/30 Brass», Journal of the Institute of Metals, vol. 96, 1968, p. 82-86.

[61] W.E. Carrington, M.L.V. Gayler, «The use of Flat Ended Projectiles for Determining Dynamic Yield Stress», Proc. Royal Society, vol. 194, 1948, p. 323-331.

[62] J. Shi, J.Y. Wang, C.R. Liu, «Modelling White Layer Thickness based on the Cutting Parameters of Hard Machining», Proceedings of the Institution of Mechanical Engineers, vol. 220, 2006, p. 119-128.

[63] O'Neil, «Hardness Measurement of Metals & Alloys», 2nd edition, Chapman & Hall, 1967.

[64] B.D. Gozin, V.F. Iankevich, «Friction and Wear in Machines», Symposium Moscow, vol. 15, 1962.

[65] D.M. Turley, «The Nature of White-Etching Surface Layers Produced during Reaming Ultra-High Strength Steels», Materials Science & Engineering, vol.19, 1975, p. 79-86.

[66] Private communication with Lance Kuhn from Hysitron.

[67] W.C. Oliver, G.M. Pharr, «An Improved Technique for Determining Hardness and Elastic Modulus using Load and Displacement Sensing Indentation Experiments», Journal of Materials Research, vol. 7, 1992, p. 1564-1583.

[68] G. Simmons, H. Wang, «Single Crystal Elastic Constants and Calculated Aggregate Properties: A Handbook», 2nd edition, M.I.T. Press, 1971.

[69] B. Cros, E. Gat, J.M. Saurel, «Characterization of the Elastic Properties of Amorphous Silicon Carbide Thin Films by Acoustic Microscopy», Journal of Non-Crystalline Solids, vol. 209, 1997, p. 273-282.

APPENDIX 1 – SCHEMATIC REPRESENTATION OF THE SAMPLES

Sample H3

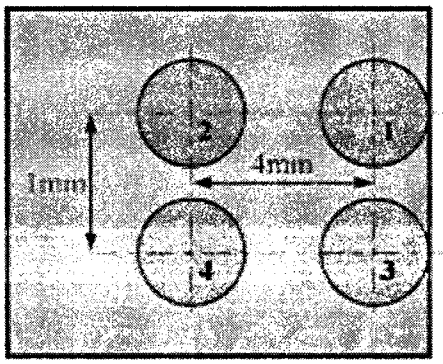

Samples EDM-F, J7, H7, H11 and H14

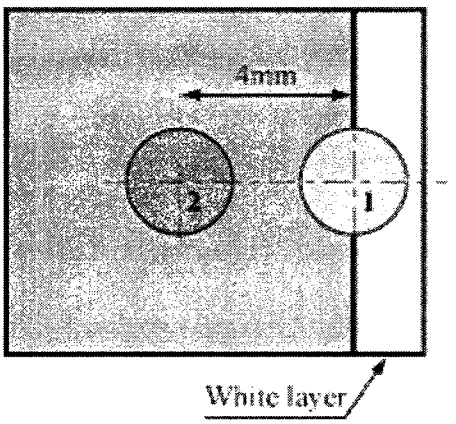

Samples EDM #35 and EDM-R

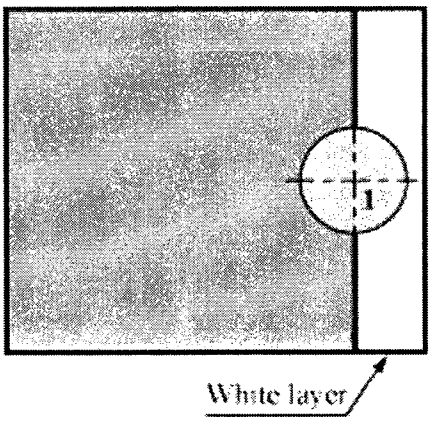

Samples Broaching #2 and Broaching #X2

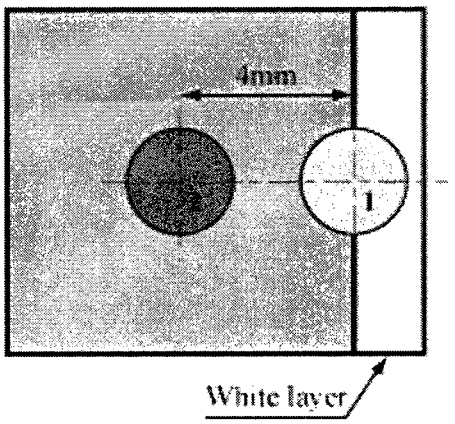

Sample Broaching #4

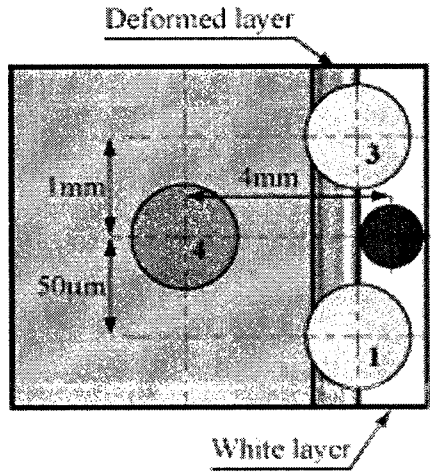

Sample Broaching #41 and H18

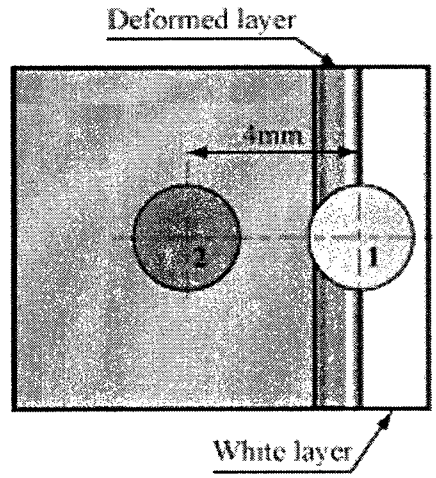

Sample J5

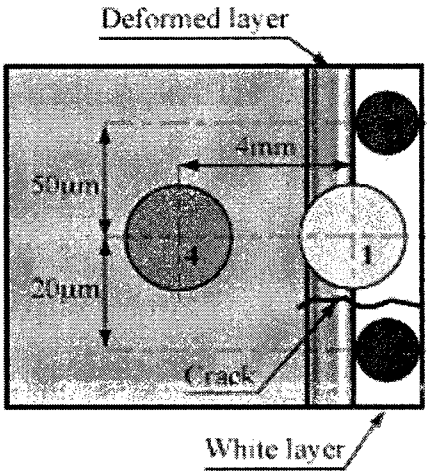

Sample H22

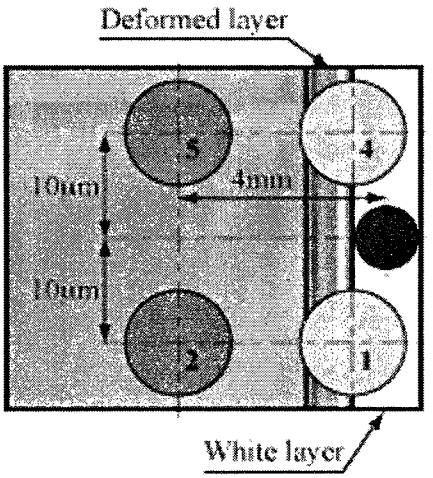

APPENDIX 2 – SAMPLE H3

Zone #1

File directory: Edouard_07_07_25

Maximum load: 5000 μN

Indent number	Distance from surface (μm)	H_{IT} (GPa)	E_r (GPa)	Displacement (nm)	Region
a	-3,0	0,5	10	418	Epoxy
b	-2,0	0,5	10	389	Epoxy
c	-1,0	1,1	23	266	Epoxy
1	0,0	4,3	106	202	Ni alloy
2	1,9	5,5	156	178	Ni alloy
3	4,4	5,5	170	178	Ni alloy
4	8,6	5,6	183	176	Ni alloy
5	12,6	5,2	168	185	Ni alloy
6	18,4	5,8	189	173	Ni alloy
7	24,2	6,3	192	164	Ni alloy
8	30,7	6,2	193	165	Ni alloy
9	41,9	5,5	198	179	Ni alloy
10	43,7	5,0	184	189	Ni alloy
11	46,5	5,6	189	177	Ni alloy
12	54,0	5,1	190	186	Ni alloy
13	56,7	5,3	183	182	Ni alloy
14	60,1	5,6	179	177	Ni alloy
15	67,5	5,7	183	174	Ni alloy

Zone #2

File directory: Edouard_07_07_25

Maximum load: 5000 μN

Indent number	Distance from surface (μm)	H_{IT} (GPa)	E_r (GPa)	Displacement (nm)	Region
100	x	5,2	170	185	Bulk
101	x	5,7	166	174	Bulk
102	x	5,7	188	174	Bulk

Zone #3

File directory: Edouard_07_08_24

Maximum load: 5000 μN

Indent number	Distance from surface (μm)	H_{IT} (GPa)	E_r (GPa)	Displacement (nm)	Region
a	-3,0	0,5	10	418	Epoxy
b	-2,0	0,5	10	389	Epoxy
c	-1,0	1,1	23	266	Epoxy
1	2,0	6,7	177	159	Ni alloy
3	9,3	5,7	177	174	Ni alloy
4	12,0	6,0	179	169	Ni alloy
6	21,3	5,4	173	180	Ni alloy
7	28,3	5,5	178	179	Ni alloy
8	36,7	5,3	177	183	Ni alloy
9	40,0	5,9	180	171	Ni alloy
10	43,7	5,5	188	178	Ni alloy
11	46,7	5,4	179	180	Ni alloy
12	50,0	5,8	189	171	Ni alloy
13	54,7	5,6	188	176	Ni alloy

Zone #4

File directory: Edouard_07_08_24

Maximum load: 5000 μN

Indent number	Distance from surface (μm)	H_{IT} (GPa)	E_r (GPa)	Displacement (nm)	Region
14	x	6,2	188	166	Bulk
15	x	6,6	207	158	Bulk
16	x	6,4	184	162	Bulk
17	x	5,6	183	177	Bulk
18	x	5,3	173	182	Bulk

APPENDIX 3 – SAMPLE EDM-F

Zone #1

File directory: Edouard_06_07_04

Maximum load: 5000 μN

Indent number	Distance from surface (μm)	H_{IT} (GPa)	E_r (GPa)	Displacement (nm)	Region
a	-3,0	0,5	10	418	Epoxy
b	-2,0	0,5	10	389	Epoxy
c	-1,0	1,1	23	266	Epoxy
3	0,7	4,2	157	211	White layer
5	0,9	3,6	196	230	White layer
6	1,0	4,1	182	213	White layer
8	1,8	3,8	173	223	White layer
4	2,0	4,8	215	194	White layer
7	2,2	4,5	206	202	White layer
9	3,5	4,5	207	203	White layer
10	5,5	3,1	178	248	Ni alloy
11	9,6	3,3	255	240	Ni alloy
13	16,2	4,4	236	204	Ni alloy

Zone #2

File directory: 06_07_04

Maximum load: 5000 μN

Indent number	Distance from surface (μm)	H_{IT} (GPa)	E_r (GPa)	Displacement (nm)	Region
201	x	3,7	254	225	Bulk
202	x	3,7	221	227	Bulk
203	x	3,8	234	223	Bulk
204	x	4,0	263	216	Bulk
205	x	2,9	224	258	Bulk

APPENDIX 4 – SAMPLE EDM #35

Zone #1

File directory: Edouard_06_06_14

Maximum load: 5000 μN

Indent number	Distance from surface (μm)	H_{IT} (GPa)	E_r (GPa)	Displacement (nm)	Region
a	-3,0	0,5	10	418	Epoxy
b	-2,0	0,5	10	389	Epoxy
c	-1,0	1,1	23	266	Epoxy
22	2,2	4,4	133	203	White layer
3	7,9	5,1	184	187	White layer
17	9,3	4,9	172	191	White layer
16	9,7	5,4	170	182	White layer
4	11,5	5,4	193	181	White layer
5	12,4	5,4	197	182	White layer
6	15,4	5,5	202	180	White layer
18	16,8	5,4	186	181	White layer
19	17,2	5,2	185	186	White layer
7	18,5	5,5	197	180	White layer
8	20,7	5,4	210	181	White layer
9	23,4	5,4	207	182	White layer
10	24,7	5,7	208	176	White layer
20	26,0	3,8	220	220	Ni alloy
13	36,2	3,2	202	245	Ni alloy
15	52,9	3,2	195	244	Ni alloy

APPENDIX 5 – SAMPLE EDM-R

Zone #1

File directory: Edouard_06_06_08

Maximum load: 5000 μN

Indent number	Distance from surface (μm)	H_{IT} (GPa)	E_r (GPa)	Displacement (nm)	Region
a	-3,0	0,5	10	418	Epoxy
b	-2,0	0,5	10	389	Epoxy
c	-1,0	1,1	23	266	Epoxy
4	3,6	5,2	175	186	White layer
1	3,7	4,5	165	201	White layer
6	5,5	4,8	197	195	White layer
5	7,1	4,6	186	198	White layer
7	7,4	4,7	208	195	White layer
13	8,2	5,1	199	187	White layer
14	8,9	4,9	159	191	White layer
9	12,9	3,7	209	225	Ni alloy
10	20,0	3,5	207	233	Ni alloy
11	34,2	4,5	231	201	Ni alloy
12	43,6	4,8	218	193	Ni alloy

APPENDIX 6 – SAMPLE J7

Zone #1

File directory: Edouard_07_05_30

Maximum load: 5000 μN

Indent number	Distance from surface (μm)	H_{IT} (GPa)	E_r (GPa)	Displacement (nm)	Region
a	-3,0	0,5	10	418	Epoxy
b	-2,0	0,5	10	389	Epoxy
c	-1,0	1,1	23	266	Epoxy
5	0,5	7,3	166	151	White layer
8	0,9	8,0	185	143	White layer
9	1,9	7,8	184	145	White layer
6	2,5	8,2	197	141	White layer
12	2,8	7,9	189	144	White layer
2	3,3	7,8	179	145	White layer
7	3,9	7,9	180	144	White layer
3	5,1	7,8	185	146	White layer
4	6,3	7,6	197	147	White layer
14	8,4	6,1	188	169	Ni alloy
15	11,8	6,2	222	167	Ni alloy
17	25,1	6,0	211	171	Ni alloy
18	35,8	5,2	188	185	Ni alloy
19	43,7	5,0	201	190	Ni alloy
20	47,4	5,1	213	187	Ni alloy
23	57,7	5,1	214	187	Ni alloy

24	63,8	4,9	196	183	Ni alloy

Zone #2

File directory: Edouard_07_05_30

Maximum load: 5000 μN

Indent number	Distance from surface (μm)	H_{IT} (GPa)	E_r (GPa)	Displacement (nm)	Region
25	x	5,1	206	178	Bulk
27	x	5,1	195	178	Bulk
29	x	4,9	190	182	Bulk

APPENDIX 7 – SAMPLE H7

Zone #1

File directory: Edouard_07_07_31

Maximum load: 5000 μN

Indent number	Distance from surface (μm)	H_{IT} (GPa)	E_r (GPa)	Displacement (nm)	Region
a	-3,0	0,5	10	418	Epoxy
b	-2,0	0,5	10	389	Epoxy
c	-1,0	1,1	23	266	Epoxy
12	0,4	8,1	196	142	White layer
8	0,9	7,7	167	146	White layer
10	1,8	8,1	176	141	White layer
7	1,9	7,5	167	148	White layer
2	3,7	7,8	172	144	White layer
5	3,9	8,4	177	138	White layer
9	5,4	7,9	192	144	White layer
3	5,6	7,7	195	145	White layer
6	6,5	8,2	204	140	White layer
14	9,3	6,0	184	169	Ni alloy
16	16,8	4,9	167	191	Ni alloy
17	19,8	6,0	195	170	Ni alloy
18	26,1	6,1	204	168	Ni alloy
19	31,6	6,1	186	168	Ni alloy
20	40,0	6,2	178	166	Ni alloy
21	44,7	6,7	202	159	Ni alloy

22	52,4	5,6	195	176	Ni alloy

Zone #2

File directory: Edouard_07_07_31

Maximum load: 5000 μN

Indent number	Distance from surface (μm)	H_{IT} (GPa)	E_r (GPa)	Displacement (nm)	Region
23	x	6,7	210	159	Bulk
24	x	5,8	209	174	Bulk
25	x	5,8	180	174	Bulk

APPENDIX 8 – SAMPLE H11

Zone #1

File directory: Edouard_07_06_05

Maximum load: 5000 μN

Indent number	Distance from surface (μm)	H_{IT} (GPa)	E_r (GPa)	Displacement (nm)	Region
a	-3,0	0,5	10	418	Epoxy
b	-2,0	0,5	10	389	Epoxy
c	-1,0	1,1	23	266	Epoxy
12	1,0	7,0	169	144	White layer
9	1,7	7,2	170	141	White layer
14	2,0	8,4	195	128	White layer
13	2,1	7,4	171	138	White layer
1	2,4	6,7	178	149	White layer
10	2,5	8,0	174	133	White layer
11	2,8	7,9	184	133	White layer
15	2,9	8,0	183	132	White layer
16	5,6	6,8	195	146	Ni alloy
17	7,4	6,7	191	148	Ni alloy
18	10,2	7,2	214	142	Ni alloy
20	14,9	6,1	194	157	Ni alloy
21	19,5	6,6	194	150	Ni alloy
22	22,3	6,1	193	157	Ni alloy
23	25,6	5,9	210	161	Ni alloy
24	27,4	6,4	204	153	Ni alloy

25	33,5	6,1	196	157	Ni alloy
26	39,5	6,7	216	148	Ni alloy

Zone #2

File directory: Edouard_07_06_05

Maximum load: 5000 μN

Indent number	Distance from surface (μm)	H_{IT} (GPa)	E_r (GPa)	Displacement (nm)	Region
27	x	6,4	202	153	Bulk
28	x	6,4	204	153	Bulk
29	x	6,0	207	159	Bulk

APPENDIX 9 – SAMPLE H14

Zone #1

File directory: Edouard_07_06_04

Maximum load: 5000 μN

Indent number	Distance from surface (μm)	H_{IT} (GPa)	E_r (GPa)	Displacement (nm)	Region
a	-3,0	0,5	10	418	Epoxy
b	-2,0	0,5	10	389	Epoxy
c	-1,0	1,1	23	266	Epoxy
1	0,0	1,5	59	441	White layer
2	1,9	6,7	126	149	White layer
3	4,3	6,8	146	147	White layer
4	6,3	6,8	157	147	White layer
5	8,4	6,9	168	146	White layer
12	10,2	6,3	166	154	White layer
6	10,7	6,9	177	145	White layer
15	13,0	7,4	190	139	White layer
7	13,2	7,9	190	134	White layer
13	14,0	7,1	188	143	White layer
8	15,4	6,9	192	146	White layer
14	16,6	6,8	187	147	White layer
16	16,7	7,1	203	143	White layer
9	17,7	7,2	192	142	White layer
10	19,5	7,0	196	144	White layer
17	19,7	6,8	189	147	White layer

11	21,6	6,8	204	147	White layer
18	22,3	5,5	181	170	Ni alloy
19	24,7	5,9	202	161	Ni alloy
20	26,5	5,9	208	161	Ni alloy
21	28,7	6,4	208	153	Ni alloy
22	31,9	5,5	205	168	Ni alloy
23	35,4	6,1	212	158	Ni alloy
25	42,8	5,9	205	161	Ni alloy
26	50,4	5,9	221	161	Ni alloy
27	x	5,7	213	164	Ni alloy

Zone #2

File directory: Edouard_07_06_04

Maximum load: 5000 μN

Indent number	Distance from surface (μm)	H_{IT} (GPa)	E_r (GPa)	Displacement (nm)	Region
30	x	6,2	213	156	Bulk
31	x	6,6	210	151	Bulk
32	x	6,5	203	151	Bulk

APPENDIX 10 – SAMPLE BROACHING #2

Zone #1

File directory: Edouard_06_11_20

Maximum load: 5000 μN

Indent number	Distance from surface (μm)	H_{IT} (GPa)	E_r (GPa)	Displacement (nm)	Region
a	-3,0	0,5	10	418	Epoxy
b	-2,0	0,5	10	389	Epoxy
c	-1,0	1,1	23	266	Epoxy
1	2,2	5,2	135	184	White layer
2	2,5	5,2	145	184	White layer
4	2,6	6,2	144	166	White layer
11	2,8	6,4	145	162	White layer
10	2,9	6,8	146	158	White layer
3	3,0	6,2	159	183	White layer
5	3,2	6,6	123	160	White layer
12	5,7	3,2	152	238	Deformed
14	6,2	3,6	160	225	Deformed
16	7,1	4,7	172	194	Ni alloy
13	9,3	4,2	175	206	Ni alloy
15	9,4	4,3	187	203	Ni alloy
17	13,2	5,5	199	178	Ni alloy
18	17,2	5,3	207	182	Ni alloy
19	20,7	5,3	221	182	Ni alloy
20	24,7	5,2	210	183	Ni alloy

22	45,9	5,9	237	172	Ni alloy
23	58,2	5,4	222	179	Ni alloy

Zone #2

File directory: Edouard_06_11_20

Maximum load: 5000 μN

Indent number	Distance from surface (μm)	H_{IT} (GPa)	E_r (GPa)	Displacement (nm)	Region
201	x	4,4	213	202	Bulk
202	x	4,1	224	208	Bulk
203	x	4,0	201	212	Bulk
204	x	3,8	207	217	Bulk
205	x	3,9	198	216	Bulk

APPENDIX 11 – SAMPLE BROACHING #4

Zone #1

File directory: Edouard_06_06_09

Maximum load: 5000 μN

Indent number	Distance from surface (μm)	H_{IT} (GPa)	E_r (GPa)	Displacement (nm)	Region
a	-3,0	0,5	10	418	Epoxy
b	-2,0	0,5	10	389	Epoxy
c	-1,0	1,1	23	266	Epoxy
1	0,4	6,6	168	142	White layer
4	1,8	7,7	210	148	White layer
2	1,9	6,6	185	143	White layer
7	2,2	6,4	179	164	White layer
6	3,1	7,0	193	173	White layer
16	3,2	7,3	178	153	White layer
3	3,3	6,2	189	147	White layer
10	8,9	4,3	174	181	Deformed
12	21,6	3,5	177	203	Ni alloy
14	41,9	3,6	205	202	Ni alloy

Zone #2

File directory: Edouard_06_06_09

Maximum load: 5000 μN

Indent number	Distance from surface (μm)	H_{IT} (GPa)	E_r (GPa)	Displacement (nm)	Region
a	-3,0	0,5	10	418	Epoxy
b	-2,0	0,5	10	389	Epoxy
c	-1,0	1,1	23	266	Epoxy
19	1,5	6,7	182	161	White layer
21	1,8	7,1	191	155	White layer
20	2,2	7,8	189	146	White layer
22	2,8	7,0	185	156	White layer
23	2,9	7,1	192	155	White layer
24	3,9	6,0	188	170	White layer
25	4,8	7,6	193	149	White layer

Zone #3

File directory: Edouard_06_07_06

Maximum load: 5000 μN

Indent number	Distance from surface (μm)	H_{IT} (GPa)	E_r (GPa)	Displacement (nm)	Region
a	-3,0	0,5	10	418	Epoxy
b	-2,0	0,5	10	389	Epoxy
c	-1,0	1,1	23	266	Epoxy
1	0,9	1,0	34	481	Epoxy
3	1,3	5,4	199	181	White layer
5	2,7	6,5	189	163	White layer
6	3,5	5,6	181	177	Deformed
7	4,4	4,8	180	195	Deformed
8	6,2	3,4	171	237	Deformed
9	6,6	2,9	188	257	Deformed
11	10,6	3,0	178	254	Deformed
13	15,4	2,8	193	263	Deformed
14	16,8	3,6	179	228	Deformed
15	18,1	3,4	188	238	Deformed
16	21,6	3,3	153	239	Deformed
17	24,3	3,7	176	227	Deformed
18	27,4	2,9	220	258	Deformed
19	30,4	3,2	205	245	Deformed
20	35,7	4,1	209	213	Deformed
21	39,7	3,7	230	224	Deformed
22	45,9	3,5	227	231	Deformed
23	48,5	3,3	251	242	Deformed

Zone #4

File directory: Edouard_06_07_19

Maximum load: 5000 μN

Indent number	Distance from surface (μm)	H_{IT} (GPa)	E_r (GPa)	Displacement (nm)	Region
201	x	4,0	233	215	Bulk
202	x	4,1	212	213	Bulk
203	x	4,0	215	215	Bulk

APPENDIX 12 – SAMPLE BROACHING #41

Zone #1

File directory: Edouard_07_08_28

Maximum load: 5000 μN

Indent number	Distance from surface (μm)	H_{IT} (GPa)	E_r (GPa)	Displacement (nm)	Region
a	-3,0	0,5	10	418	Epoxy
b	-2,0	0,5	10	389	Epoxy
c	-1,0	1,1	23	266	Epoxy
1	1,7	4,7	107	195	White layer
7	2,0	8,7	134	134	White layer
6	2,5	9,1	140	131	White layer
3	3,2	8,7	143	134	White layer
9	3,3	8,8	140	133	White layer
8	4,3	9,5	154	127	White layer
4	5,0	9,2	160	130	White layer
11	5,3	9,0	160	131	White layer
5	5,9	9,4	163	128	White layer
2	6,0	8,8	158	133	White layer
10	6,7	8,5	162	136	White layer
12	8,7	7,3	157	149	Deformed
13	11,3	7,2	160	151	Deformed
14	13,3	7,0	157	153	Deformed
15	16,3	7,6	170	146	Deformed
16	21,3	6,8	170	156	Deformed

17	24,7	6,4	155	162	Deformed
18	30,7	6,5	168	160	Deformed
19	37,3	6,2	163	165	Deformed
20	45,3	6,5	166	161	Deformed
21	47,2	5,9	181	170	Deformed
22	49,1	6,2	167	165	Deformed
23	51,2	5,6	159	176	Ni alloy
24	53,4	5,3	161	182	Ni alloy
25	54,2	5,7	179	173	Ni alloy

Zone #2

File directory: Edouard_07_08_28

Maximum load: 5000 μN

Indent number	Distance from surface (μm)	H_{IT} (GPa)	E_r (GPa)	Displacement (nm)	Region
26	x	5,7	188	175	Bulk
27	x	5,1	175	186	Bulk
28	x	5,7	172	173	Bulk
29	x	5,5	198	178	Bulk

APPENDIX 13 – SAMPLE BROACHING #X2

Zone #1

File directory: Edouard_07_08_31

Maximum load: 5000 μN

Indent number	Distance from surface (μm)	H_{IT} (GPa)	E_r (GPa)	Displacement (nm)	Region
a	-3,0	0,5	10	418	Epoxy
b	-2,0	0,5	10	389	Epoxy
c	-1,0	1,1	23	266	Epoxy
9	2,7	6,2	155	166	Deformed
10	5,7	6,7	170	158	Deformed
11	8,7	7,5	199	148	Ni alloy
12	11,3	7,4	205	149	Ni alloy
13	14,7	7,6	222	147	Ni alloy
14	18,7	6,4	191	163	Ni alloy
15	22,7	6,4	206	162	Ni alloy
16	25,3	6,1	206	168	Ni alloy
17	29,3	5,8	187	174	Ni alloy
18	34,0	6,5	194	161	Ni alloy
19	40,7	6,0	211	170	Ni alloy
20	46,0	6,8	219	156	Ni alloy
21	56,0	6,1	197	168	Ni alloy
22	61,3	5,9	198	171	Ni alloy
23	64,0	6,1	211	167	Ni alloy
24	66,0	6,8	205	157	Ni alloy

25	69,3	7,0	216	154	Ni alloy
26	72,7	6,3	196	164	Ni alloy
27	75,3	6,3	215	165	Ni alloy

Zone #2

File directory: Edouard_07_08_31

Maximum load: 5000 μN

Indent number	Distance from surface (μm)	H_{IT} (GPa)	E_r (GPa)	Displacement (nm)	Region
32	x	6,0	195	169	Bulk
33	x	6,4	182	163	Bulk
34	x	7,4	210	149	Bulk
35	x	6,3	194	164	Bulk
36	x	7,4	213	149	Bulk
37	x	6,5	206	161	Bulk

APPENDIX 14 – SAMPLE H18

Zone #1

File directory: Edouard_07_08_31

Maximum load: 5000 μN

Indent number	Distance from surface (μm)	H_{IT} (GPa)	E_r (GPa)	Displacement (nm)	Region
a	-3,0	0,5	10	418	Epoxy
b	-2,0	0,5	10	389	Epoxy
c	-1,0	1,1	23	266	Epoxy
9	1,3	8,9	155	133	White layer
8	1,7	10,6	179	119	White layer
2	2,0	10,2	185	122	White layer
1	2,1	11,1	190	115	White layer
7	2,4	10,3	189	121	White layer
3	2,5	10,7	199	118	White layer
5	2,7	10,4	202	121	White layer
4	2,8	10,3	195	121	White layer
6	3,7	11,1	198	115	White layer
10	4,0	8,7	188	135	Deformed
16	4,9	10,2	203	122	Deformed
17	6,0	8,2	178	141	Deformed
18	8,0	8,9	188	133	Deformed
12	8,3	10,7	200	118	Deformed
11	8,7	9,4	176	129	Deformed
31	10,0	8,9	208	133	Deformed

19	11,0	10,9	207	117	Deformed
13	14,3	9,9	198	124	Deformed
20	14,7	9,5	202	127	Deformed
32	16,0	8,9	197	133	Deformed
21	19,0	9,2	192	131	Deformed
33	22,7	8,8	197	134	Deformed
22	23,3	8,0	186	143	Deformed
14	24,7	7,7	159	146	Deformed
34	26,7	7,8	194	144	Deformed
23	28,7	7,8	192	145	Deformed
15	30,7	8,2	179	140	Deformed
24	32,7	6,9	193	157	Ni alloy
25	35,4	7,3	196	151	Ni alloy
26	37,2	6,8	199	158	Ni alloy
27	42,5	5,9	167	173	Ni alloy
28	45,7	6,2	178	167	Ni alloy
29	49,0	6,6	187	161	Ni alloy
30	52,3	6,5	178	162	Ni alloy

Zone #2

File directory: Edouard_07_08_31

Maximum load: 5000 μN

Indent number	Distance from surface (μm)	H_{IT} (GPa)	E_r (GPa)	Displacement (nm)	Region
35	x	5,8	191	174	Bulk
36	x	6,0	185	171	Bulk
37	x	5,8	194	174	Bulk
38	x	6,1	212	169	Bulk
39	x	5,8	195	174	Bulk

APPENDIX 15 – SAMPLE J5

Zone #1

File directory: 07_05_29

Maximum load: 5000 μN

Indent number	Distance from surface (μm)	H_{IT} (GPa)	E_r (GPa)	Displacement (nm)	Region
a	-3,0	0,5	10	418	Epoxy
b	-2,0	0,5	10	389	Epoxy
c	-1,0	1,1	23	266	Epoxy
1	0,9	3,8	113	221	White layer
2	2,6	10,7	201	119	White layer
3	3,1	10,8	210	118	White layer
4	4,7	10,7	201	119	White layer
5	6,5	11,2	219	116	White layer
6	8,6	10,6	210	120	White layer
7	11,2	11,3	222	115	White layer
8	14,0	11,2	217	115	White layer
9	16,7	10,6	228	120	White layer
10	19,5	10,2	217	123	White layer
11	21,4	10,7	220	119	White layer
12	24,4	9,7	208	127	White layer
13	27,4	9,7	212	127	White layer
14	30,7	10,1	215	123	White layer
15	33,5	10,1	217	124	White layer
16	36,3	10,0	218	124	White layer

17	39,1	10,2	216	123	White layer
18	41,9	10,1	213	123	Deformed
19	44,7	10,4	212	121	Deformed
20	47,4	10,8	217	118	Deformed
21	49,8	10,0	216	124	Deformed
22	52,1	9,9	214	125	Deformed
23	54,0	8,9	204	134	Deformed
25	60,5	9,7	214	127	Deformed
26	63,7	9,6	217	127	Deformed
27	65,1	9,1	215	132	Deformed
28	67,9	9,4	215	129	Deformed
29	72,6	8,7	203	136	Deformed
30	75,4	8,8	205	135	Deformed
31	81,9	8,6	208	137	Deformed
32	86,5	9,0	221	133	Deformed
33	90,2	9,3	224	130	Deformed
34	97,7	8,4	206	138	Deformed
35	102.3	7,6	190	147	Deformed
36	107,9	8,2	210	141	Deformed
37	111,6	8,2	215	140	Deformed
38	115	8,1	221	142	Deformed
40	125,6	7,5	211	148	Ni alloy
41	130,2	8,3	201	140	Ni alloy
42	134,9	7,6	215	147	Ni alloy
43	139,5	8,9	224	134	Ni alloy

Zone #2

File directory: Edouard_07_05_29

Maximum load: 5000 μN

Indent number	Distance from surface (μm)	H_{IT} (GPa)	E_r (GPa)	Displacement (nm)	Region
44	1,4	10,5	170	120	White layer
45	12,1	11,1	193	116	White layer
46	29,8	10,0	199	125	White layer
47	51,2	8,9	184	134	White layer

Zone #3

File directory: Edouard_07_05_29

Maximum load: 5000 μN

Indent number	Distance from surface (μm)	H_{IT} (GPa)	E_r (GPa)	Displacement (nm)	Region
48	0,9	10,5	184	120	White layer
49	3,9	11,5	202	114	White layer
50	4,7	10,2	218	123	White layer
51	14,0	11,3	210	115	White layer
52	23,3	10,5	215	121	White layer
53	35,4	10,3	211	122	White layer

Zone #4

File directory: Edouard_07_05_29

Maximum load: 5000 μN

Indent number	Distance from surface (μm)	H_{IT} (GPa)	E_r (GPa)	Displacement (nm)	Region
54	x	6,2	207	168	Bulk
55	x	6,1	215	168	Bulk
56	x	6,8	221	158	Bulk

APPENDIX 16 – SAMPLE H22

Zone #1

File directory: Edouard_07_05_31

Maximum load: 5000 μN

Indent number	Distance from surface (μm)	H_{IT} (GPa)	E_r (GPa)	Displacement (nm)	Region
a	-3,0	0,5	10	418	Epoxy
b	-2,0	0,5	10	389	Epoxy
c	-1,0	1,1	23	266	Epoxy
1	0,5	8,3	174	129	White layer
2	2,3	9,9	209	115	White layer
3	4,4	9,8	203	116	White layer
4	6,1	9,7	203	117	White layer
5	7,6	9,7	201	117	White layer
6	9,8	8,8	202	124	White layer
11	9,9	9,8	205	116	White layer
10	10,1	9,3	203	120	White layer
7	11,2	9,0	205	123	White layer
8	13,0	9,5	201	119	White layer
9	14,2	9,1	198	122	White layer
12	15,5	8,7	204	125	Deformed
13	16,7	8,4	199	128	Deformed
14	19,5	8,8	202	125	Deformed
15	20,7	8,3	207	129	Deformed
16	22,8	7,6	193	137	Deformed

17	23,7	8,4	203	128	Deformed
18	27,2	8,2	202	131	Deformed
19	31,6	7,5	195	137	Deformed
20	33,7	8,0	209	132	Deformed
21	39,9	7,2	194	142	Deformed
22	42,8	7,9	202	133	Deformed
23	48,2	6,9	198	145	Deformed
24	62,3	5,9	219	160	Deformed
25	71,6	6,0	189	159	Ni alloy
26	78,1	6,0	202	159	Ni alloy
27	86,5	5,6	193	166	Ni alloy
28	?	5,6	188	167	Ni alloy

Zone #2

File directory: Edouard_07_05_31

Maximum load: 5000 μN

Indent number	Distance from surface (μm)	H_{IT} (GPa)	E_r (GPa)	Displacement (nm)	Region
29	x	5,7	188	165	Bulk
31	x	5,2	184	174	Bulk
34	x	5,7	204	164	Bulk

Zone #3

File directory: Edouard_07_08_01

Maximum load: 5000 μN

Indent number	Distance from surface (μm)	H_{IT} (GPa)	E_r (GPa)	Displacement (nm)	Region
a	-3,0	0,5	10	418	Epoxy
b	-2,0	0,5	10	389	Epoxy
c	-1,0	1,1	23	266	Epoxy
35	0,2	10,3	172	121	White layer
39	0,7	10,6	186	119	White layer
41	0,7	11,7	189	112	White layer
43	0,8	11,7	207	112	White layer
42	0,9	11,3	200	115	White layer
36	1,0	11,4	192	114	White layer
37	1,1	10,1	176	123	White layer
38	1,3	10,2	177	123	White layer
40	1,4	10,6	194	119	White layer

Zone #4

File directory: Edouard_07_08_01

Maximum load: 5000 μN

Indent number	Distance from surface (μm)	H_{IT} (GPa)	E_r (GPa)	Displacement (nm)	Region
a	-3,0	0,5	10	418	Epoxy
b	-2,0	0,5	10	389	Epoxy
c	-1,0	1,1	23	266	Epoxy
44	1,0	11,3	203	115	White layer
45	3,3	11,5	199	113	White layer
46	5,1	11,0	215	116	White layer
47	7,9	11,2	209	115	White layer
48	10,2	10,4	207	121	White layer
49	12,1	10,5	207	120	White layer
50	14,4	9,4	209	129	Deformed
52	15,8	9,6	198	127	Deformed
53	22,3	7,9	194	143	Deformed
54	32,7	9,3	206	130	Deformed
55	38,6	8,7	209	135	Deformed
56	47,4	8,1	193	141	Deformed
57	53,0	7,9	198	143	Deformed
58	59,5	6,7	188	159	Ni alloy
59	62,3	6,5	203	162	Ni alloy

Zone #5

File directory: Edouard_07_08_01

Maximum load: 5000 μN

Indent number	Distance from surface (μm)	H_{IT} (GPa)	E_r (GPa)	Displacement (nm)	Region
60	x	6,0	185	170	Bulk
61	x	6,0	193	170	Bulk
62	x	5,7	177	175	Bulk
63	x	6,0	193	170	Bulk
64	x	5,9	183	171	Bulk